THERMAL AND OPTICAL INTERACTION OF TIGHTLY PACKAGED LEDS IN AUTOMOTIVE LIGHTING APPLICATIONS

A Thesis

by

Umut Zeynep Uras

Submitted to the
Graduate School of Sciences and Engineering
In Partial Fulfillment of the Requirements for
the Degree of

Master of Science

in the
Department of Mechanical Engineering

Özyeğin University
November 2018

THERMAL AND OPTICAL INTERACTION OF TIGHTLY PACKAGED LEDS IN AUTOMOTIVE LIGHTING APPLICATIONS

Approved by:

Professor Mehmet Arık, Advisor
Department of Mechanical Engineering
Özyeğin University

Assistant Professor Mete Budakl
Department of Mechanical Engineering
Turkish-German University

Assistant Professor Altug Basol,
Department of Mechanical Engineering
Özyeğin University

Assistant Professor Polat Sendur
Department of Mechanical Engineering
Özyeğin University

Date Approved: 20 November 2018

Associate Professor Cenk Demiroglu
Department of Electrical and Electronics Engineering
Özyeğin University

To my lovely family..

ABSTRACT

This study aims to enhance the thermal management of an LED light engine for automotive exterior lighting with an advanced heat spreader. Although LEDs have many advantages, their applications require an accurate thermal management. To house driver electronics and LEDs in a typical automotive exterior lighting, conventionally FR4 based printed circuit board is usually used. Over the board, local hotspots are observed due to low thermal conductivity of FR4 based PCB and high heat flux caused by LEDs and electronics. LEDs in automotive back lighting units operated with different input power for position, stop and signal lights. Moreover, in some instances, these three lights perform simultaneously in the automobiles. Therefore, heat flux dissipation over LEDs and electronics become abundant making thermal performance of the FR4 board inadequate to diffuse this flux. Thus, in this study, an advanced heat spreader board technology was investigated and compared with the conventional FR4 based and Al metal core printed circuit boards. An experimental study was conducted via thermal imaging technique in order to inspect local hot spots. Also, an optical performance investigation for advanced heat spreader based LED light engine is conducted. Then, a numerical analysis is also performed in order to validate experimental results. According to experimental data, advanced heat spreader has performed 7.4% better thermal performance than Al metal core board and 25.8% FR4 based board. Besides, when advanced heat spreader board base used instead of FR4 board base, luminous efficacy can be improved by 25.9%.

In addition, improving thermal spreading capability of PCBs is one of the alternative solution in order to distribute heat from source, efficiently. Various type of materials is investigated to improve thermal characteristics of PCBs. In this study,

multilayer ceramic flex PCB is analyzed as alternative PCB solution to overcome thermal problems. To analyze thermal performance of the PCB, it is compared with that of FR4 flex PCB experimentally and computationally. While thermal performance degrades 36.5% when FR4 flex PCB is used, radiant flux and luminous flux of the LED light engine decrease by 13.3% and 14.6%, respectively.

Besides, there is strong dependency between photometric, electrical and thermal properties of LEDs. Hence, while a lighting system is designed, thermal and electrical parameters of the system should be considered to achieve desired performance. Therefore, another aim of the study is to analyze dependency between photometric, electrical and thermal parameters of the FR4 LED light engine with FR4 flex PCB is analyzed.

On the other hand, in recent years, paradigm of Internet of Things which will be effective in all areas of our lives is in the foreground and lighting systems with over 500 billion fixtures globally are seen as a great opportunity for a widespread application. In addition, automobiles may constitute a platform for IoT applications due to their current electronics system and mobility feature. Thus, in this study, a possible candidate automotive rear LED lighting system is evaluated in terms of thermal performance for new generation IoT added applications. Firstly, thermal performance of FR4 based LED engine is evaluated and it is modeled in a CFD program. Then, computational model is solved for different cases such as; 25%, 50% and 70% power addition to electronics to determine the adverse effects due to IOT power needs. Metal and advanced heat spreader substrate technologies are presented as solution to overcome thermal problems. While power consumption of electronic increases by 70%, maximum temperatures that is experienced on electronics increase by +38.4%. Maximum temperatures of amber LEDs increased by +12.5%, when temperature rise of +11.2% is experienced on red LEDs. As conventional FR4 substrate is not adequate for future electronic systems, advanced heat spreader board

technology which consists of vapor chamber structure can be a possible substrate technology for new generation smart applications.

ÖZETÇE

Bu çalışma gelişmiş ısı dağıtıcı elektronik kart kullanımı ile LED otomotiv dış aydınlatma sistemlerinin termal yönetimini iyileştirmeyi amaçlamaktadır. LED'ler geleneksel aydınlatma sistemlerine kıyasla birçok avantaj sunmasına rağmen, LED uygulamaları da gelişmiş bir termal yönetim gerektirmektedir. Genellikle, otomotiv dış aydınlatma sistemlerinde elektronik kart malzemesi olarak FR4 malzemesi kullanılmaktadır. FR4 malzemesinin sahip olduğu düşük termal iletkenlik katsayısı sebebiyle elektronik kartlar üzerinde çeşitli bölgelerde kritik ısı yoğunlukları oluşmaktadır ve LED ve elektronikler yüksek miktarda ısı akısı yaymaktadırlar. Otomotiv dış aydınlatma sistemleri pozisyon, sinyal ve stop fonksiyonlarını gerçekleştirmek ile sorumludur. Her bir fonksiyon için LED'ler farklı güç değerlerinde sürülürler. Bazı durumlarda, bu üç fonksiyon simultane olarak çalışır. Bu durum komponentlerin ısı akısını daha da kritik hale getirir. Dolayısıyla bu çalışmada, geliştirilmiş bir ısı dağıtıcı elektronik kart tabanı, FR4 ve Alüminyum elektronik kartlar ile karşılaştırılarak analiz edilmiştir. Lokal ısı yoğunluklarının tespit edilmesi amacı ile infrared termografi metodu kullanılmıştır. Ayrıca, LED kartlarının optik performans analizleri de gerçekleştirilmiştir. Bunun yanı sıra, deneysel sonuçları doğrulamak amacı ile hesaplamalı akışkanlar dinamiği (HAD) çalışması gerçekleştirilmiştir. Deneysel dataya göre, geliştirilmiş ısı dağıtıcı kart ile Alüminyum karta göre %7.4, FR4 karta göre %25.8 gelişim elde edilmiştir. Ayrıca, geliştirilmiş ısı dağıtıcı kart sayesinde efikasite değeri FR4 karta göre %25.9 arttırılmıştır.

Baskılı devre kartının ısıl dağıtım kapasitesini arttırmak termal yönetimi geliştirmenin bir başka yoludur. Bunun için elektronik kart malzemesi olarak birçok farklı malzeme çeşidi denenmiştir. Bu çalışmada, termal sorunları gidermek amacı ile çok katmanlı

seramik esnek baskılı elektronik kart, FR4 esnek baskılı elektronik karta alternatif olarak deneysel ve sayısal olarak analiz edilmiştir. Seramik kart yerine FR4 kart kullanıldığında termal performansın %36.5 düştüğü saptanırken, ışınım akısının ve ışık akısının sırasıyla %13.3 ve %14.6 azaldığı belirlenmiştir.

Ayrıca, LED'lerin fotometrik, elektriksel ve termal özellikleri arasında güçlü bir bağ vardır. Bu nedenle, bir aydınlatma sistemi tasarlanırken tüm bu özelliklere dikkat edilmelidir. Dolayısıyla, bu çalışmanın bir diğer amacı da fotometrik, elektriksel ve termal parametreler arasındaki ilişkiyi saptamaktır ve FR4 kart bu doğrultuda analiz edilmiştir.

Bir diğer yandan, son yıllarda, en az 500 milyar cihazın kullanacağı Nesnelerin İnterneti birçok uygulama için büyük bir potansiyel oluşturmaktadır. Ayrıca, otomobiller hlihazırda sahip oldukları elektronik sistemlerden dolayı Nesnelerin İnterneti uygulamaları için potansiyel bir platform olarak görülmektedir. Bu sebeple, bu çalışmada, Nesnelerin İnterneti uygulamaları için otomotiv aydınlatmasında kullanılan bir elektronik LED kartı potansiyel bir aday olarak analiz edilmiştir. İlk olarak, FR4 kart deneysel ve sayısal olarak analiz edilmiştir. Sonrasında, hesaplamalı akışkanlar mekaniği modeli, elektronik komponentlere %25, %50 ve %70 daha fazla güç verilerek Nesnelerin Interneti uygulamalarının sonucunda oluşabilecek güç gereksinimi artışlarını simule edebilmek amacıyla analiz edilmiştir. Elektroniklerin güç tüketimi %70 arttırıldığında, maksimum elektronik komponent sıcaklığının %38.4, maksimum amber LED sıcaklığının %12.5 ve maksimum kırmızı LED sıcaklığının %11.2 arttığı gözlemlenmiştir. Dolayısıyla, ileride kullanılabilecek elektronik sistemler için FR4 malzemesinin kart malzemesi olarak kullanılmasının mümkün olmadığı saptanmıştır. Geliştirilmiş ısı dağıtıcı kart tabakasının yeni jenerasyon akıllı sistemlerde kullanılabilecek potansiyel bir kart tipi olduğu analiz edilmiştir.

ACKNOWLEDGEMENTS

I would first like to thank my thesis advisor Professor Mehmet Arık for the continuous support of my master study and research, for his patience, motivation and knowledge. His guidance helped me in all the time of research and completing of this thesis. I would also like to thank for the partial financial support from FARBA Corporation of Bursa. I would also like to thank EVATEG Center for the utilization of laboratories and infrastructure. I would also like to thank to rest of my thesis committee: Assistant Professor Altuğ Başol, Assistant Professor Cenk Demiroğlu, Assistant Professor Mete Budaklı, Assistant Professor Polat Şendur. Besides, I must express my very profound gratitude to my family for providing me with unfailing support and continuous encouragement throughout my years of study and through the process of researching and writing this thesis. Especially, I want to thank my brother and father for their language reviews for my papers. This accomplishment would not have been possible without them. Also, I want to thank my dearest friends Ece Ulusu, Ezgi Karaca, Şebnem özbek and Ezgi Gülccay for their presence in every aspects of my life. In addition, I thank Ali for all his help for this thesis. My final thank goes to Hayati Yaşamak İsteyenler for being like family in these 3 years. Thank you!

TABLE OF CONTENTS

LIST OF TABLES

LIST OF FIGURES

CHAPTER I

INTRODUCTION

In recent years, LEDs have been used in many areas because of their unique advantages such as high lumen output, energy savings, exceptional color features, precise optical control and long life span [1]. Automotive sector is one of these areas that used LEDs in both exterior and interior lighting of vehicles during the last decade. However, due to tight volumes and severe environmental conditions of transportation applications, challenging thermal problems such as elevated junction temperatures are confronted. An increase in junction temperature may cause lumen degradation, wavelength shift and catastrophic failures in LEDs [2]. Therefore, compact packaging with proper thermal management has become a required system solution for LED lighting systems in vehicles. Moreover, automotive headlamps have been exploring novel technological applications such as smart lighting and Li-Fi. For example, with the Li-Fi technology, headlamps have been used for vehicle-to-vehicle communication (i.e. visible light communication (VLC)) [3]. Thus, with these kinds of technological improvements, the importance of compact packaging will increase due to crammed components into tight volumes and foot print areas. However, when electronics are placed closely, distributing heat from surfaces of components poses significant problems [4]. Therefore, thermal problems should be anticipated before designing component placement over a light engine. In addition, system level cooling technologies should be implemented so that effective heat removal is assured for hermetically sealed automotive lighting systems. To meet system level cooling challenges, there are a number of active cooling techniques such as rotary fans and synthetic jets but due to their reliability and noise issues [5], passive cooling techniques are more

applicable for automotive lighting systems. Although developing a system level solution is possible with known technologies, local hot spots at the double-sided PCB populated with electronics components and LEDs are still problems that design engineers face with. Conventional FR4 substrates are used in many applications due to ease of manufacturing and low-cost. However, their poor thermal conductivity creates shortages to meet todays demanding thermal needs. Therefore, recent compact packaged high lumen light engines require novel thermal solutions. In light commercial vehicles exterior lighting system, three distinct functions are required such called position, stop and signal. While using a FR4 based printed circuit board with LEDs, to combine all these functions into a single PCB is not possible due to thermal problems. Therefore, to improve thermal performance of PCBs, FR4 substrates are soon expected to be replaced with high performing substrate technologies as the cost of those substrates will shrink. Metal clad printed circuit boards (MCPCBs) have capability of multidimensional heat transfer with a low constriction resistance; they show better thermal performance than conventional FR4 substrates [6]. This is particularly due to approximately a factor of three increase (200/0.2) in the thermal conductivity. Therefore, metal clad printed circuit board technology may be an option for LED automotive lamps. A further increase in the thermal performance at the same or similar cost will extend the lumen extraction and reduce system cost by other novel approaches. During last couple of decades, vapor chamber technology which is capable of diffusing heat from a surface is investigated for electronic cooling applications [7, 8]. Due to the fact that phase change heat transfer occurs in vapor chambers, its cooling performance is reported to be over 10-100 times of copper (400 W/m-K) [9]. Therefore, vapor chamber technology may be used in printed circuit boards as a possible substrate for LED light engines as well. While the technology is still at the exploration phase, it is expected to offer unique performances.

For automotive exterior lighting applications, advanced vapor chamber based

board is a possible alternative. In this study, three distinct substrates for thermal performances of LED boards have been studied. Technological investigation started with FR4 based conventional board (PCB), and then extended to metal-clad board (Al) and a further this study conducted with an advanced thin vapor chamber substrate. Currently, single vapor chamber heat spreader has not been used as a board substrate for exterior automotive lighting. Thus, this study aims to contribute current technology via investigating advanced vapor chamber based board for automotive exterior lighting systems. Both experimental and computational findings are presented and discussions are given in the Chapter III and VI, respectively. Also, optical performance of the light engines were tested and results were discussed in Chapter IV.

Another aim of the study is to analyze thermal performance of ceramic flex PCBs. Therefore, in the study, two multichip LED light engines which have distinct flex PCBs are compared in terms of thermal spreading performance. The first flex PCB consists of one copper and one glass fiber epoxy sub layers while the other one is composed of one ceramic-polymer blend and two copper sub layers. IR thermography technique is used to obtain thermal performance of these two LED engines. In order to validate experimental study, LED light engines are modeled in computational environment. Then, optical tests were conducted with an integrating sphere on LED engines in order to understand the relation between thermal and optical performances. Thermal performance tests are presented in Chapter III while results of optical investigation is shared at Chapter IV. In addition, computational findings of the study is given in Chapter VI.

Photometric, electrical and thermal properties of LEDs are highly dependent with each other. Therefore, while a lighting system is designed, thermal and electrical parameters of the system should be considered to achieve desired optical performance. Luminous efficacy of the LED systems are highly sensitive to junction temperature of the LEDs because optical output of the LEDs is changing with temperature. Thus, a

relationship between photometric, electrical and thermal parameters of the FR4 LED light engine with FR4 flex PCB is investigated in Chapter V.

Another recent technological area, Internet of things (IOT) has been rapidly evolving, and lighting systems with over 550 Billion fixtures globally seen as a great opportunity for a widespread application space. Added electronics due to communication, control, sensing and power for IOT features are expected to contribute an additional amount of over 70 percent to overall heat generation. Therefore, a hard problem will be harder at the same volume, footprint area and cost. This study also aims emphasizing the severity of the anticipated thermal problems of IOT added future lighting systems besides presenting some of the current local hot spot thermal issues due to LED tight packaging. In Chapter VII, electronics of the LED light engines are modeled in computational environment with higher input power in order to mimic the same system adding IOT features.

1.1 Literature Review

This section discusses properties of light-emitting diodes, thermal management technologies for cooling of the LEDs and their place in Internet of Thing applications. In the first part of the section, packaging development of LEDs and their advantages over conventional light sources are mentioned. Then, historical evolution, radiative and non-radiative recombination, junction temperature and optical properties of the LEDs are explained. In the second part, thermal management problems of LEDs and possible cooling techniques to solve these problems are discussed. In the last part, importance of LEDs for Internet of Things applications is analyzed.

1.1.1 Light-Emitting Diodes (LEDs)

As it can be easily inferred from their name, light emitting diodes (LEDs) are a kind of diodes. However, they have some properties different from regular rectifier diodes. One of the most distinctive property of LEDs is that forward voltage of LEDs are

much higher than normal diodes due to achieve efficient light emission [10].

LED production begins with manufacturing of bare wafer such as sapphire, GaN, GaAs, Si wafers. Then, a couple of epilayers are grown on the bare wafers. To attain different LED colors, distinct epiwafers are using such as for green, blue and UV range light, InGaN and AlGaN epiwafers; for red and yellow light, InAlGaP and for red and infrared range light, AlGaAs epiwafers are used. After that, electric contact pads are assembled with the epiwafers and epiwafers are shaped as LED die. At the end of the manufacturing process, LED die is packaged.

LED package has complicated structure that composed of multiple components. In Figure 1, the components of an LED are demonstrated as an example of an LED structure [11]. The LED consists of bond wire, LED die, encapsulant, lead frame, die attach and housing. Bond wire which provides electrical connection between LED die and lead frame are generally made of gold. The die is made up of a semiconductor compound. Encapsulant is formed on top of the structure as a dome and generally silicon or epoxy resin is used as encapsulant material. Lead frame provides connection between external power source and LED die. Die attach constitutes a medium to connect LED die mechanically and thermally to lead frame. Housing forms a protected structure for an LED [11].

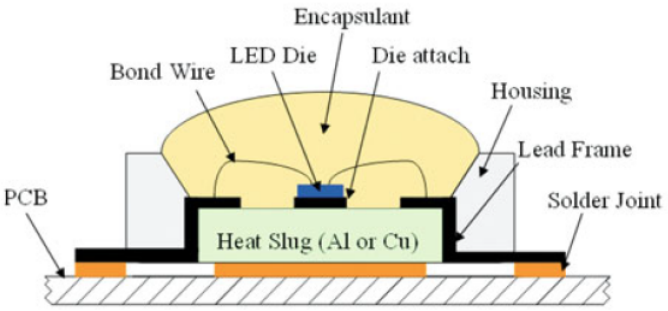

Figure 1: Cross-sectional side view of a typical white LED [11]

LEDs require proper packaging to ensure cooling, protection, optical configurations and enclosing. In the early LEDs, packaging structure was quite simple with just a couple of components whereas today, with the increasing demand to high power LED applications, package structure become more advanced. Especially, while power of LEDs continuously increasing, thermal management become more and more important to provide efficient heat dissipation from the chip. Achieving advance thermal management, there are four LED packaging types which are chip-level, frame-level, board-level and system-level packaging [11].

Surface Mount Technology (SMT) is a novel mount technology for microelectronic. Due to smaller volume and low thermal resistance characteristics of the SMT, it has been also popular for LED packaging. Besides, ceramic substrates are another packaging solution in LED industry due to its high thermal conductivity. For high-power applications that need more than a chip, chip on board (COB) technology offers a solution with low thermal resistance [11].

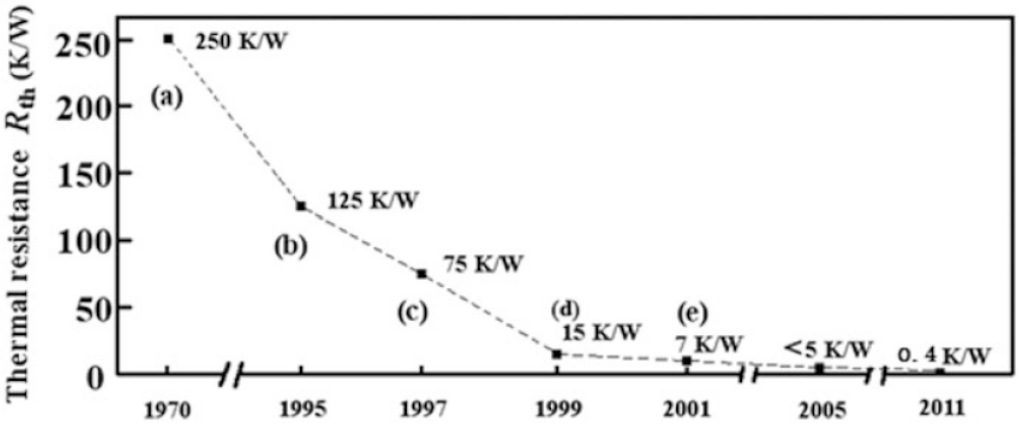

Figure 2: Revolution of LED Thermal Resistance [11]

As it is represented in Figure 2, in early LEDs, thermal resistance of the package reached up to 250 K/W (junction-to-ambient). However, recent developments like COB and novel substrate technologies enable decrease in thermal resistance under

10 K/W. Moreover, with various passive and active cooling technologies, thermal resistance can be decreased more in system-level [11].

According to Commercial Buildings Energy Consumption Survey of U.S. Energy Information Administration [12], in 2012, lighting constitutes 17% of the electricity consumption in buildings. Lighting has the highest share in the survey. Therefore, energy efficiency in lighting has crucial effect to decrease electricity consumption and provide economic contribution. In this regard, because of their high energy efficiency, popularity of LEDs have been tremendously increasing in recent years. While the efficiency of conventional light sources is about 5%, LEDs reaches up to energy efficiency of 20%-30% [13, 4]. Furthermore, according to the Haitz Law, it is predicted that luminous output of the LEDs rises 35% per year while price of the LEDs in terms of cost per lumen decreases 20% per year [10]. Prediction trend of the Haitz Law is represented in Figure 3 [10].

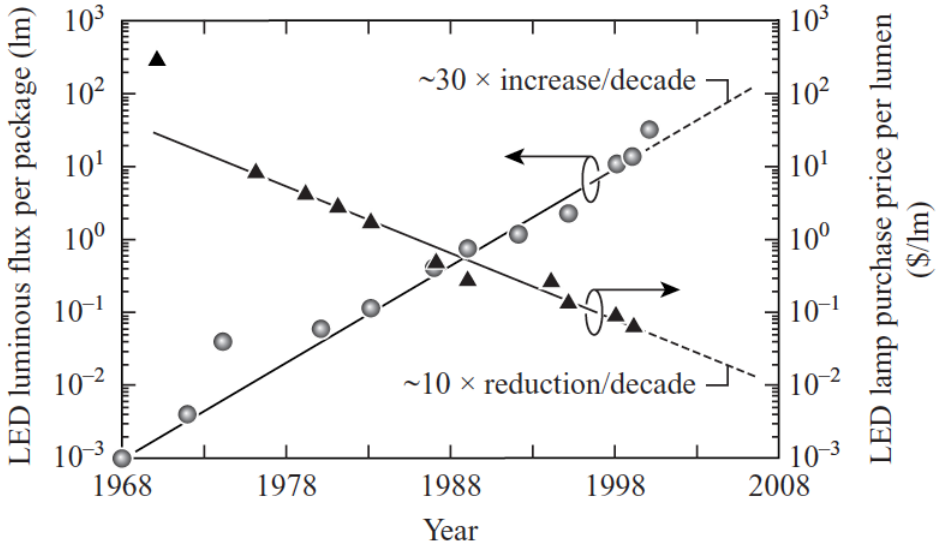

Figure 3: Haitz Law [10]

Besides high energy efficiency of LEDs, their lifetime is about 50,000 hours which is

much higher than regular lighting fixtures. Moreover, quick response as microsecond-level on-off switching, wide range controllable color temperatures, no low temperature start-up problems, low ultra violet radiation and non-toxic emission are another major advantages of LEDs over conventional light sources [11].

1.1.1.1 Evolution of LEDs

First light emitting diode (LED) had been found by Henry Joseph in 1907. However, the first diode is not an p-n junction diode, it is a Schottky diode. In 1936, Destriau published first LED made up of zincblende (ZnS). III-V compound semiconductors firstly developed by Heinrich Welker in early 1950s. The III-V compounds which can not found in nature are very suitable to optical applications so development of the III-V compounds is a milestone for LED technology [14].

In early 1960s, III-V GaAs devices have begun to be investigated. First commercial GaAs LED is developed by the Texas Instrument Corporation in early 1960s.

For achieving visible emission, GaAsP and AlGaAs were also researched. GaAsP LEDs firstly used on circuit boards as indicator lights [14].

In 1962, Holonjak and Bevacqua declared visible light emission from GaAsP junction. This declaration is a remarkable progress as the first step of applicable p-n junction LEDs with visible light emission [14].

In 1968, with the first mass production of LEDs by Monsanto Corporation, price of the LEDs decreased. As a result of the price reduction, solid-state lamps entered to the lighting market. Product portfolio of the company was consisting of GaAsP p-n junctions LEDs grown on GaAs substrate. The LEDs were emitting visible light in red wavelength region of the spectrum [14].

It is revealed that the external efficiency of GaAsP LEDs was limited as 0.2% or less due to high density dislocations caused by large lattice mismatch between the GaAs substrate and GaAsP epilayer. Also, because of direct-indirect transitions,

brightness of GaAsP LED remained low. Therefore, from 1960s to middle of 1970s, GaAsP LEDs were used to low-brightness applications such as LED displays of calculators and watches [14].

In early 1960s, GaP-based red and green LEDs were developed. Light emission of the GaP is limited since GaP is an indirect-gap semiconductor and probability of radiative recombination is low [14]. Over the years, to improve the efficiency of GaP LEDs, different doping and growth techniques were investigated. Vapor-phase epitaxy (VPE) was applied as a growth method so that it led to n-doping just in the near of p-n junction. Consequently, less light absorption in the layers and greater overall efficiency were achieved in 1970s [14].

Later, for low-brightness applications with green light emission, n-doped GaP LEDs are the essential LED material [14]. During 1970s, GaP, GaInP and GaAsP was utilizing widely in dial pads of telephones and displays of watches and calculators [14].

At the end of 1960s, Tietjen from Radio Corporation of America (RCA) aimed to produce flat panel televisions which required red, green and blue pixels. There were already LED technology for green (GaP:N LEDs) and red (GaAsP LEDs) pixels. Therefore, in 1968, in order to obtain blue pixels, he and his group began to work on a technique for growing single-crystal films of GaN. However, they could not achieve an efficient method. Until 1982, there were only single published paper about GaN LEDs. Then, Mg-doping of GaN made an era for all nitride based LEDs [14].

Team of Nakamura and Mukai [14], has contributed GaN growth, LEDs and lasers, significantly. First applicable green and blue GaInN double heterostructure LED which reached efficiency of 10% was developed by them. After these improvements in GaInN LEDs, they have been started to be used in high-brightness applications [14].

AlGaInP LEDs are developed in Japan at the end of 1980s. With multiple quantum well (MQW) active regions, efficiency of AlGaInP LEDs were considerably improved. AlGaInP material is utilized to high-brightness light emission of red, yellow and orange applications [14].

1.1.1.2 Radiative and Non-Radiative Recombination

For semiconductors, using p-n junction diode is efficient way to generate light emission. The light emission in p-n junction diodes happens as a result of radiative recombination. As illustrated in Figure 4, radiative recombination can be defined as transition of an excited electron from conduction band to valance band via recombining with a hole in the valance band [11]. Bandgap energy is the difference of conduction band energy and valance band energy ($W_g = W_c W_v$). Frequency of the photon is determined by following relationship [11].

$$f = \frac{W_g}{h} \tag{1}$$

where f is frequency of photon, W_g is bandgap energy and h is Plank's constant.

Wavelength of the photon is also determined by bandgap energy with following equation [11]

$$\lambda = \frac{c}{f} = \frac{ch}{W_g} \tag{2}$$

where c is the speed of light.

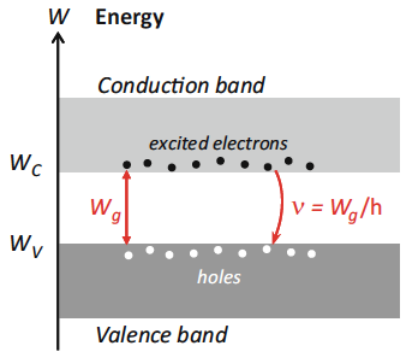

Figure 4: Illustration of radiative recombination [11]

Characteristics of the light emission is designated by bandgap structure of the semiconductor material. There are two classes of semiconductors which are direct bandgap and indirect bandgap materials. In direct bandgap semiconductors, the minimum energy level of the conduction band and the maximum energy level of the valence band are at the same k-wavelength number. Therefore, electrons and holes have the same momentum. However, in indirect bandgap semiconductors, the minimum energy level of the conduction band and the maximum energy level of the valence band are not located at the same k-wavelength number. In other words, momentums of electrons and holes are different. Thus, in indirect bandgap, recombination of electrons and holes only happens with the presence of phonons. Recombination energy of electrons is transmitted to vibration energy via phonons. As a result of the non-radiative recombination, heat formation occurs [11].

Bimolecular recombination coefficient B depends on $T^{-3/2}$. Therefore, recombination probability is inversely proportional with temperature. As it is indicated in Figure 5, carrier distribution in k space is more dense at low temperatures. Due to the fact that electron and holes can recombine only if their momentums are the same, recombination probability is higher at low temperatures [11, 14].

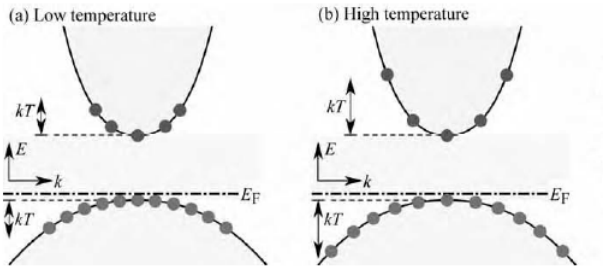

Figure 5: Carrier distribution at low (a) and high (b) temperatures [14]

1.1.1.3 Junction Temperature of LEDs

Junction temperature defines the temperature of the active region crystal lattice [14]. Junction temperature is a significant characteristic of LEDs because of many reasons. Mechanical strength of the encapsulation, internal quantum efficiency and lifetime of the LED depends on junction temperature. Thus, measuring junction temperature of the LEDs is essential for lighting designers. There are various junction temperature measurement methods such as forward voltage, micro-Raman spectroscopy, microinfrared imaging, thermal resistance methods and a method which estimates junction temperature according to peak wavelength shift [14].

Bandgap energy is temperature dependent because of electron-phonon interactions and lattice vibrations [15]. As a result of energy bandgap shrinking, peak wavelength of an LED is shifted. Junction temperature method based on peak wavelength shift uses the dependency between energy bandgap and temperature. In this method, there are two stages: calibration measurement and junction temperature measurement according to calibration data. In the first stage, LED are driven with different pulsed currents without any Joule heating in a thermal chamber. Peak wavelength is measured at different chamber temperatures for different current levels. As a results of calibration measurement, a correlation between peak wavelength and temperature

is attained for different current levels. Then, calibration correlation is used to determine junction temperatures with respect to measured peak wavelengths. Although wavelength shift method is using to estimate junction temperature of LEDs, there are more accurate and easier methods like forward voltage methods [14].

There is a dependency between forward voltage and junction temperature. Forward voltage method uses this dependency to estimate junction temperature of LEDs. Forward voltage method is also consists of two stages: calibration measurement and junction temperature estimation based on calibration data. In the calibration measurements, LEDs pulsed with different current levels in a temperature-controlled chamber. Forward voltage of the LED is measured at different ambient temperatures. Therefore, a calibration correlation between forward voltage and temperature for different current levels is obtained. Then, with steady state measurement, LED drive with same current range and for each voltage level, junction temperature of the LED is determined according to calibration correlation [14].

As it is mentioned, there are many junction temperature measurement techniques. Tamdogan et al. presents a detailed comparison study for Raman spectroscopy, microinfrared (IR) imaging, and forward voltage methods in [16].

1.1.1.4 Photometric and Radiometric Quantities of LEDs

Optical energy generated by light is measured in Joules but it usage rate of the energy is quantified in Watts. Radiated energy is equal to multiplication of Plank constant and frequency of light. Therefore, energy of light is proportional with frequency [10].

$$E = hf \tag{3}$$

In addition, frequency of light is equals to ratio of speed of light c and wavelength λ. Therefore, energy of the light is inversely proportional with the wavelength. It is defined as following equation [10].

$$E = h\frac{c}{\lambda} \tag{4}$$

Radiated energy per second is described by radiant power which is radiometric quantity. Most of the light sources emits lights which includes multiple colors. LEDs also emits light which have wide wavelength spectrum. Therefore, radiated power of LEDs is calculated with sum of the all powers in each frequency [10].

Radiant flux is the sum of the light in every wavelength but human eye is sensitive only a part of the emission spectrum (about 390 to 700nm). Therefore, the term luminous flux is derived by radiant flux according to spectral response of the human eye as in the following equation. Due to the fact that it is weighted by eye response, it is photometric quantity.

$$\Phi_v = K_m \int_0^\infty \frac{d\Phi_e(\lambda)}{d\lambda} V(\lambda) d\lambda \tag{5}$$

where, K_m is the maximum luminous efficacy, $V(\lambda)$ is the spectral luminous efficiency function and $\Phi_e(\lambda)$ is the spectral distribution of the radiant flux [11].

Various quantities are utilizing in order to evaluate optical performance of LEDs. Primarily, efficiency of a system is one of the key performance parameters. Therefore, to analyze optical performance of an LED, determining the efficiency is the first goal of engineers or scientists. There are four types of efficiency which are internal, extraction, external and power efficiency.

In active region of ideal LEDs, as a result of every electron injection, a photon emission originates [14]. Therefore, quantum efficiency of the ideal region is equal to unity. However, in real case, not all electron injection ends up with photon emission. Therefore, internal quantum efficiency of an LED is calculated with following equation.

$$\eta_{int} = \frac{Number\ of\ photons\ emitted\ from\ active\ region\ per\ second}{number\ of\ electrons\ injected\ into\ LED\ per\ second} \tag{6}$$

After the photon emission, in ideal LEDs, all photons should leave the active region to free space but in regular LEDs, not all emitted photons can escape from the LED die due to various failure mechanisms. For instance, reflected light can be received by metallic surface and absorbed by it and this phenomenon is called total internal reflection [14]. Extraction efficiency of an LED is described as

$$\eta_{extraction} = \frac{Number\ of\ photons\ emitted\ into\ free\ space\ per\ second}{number\ of\ photons\ emitted\ from\ active\ region\ per\ second} \tag{7}$$

In order to obtain how many injected electrons results with light emission into free space, the external quantum efficiency term calculated with the following equation [14].

$$\eta_{ext} = \frac{Number\ of\ photons\ emitted\ into\ free\ space\ per\ second}{number\ of\ electrons\ injected\ into\ LED\ per\ second} \tag{8}$$

Another important performance parameter for an LED is power efficiency which is also named as wallplug efficiency. Wallplug efficiency of the LED shows that amount of the electrical power which transfers into radiant power [14]. It is defined as

$$\eta_{power} = \frac{P}{IV} \tag{9}$$

where P is the radiant power, I is the input electrical current and V is the input voltage.

1.1.2 Thermal Management of Exterior Automotive LED Lighting Systems

1.1.2.1 Possible Cooling Technologies for Thermal Management Problems of LEDs

In recent years, light-emitting diodes (LEDs) have been widely utilized in various lighting applications due to high efficacy, longer lifespan and low electricity consumption[1].

Despite low energy consumption in LEDs compared to conventional lighting, in which about 70- 80% of the electrical energy converts into thermal energy results in elevated junction temperatures [1, 4] which affects the optical quality and reliability of the system [2, 17]. According to Arik et al., light output degradation, wavelength shift and catastrophic failures are the possible consequences of elevated junction temperatures in LEDs [2]. Especially, in automotive lighting, where LEDs junction temperature increases, amber LEDs can emit red color light instead of amber color due to wavelength shift [2]. Therefore, increased junction temperature is become a critical issue for automotive lighting manufacturers. In order to control the junction temperature, proper thermal management is required for LED based lighting systems. Thus; for thermal management of LEDs, various active and passive cooling techniques have been investigated such as thermoelectric, heat pipe, synthetic jets and forced air cooling. However, due to reliability concern, undesired noise and energy consumption problems of active cooling [6] [5], passive cooling is become more preferable method for lighting applications. One of the most ideal passive cooling techniques is to enhance the heat conduction throughout the printed circuit board on which LEDs are mounted. Selection of PCB substrate is a significant subject since thermal conductivity depends on material type. In the literature, there are some studies which focus on replacement of low conductive FR4 based PCB with high conductive metal core printed circuit boards (MCPCB) in order to improve heat conduction capability of the LED boards. K. C. Yung et al. [6], concluded that metal core PCBs are more convenient to heat dissipation in all directions than FR4 based PCBs which permit heat dissipation only in single direction due to its low thermal conductivity. According to this study, difference in thermal performance directly affects the optical performance of LEDs. Therefore, optical output efficiency of LEDs that are mounted to MCPCB is higher than that of LEDs mounted to FR4 based PCB. In another study of K.C. Yung et al., they claim that the most effective thermal conduction path can

be reached by optimizing optical performance, energy consumption and cost of the system [6]. Although MCPCBs improve thermal performance of LED applications significantly, whether in harsh ambient conditions, there is still a need for more advanced board technology in order to achieve improved heat dissipation. Automotive exterior lighting can also be challenging due to significant thermal problems. These thermal problems are mainly caused by harsh ambient conditions, tight volume and low conductive boards. Therefore, a novel approach for advanced heat spreader board technology is required which will have better thermal performance than FR4 PCB and MCPCB, for automotive exterior LED lighting system.

In the literature, in order to improve thermal performance of the board, heat sink technologies have been studied. However, in high heat flux applications, heat sink technology has become inadequate for removing heat efficiently from the heat source. In recent years, flat plate heat pipe technology has been utilized to enhance heat spreading capability of heat sink [7, 8]. Working principles of this flat heat pipe which is also named as vapor chamber is based on two dimensional heat transfer [5]. Inside the vapor chamber, working fluid evaporates into hotter section via absorbing heat from the source and evaporated fluid comes to condenser part in order to release the heat energy [7, 8]. The intended usage of vapor chambers and heat pipes are different. While heat pipe transports heat from one medium to another, where vapor chamber is widely utilized to spread heat from high density place to low dense and larger place [7]. Due to larger dimensions of heat sinks, this kind of cooling technology is not applicable for compact systems. Thus, vapor chambers can be designed without any heat sink assembly. Khosroshahi et al. [18] reveals that the local hot spots, which occur on LED substrates, can be removed via embedding heat pipes into light engine substrates. For automotive exterior lighting applications, advanced vapor chamber based board is a possible alternative due to its compact structure and high thermal conductivity.

1.1.2.2 Printed Circuit Board Alternatives as Thermal Solutions

As it is mentioned in previous section, LEDs require advanced thermal management technologies. Vapor chamber board technologies is one of the solution for thermal problems. However, there is not proper technology to mount electronics on vapor chamber based boards directly. Hence, a flex printed circuit board is required to mount components and provide electrical connections of the system. Therefore, flex circuit boards are also open to improvements in order to enhance thermal performance of the overall lighting systems.

Only negligible amount of the heat load transferred by natural convection and infrared radiation from side of the electronics [19]. Thus, to dissipating heat loads from electronics through a conduction path is one of the most effective thermal management techniques for compact electronic devices [20]. In this regard, printed circuit boards (PCBs) with thermally conducting layer provides conduction heat transfer medium that directly contact with high heat flux electronics [21]. In order to enhance thermal performance of the electronic systems, characteristics of PCB can be modified via material selection. There are some requirements that PCB material have to meet. First of all, coefficient of the thermal expansion (CTE) have to be appropriate for placements of electronic components in different forms [22]. Also, PCB material should be highly thermally conductive, robust for deformity, lightweight and reasonably priced [22]. In the industry, due to its low cost and easy manufacturability, FR4 material has been used generally. However, FR4 PCBs have become inadequate since high power electronics have been introduced to the market. Therefore, to improve thermal performance of the high power electronic systems, novel PCB materials have been evaluated in different studies.

Saums et al. analyzed and compared different composite materials as candidate PCB material such as carbon composite copper laminate and copper-graphite composite in terms of CTE matching, thermal conductivity, resistance to deformity, cost

and weight for aerospace applications [22]. Juntunen et al. reported that ceramics such as Al_2O_3, AlN and BeO; metal core printed circuit boards (MCPCB) and insulated metal substrates (IMS) are PCB substrates using for electronic systems and LED modules [23]. While ceramics are suitable for multilayer structures and able to endure difficult conditions, MCPCBs and insulated metal substrates present high thermal conductivity with affordable cost [23]. Dieker et al. reveals that Alumina (Al_2O_3) PCBs shows considerably higher thermal performance than that of FR4 PCB. Due to low thermal conductivity of FR4 PCB, heat can only dissipate through copper plate inside, while on the Al_2O_3 PCB, heat diffuses uniformly across the substrate [19]. FR4, Copper Al_2O_3 and AlN substrates are compared in terms of thermal and optical performances by Kckmann et al. Although AlN performs better than others, due to its considerably high price and brittle structure of AlN, it is not commonly preferred substrate type [20]. In order to enhance the thermal performance of high power LED systems, Weilguni et al. emphasizes providing heat spreading through copper layer in lateral direction and heat conduction through thermal vias in vertical direction [24].

Recent years, LEDs have been used in high lumen output required applications such as general lighting and automotive lighting. Besides, due to compact lighting designs, heat flux densities of LEDs increase. High heat loads led to rise in junction temperatures of LEDs. High junction temperature causes reliability issue, optical output degradation and wavelength shift [21, 23, 24, 25]. Therefore, in order to keep junction temperature under the critical operation temperature (100°C), these different substrate technologies have been also used for LED based lighting systems.

1.1.3 Internet of Things (IOT) for Next Generation Solid State Lighting Systems

Light emitting diodes (LEDs) bring unique advantages to a wide range of lighting applications such as automotive lighting, security lighting and display technologies.

Due to their various color options with high luminous efficacy, LEDs have dominated the lighting industry. Although LEDs are considerably high energy efficient sources compared to conventional old-fashioned systems, still 70-80% of input electrical input power is converted to heat [13, 4]. If released heat cannot be transferred to ambient, it causes elevated junction temperatures of LEDs which lead to optical losses, catastrophic defects and lifetime problems [2, 17]. Therefore, thermal management is a significant concern for sustainability of LED lighting systems. Several thermal management solutions have been studied in the literature. According to the ambient conditions and requirements of problem, passive or active cooling technologies can be used to overcome some of those thermal issues. Internet of things (IOT) have gained tremendous attention during the last decade and more focus on how to utilize IOT in LED systems for the last five years. Though smart sensors and network capabilities are some of those first technologies in smart lighting systems, they will offer tremendous opportunities in upcoming years. However, none of the current LED lighting applications reach the dream of IOT goals yet. Therefore, it would be interesting to see some of those high ends and high functionality features in possible LED systems. As thermal management is still a major challenge in LED systems, more functionality with IOT will pose substantially harder problems for scientists and design engineers. It is important to review some of the current approaches to understand the thermal issues in LEDs, and then attention will be turned to IOT embedded LED systems.

A current automotive rear lighting system is perhaps the closest LED technology in a compact packaging form factor that will IOT features will pose on new systems. A double sided LED light engine houses LEDs at the front side, while densely populated electronics and sensors are used in the backside of the board [18, 25]. A detailed study has been presented by Uras et al [25] on the thermal management issues of an LED automotive lighting system. The system has tight packaging problems, limited lifetime, vibration issues, aggressive power needs. It cannot easily adopt active

cooling technologies, so they have chosen to investigate passive thermal management solutions. As a passive thermal management technique, thermal performance of conventional PCB can be enhanced via high thermally conductive PCB substrates [5]. Due to poor thermal conductivity of conventional FR4 PCBs, LEDs and electronic components cannot diffuse excessive heat. Therefore, local hot spots occur over the PCB and junction temperature gets higher. In this regard, metal core PCB improves thermal performance of the system because of its higher thermal conductivity [6]. However, in compact and dense lighting engines, MCPCBs are not efficient to meet operational requirements of LEDs as well. Thus, a novel heat spreader technology is required.

Tamdogan et al. [26] reports that high power LEDs and electronics require novel thermal management techniques such as micro jet, micro channel and immersion cooling methods. They studied computationally and experimentally thermal characteristics of a high-power LED light engine utilizing various cooling methods with different coolants. Despite of the fact that multiphase liquid cooling performs better, bubble generation around the LED chip leads to significant lumen degradation. However, light engine with single phase liquid cooling showed efficient thermal performance while enhancing light extraction by 15%. Therefore, the study reveals that single-phase immersion liquid cooling is a possible cooling method to enhance the thermal performance of high power LEDs. In another study, Arik et al. [27] presented synthetic jets as novel cooling devices for high power electronics. Synthetic jets are practical for many applications due to their small sizes compared to other forced convection devices.

IoT will bring along many sensors and communication features so electronic component density of the PCBs, possibly light engine, will increase significantly while

power consumption of the present electronic components rises. IOT is an environment that smart devices, sensors and actuators are connected and able to communicate with each other via internet platform [28]. In recent years, IOT has been rapidly evolving, and it is expected that in five years 50 billion smart devices will be connected [29]. Smart devices will be effective in many different areas such as healthcare, energy, lighting, automotive, smart grids and home automation [29, 30]. IoT will also integrate these individual areas. Such as smart buildings will manage energy efficiency of houses, it will also analyze comfort and health of households [30]. Although IoT provide many benefits, it also has some challenges and concerns such as privacy, security, openness [31, 32] and power consumption [33]. As it is mentioned, by 2020 approximately 50 billion smart devices will be connected to each other. Therefore, number of smart sensors, communication devices and electronic components will be considerably higher than today and their power consumption will be higher. Thus, power will be a significant concern for the IoT applications. For IoT devices, mobility is very important so they should operate with batteries [28]. However, present batteries have limited lifetime and energy storage problems. With the enhancing utilities of smart devices, more power requirement will occur. In order to solve high power consumption problem, Ju and Zhang [33] suggest that energy harvesting for low power IoT devices with small size and proper energy storage volume is a need and they propose Internet of Battery-less Things (IoBTs). One of the major goal of the Internet of Things is to enhance the capacity of devices and electronics while reduce their energy consumption. In this regard, besides investigating novel low power technologies, minimizing the power loss of the components is crucial. New devices have been developed with the concept of low power consumption. However, due to small size constraint and high usage of sensors, actuators and electronics, increase in total heat flux of the system constitutes efficient thermal management requirement. As it is mentioned before, even today thermal problems in electronic systems, with

the increasing number of sensors and electronics which provide connectivity of things, heat flux over electronics is expected to increase over 70%. Because of poor thermal conductivity of conventional PCBs, local hot spots which affect the reliability of the system will occur. Thus, novel PCB solutions should be improved.

Lighting systems with over 550 Billion fixtures globally are seen as a great opportunity for a widespread application. Lighting systems are used almost in all living spaces and a large number of outdoor areas. IoT applications will also be active in all of these places so lighting fixtures may constitute a platform. According to Lowe [34], automobiles have a great number of microcontrollers and due to their mobility, they can be defined as ultimate smart mobile device so automobile industry will take a critical role in IoT conversion. Lighting fixtures of automobiles can be enhanced to collect and sense data from the environment due to their present electronic structure and place where they mounted on automobile. Therefore, in this study an automotive rear lighting system is studied. Thermal challenges which are caused by the increase of heat flux from components with IoT will also be faced in automotive lighting systems. Due to size and cost concerns, LEDs and electronics are integrated on the same board. Moreover, all lamp functions, stop, signal and position operate on a single PCB. Therefore, even at the present condition, complex thermal problems occur on the selected LED lighting system. When IoT added over traditional lighting fixtures are considered, hard problem will be harder at the same volume and footprint area.

CHAPTER II

SYSTEM DEFINITION AND EXPERIMENTAL PROCEDURE

2.1 Problem Definition

Four types of lamps are used in automotive rear-lighting for position, stop, signal and fog purposes. These types of LED lamps are placed in separate printed circuit boards. LEDs allows utilizing all those different functions in one single board at the same time. When all LEDs operate at the same time on a single PCB, junction temperatures of LEDs exceed the optimal temperature which is about 100°C [2] increasing the risk of fire and catastrophic failures. Therefore, advanced thermal management technology is necessary for new generation of LED automotive exterior lighting systems. In this study, investigation of conventional and advanced vapor chamber heat spreader based double sided PCB where LEDs and electronics are mounted has been investigated in order to resolve the thermal issues for 3-purpose LED rear lamp.

2.2 System Definition

The proposed advanced heat spreader based LED light engine is an alternative solution for enhancing thermal performance of exterior automotive lighting systems. To analyze thermal and optical performance of the advanced heat spreader substrate, it is compared with FR4 and Al substrates. First of all, advanced heat spreader substrate is manufactured as flat plate vapor chamber with micro-channels. Then, FR4 and Al substrates are prepared to form a baseline for performance analysis of the advanced heat spreader substrate. These three substrates are briefly explained in the following.

2.2.1 LED Board Substrates

Vapor chambers are cooling devices that achieves high thermal conductivity values via phase change heat transfer. Therefore, the advanced heat spreader substrate is designed as flat plate vapor chamber with micro-channels due to its high heat diffusion capability.

FR4 is a commonly used electronic board substrate due to its low cost, high machinability and high CTE matching. Thus, it is used in this study as baseline. FR4 plate is shaped as 66x80x2.75 mm^3 board substrate.

Aluminum have been used in recent years in electronic industry as alternative board material due to its high thermal conductivity. Hence, an Al board substrate is also prepared to analyze performance of the novel board substrate. For the study, an Al plate is formed with the same dimensions as FR4 board substrate.

After all of advanced heat spreader, FR4 and Al substrates are prepared, flex printed circuits boards (PCB) are attached to front and back of the substrates to provide electrical connection. In the study, two types of flex PCBs are used. These flex PCBs are described in the following.

2.2.2 Flex Printed Circuit Boards

In the study, FR4 based and ceramic based flex printed circuit boards are utilized. Firstly, properties of the FR4 flex PCB will be given. Then, characteristics of the ceramic based PCB will be explained. Their thermal and optical performances are analyzed in the following chapters.

2.2.2.1 FR4 Based Flex PCB

FR4 flex PCB compose of two layer that are one trace of copper layer and one glass of fiber epoxy (FR4) sub layer. Thickness of copper and FR4 layers are 40 and 160 microns, respectively. These flex PCBs are attached to front and back of the substrates with highly conductive doubled sided tapes. Thickness and thermal conductivity of

the tape are 100 microns and 0.6 W/m-K, respectively. The microscopic image of the cross section of the PCB is presented in Figure 6.

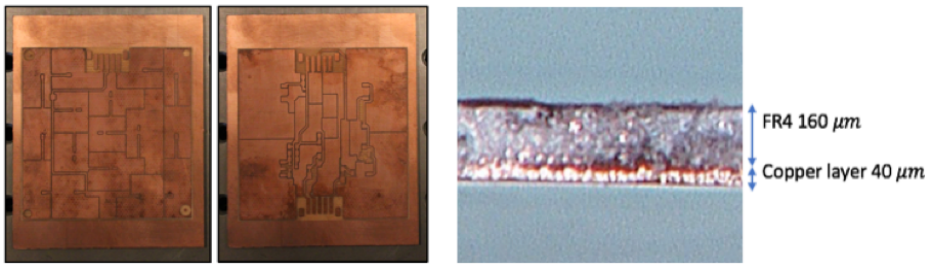

Figure 6: FR4 based flex PCB and micrograph of its cross-section

2.2.2.2 Ceramic Based Flex PCB

PCBs with ceramic structures like Alumina (Al2O3) shows considerably higher thermal performance than that of FR4 PCB. Due to low thermal conductivity of FR4 PCB, heat can only dissipate through copper plate inside, while on the Al_2O_3 PCB, heat diffuses uniformly across the substrate [19]. Therefore, ceramic based flex PCB is investigated in this study as alternative for FR4 flex PCB due to its higher thermal conductivity. Ceramic based flex PCB which comprises of five layers: a copper foils, a white solder mask (paint), a copper foil, a ceramic-polymer blend dielectric layer (Thermal Clad HT 6), second copper foil and an adhesive layer (Bond-Ply) is produced in Bergquist Company. As illustrated in Figure 7, thicknesses of the layers are 50, 70, 152, 70 and 127 microns, respectively. Thermal conductivity of copper foils, ceramic-polymer blend dielectric layer and adhesive layer are 400 W/m-K, 2.2 W/m-K and 0.8 W/m-K, respectively [35], [36].

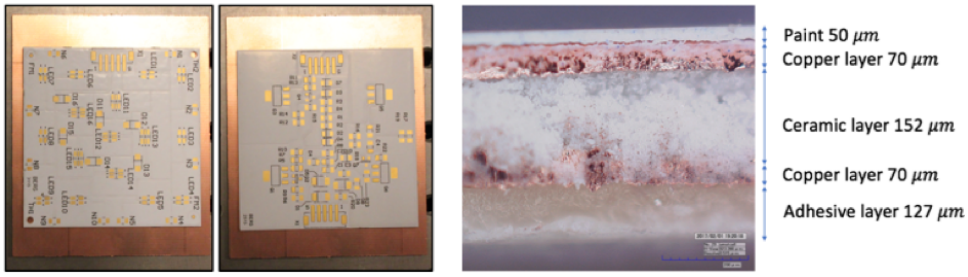

Figure 7: Ceramic based flex PCB and micrograph of its cross-section

While FR4 based flex PCB is attached with double sided tape, manually, possible air gaps between substrate and tape and also between tape and flex board can be occurred. Thus, these air gaps can cause increase in thermal resistance of the system. However, ceramic based boards has its own adhesive so there is no possibility of air gap presence between adhesive and flex board. In this regard, ceramic based flex boards gain an advantage over FR4 based flex boards in terms of thermal resistance.

2.2.3 LEDs and Electronic Components

After flex PCBs were attached to substrates, LEDs and electronic components are mounted to front and back of the flex PCBs, respectively. Types of LEDs and electronic components will be describe in following subsections.

2.2.3.1 LEDs

16 LEDs are assembled front of the PCBs. While ten of them are identical OSRAM LR E6SF red LEDs, the other six of them are identical OSRAM LA G6SP amber LEDs. While the red LED packages are in charge of stop and position functions of automotive rear lighting system, the amber LED packages are in charge of signal function. Power conditions of LEDs are demonstrated in Table 1.

Table 1: Specifications of LEDs.

Component	*Package*	*Color*	*Power(mW)*
LED 1-10	TOPLED OSRAM LR E6SF	RED	110
LED 11-16	TOPLED OSRAM LR G6SP	AMBER	305

Package of the LR E6SF red LEDs is white PLCC-4 package and made of silicon resin. InGaAlP thinfilm which is suitable for red, yellow and amber lighting applications due to its emission in that wavelength range (from 560nm to 630nm) is used as die technology [11] [14] [37] [38]. Package geometry of LR E6SF LED is presented in Figure 8. Micrograph of the LED die can be seen in Figure 9. According to microscopic measurement, dimensions of the die is 300 microns to 300 microns.

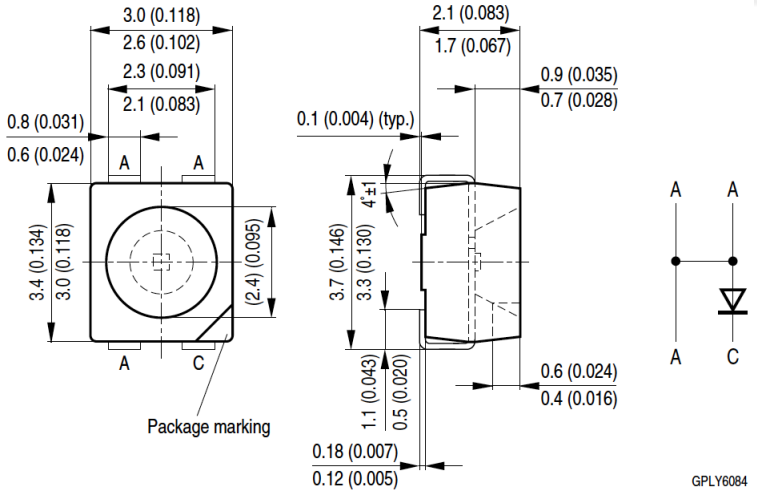

Figure 8: Package geometry of LR E6SF LED [37]

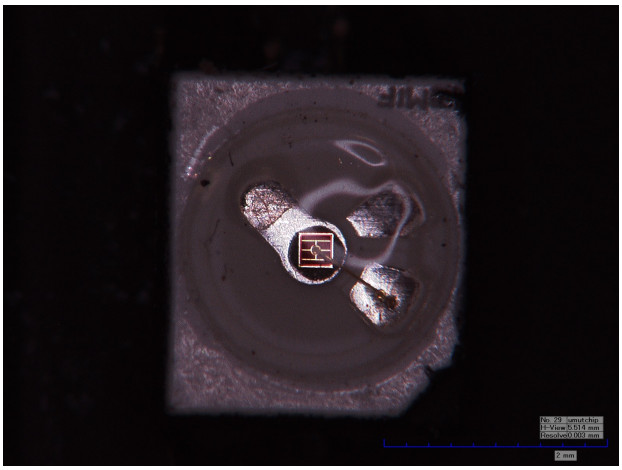

Figure 9: Microscopic image of the LR E6SF LED die

Package of LA G6SP amber LED is white PLCC-6 package and made of colorless clear resin. InGaAlP die is used in LED package [37] [38]. Package geometry of the LA G6SP LED is presented in Figure 10. Dimensions of the LED die is measured as 500 microns to 500 microns via digital microscope.

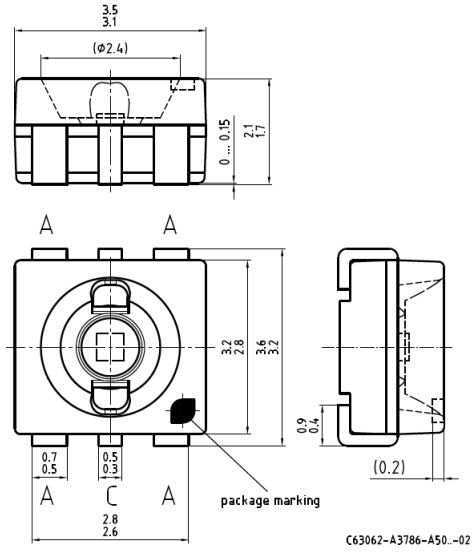

Figure 10: Package geometry of LA G6SP LED [38]

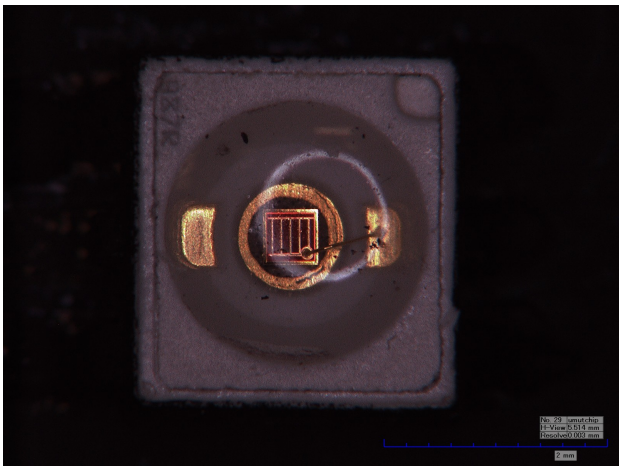

Figure 11: Microscopic image of the LA G6SP LED die

2.2.3.2 Electronics

Multiple electronic components are attached to back of the LED light engines in order to regulate and direct the current flow. In total, 23 resistors, 7 transistors, 4 capacitors and 10 diodes are utilized. Most of the electronic components are SMD (surface mount device) type components. Specifications of the components are presented in Table 2.

Table 2: Specifications of electronic components.

Component	*Package*	*Power(mW)*
R1, R2, R3, R4	1206	45
R5, R7, R11	1206	16
R6, R12	1206	13
R8, R20	1206	25
R9, R10, R14, R15	1206	3
R16, R18	1206	50
R17, R19	1206	224
R21	1206	40
R23	1206	1.8
D2, D3	SOD123F	4.3
D1, D5, D9	DO-214AA	0
D4, D6, D7, D8, D10	SOD123F	0
Q1, Q3	SOT-223	480
Q5	SOT-223	442
Q6	SOT-223	530
Q2, Q4	SOT-23	4.5
Q7	SOT-23	7.2
C1, C2, C3,C4	1206	0

Final version of one of the LED light engine is demonstrated in Figure 12. Figure 12 a presents LEDs' side of the light engine and Figure 12 b shows electronics' side of the light engine.

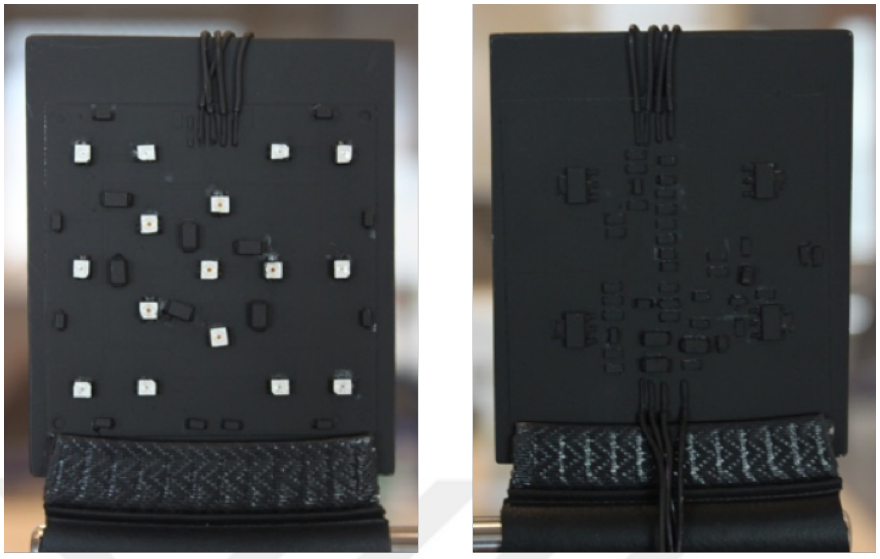

Figure 12: Final version of one of the LED light engine: (a) LEDs' side, (b) electronics' side

Configurations of the LEDs and electronic components on the light engine can be seen from the Figure 13.

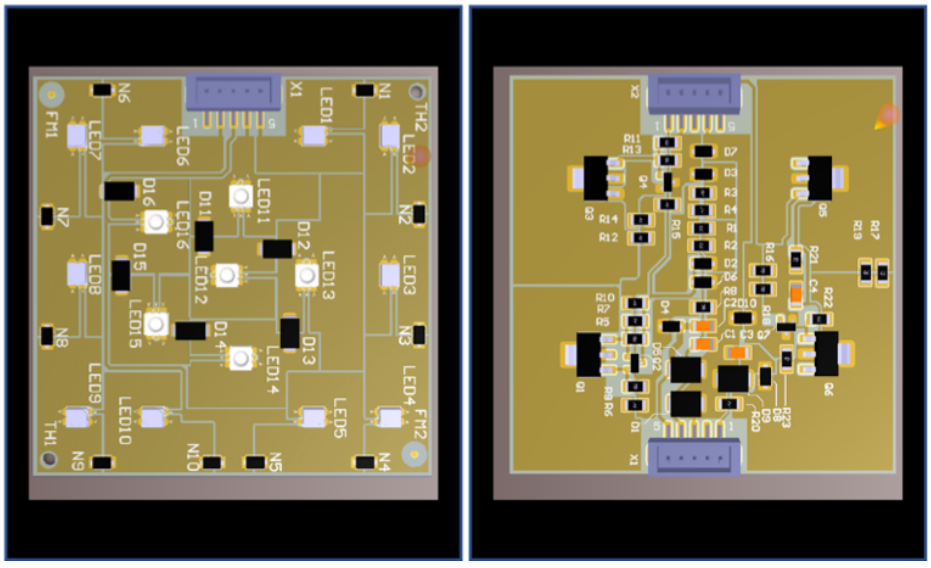

Figure 13: Configurations of the LEDs and electronic components on the light engine

2.3 Experimental Methods

As it mentioned in the problem definition section, there are four type of lamp functions in automotive rear-lighting which are position, stop, signal and fog functions. In this study, the LED light engines are operated for these three functions. In addition, the LED light engines are also operated while all kind of lamps are working simultaneously. Therefore, experiments are conducted on four cases; case 1 - position function, case 2 - stop function, case 3 - signal function, and case 4 - multi function.

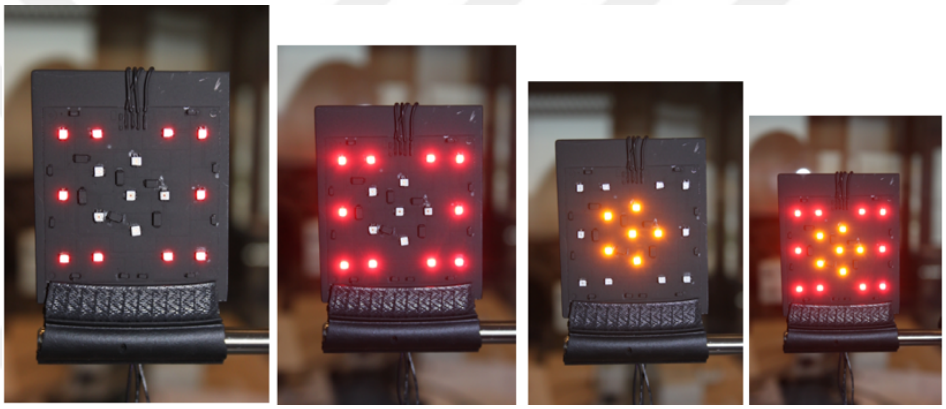

Figure 14: Case 1- Position function, Case 2- Stop function,Case 3- Signal function and Case 4- Multi-function, respectively

Case 1 represents the condition when occurs only position headlamps turned on in automobiles. In this case, only 10 red LEDs which are placed side of the board are operated with 10 mW per LED.

Case 2 represents the condition when happens only stop headlamps are turned on in automobiles. In this case, again same 10 red LEDs are operated but the input power per LED increase to 100 mW.

In Case 3, power conditions of LEDs and electronics are same as power conditions when occurs only signal headlamps of automobile are operated. In this case, 6 amber LEDs which are placed on the middle of the board are supplied with 305 mW power

per LED.

In some situations; stop, signal and position headlamps operates simultaneously. In Case 4, all LEDs on the test vehicle are turned on at the same time in order to enable this real situation in the test environment. 6 red LEDs which used in the Case 3 are operated with 305 mW per LED and the other 10 red LEDs are worked with 110mW per LED that was summation of power amount used in case 1 and case 2.

Table 3: Corresponding driving power conditions for each LED and the LED light engine

Case	*Function*	*Numberof LEDs*	*Power/LED (mW)*	*Total Power/LED Light Engine(mW)*	*LED Light Engine*
Case 1	Position	10 Red LEDs	10	288	FR4 Aluminum Adv. Heat Spreader
Case 2	Stop	10 Red LEDs	100	2424	FR4 Aluminum Adv. Heat Spreader
Case 3	Signal	6 Amber LEDs	305	3433	FR4 Aluminum Adv. Heat Spreader
Case 4	Multi	10 Red + 6 Amber LEDs	305 + 110	5953	FR4 Aluminum Adv. Heat Spreader

Cases are repeated for Al based, FR4 based and vapor chamber based boards. Power conditions of each case is demonstrated in Table 1. Picture of each experimental case are presented in the Figure 2. In the study, to analyze thermal performance

of LEDs, firstly, thermal experiments are conducted for each LED light engines. Secondly, optical experiments are conducted for each LED light engines. For each LED engine, thermal and optical experiments are conducted in these four experimental cases.

2.3.1 Thermal Experiments

Thermal experiments are conducted to analyze thermal distribution over the LED light engines and also estimate junction temperatures of LEDs during different experimental cases. To obtain thermal distribution across an object surface, infrared thermography is commonly used method [39] [40]. Therefore, in this study, IR thermography method is used for thermal experiments. Firstly, infrared thermography will be briefly introduced and then, experimental procedure for thermal experiments will be defined.

2.3.1.1 Infrared Thermography

IR systems have been firstly used by Swedish Defense Department in 1950s. Working principle of the first IR system is based on transfer incoming heat radiation to IR sensor via multiple mirrors and optics. Detector type of the first IR system was thermistor bolometer which is very similar to today's technology [41].

IR systems works based on heat transfer mechanism of infrared radiation. The infrared spectral band range is between 0.75 and 1000 microns [41]. If the temperature of an object is greater than the absolute zero, it emits electromagnetic radiation. Thus, electromagnetic radiation emitted by an object is related to its surface temperature [41]. According to Stefan-Boltzmann Law, upper limit of the emitted radiation from a object is

$$W = \sigma T^4 (W/m^2) \tag{10}$$

where W is the total radiated energy, σ is the Boltzmann constant and T is the surface temperature of the object [41][42][43]. However, this law is applicable for

blackbodies whose emissivity is equal to 1. For the other bodies whose emissivity, which is the ability of a surface to emit energy, is different than 1, Stefan-Boltzmann Law is formed as

$$W = \epsilon\sigma T^4 (W/m^2) \tag{11}$$

where W is the total radiated energy, ϵ is the emissivity, σ is the Boltzmann constant and T is the surface temperature of the object [41][42][43]. Therefore, emissivity of the object surface is very significant property for the IR thermography.

Most important part of the IR thermographic devices is the detector which absorbs the infrared radiation emitted by an object and transform it into a signal [41]. These transformed signals can be converted into temperature map [41]. There are two types of detector type which are thermal and quantum detectors. Quantum detectors that are made of InSb, InGaAs, GaAs etc. are more faster and sensitive than thermal detectors. In quantum detectors, electrons changes their states in a crystal structure responding to incident photon [41].

In IR thermography measurements, there are three different radiation energy sources coming to camera lens. These are radiation from the object surface, radiation from the surroundings of the object caused by reflection from the object surface and radiation absorbed by the atmosphere [43]. In this regard, formula to calculate total radiation coming to camera lens becomes as

$$W_{total} = \epsilon\tau W_{object} + (1-\epsilon)\tau W_{ambient} + (1-\tau) W_{atmosphere} \tag{12}$$

where τ is the transmission through the atmosphere.

2.3.1.2 Experimental Procedure

As it is mentioned before, there are two sets of LED light engines and each set has 3 different LED light engines. In the first set of LED engines, there are 3 LED light engines with FR4, Al and advanced heat spreader substrates. These LED light engines have FR4 flex PCBs. In the second set of LED light engines, there are also

3 LED light engines with FR4, Al and advanced heat spreader substrates but the difference from the first set is that they have ceramic flex PCBs. Therefore, thermal experiments conducted in two stage: first one for the first set of LED engines (which has FR4 flex PCBs) and second one for the second set of LED engines (which has ceramic flex PCBs).

Firstly, FR4 based LED light engine with FR4 flex PCB is connected to a holder with a low thermal conductivity. The corresponding DC input power is supplied according to our design of experiments (DOE) plan. LEDs continue to operate until board temperature reaches the steady state meaning that there is no temperature fluctuation over + 0.1 on the board in 5 minutes. Surface temperatures are obtained by microscopic IR thermal imaging technique. As mentioned earlier, boards are painted with a black paint whose emissivity is about 0.97. Therefore, a calibration study has been done similar to earlier studies [39]. Thermal images of the board are obtained in order to investigate the thermal distribution and hotspots across the board. Ambient temperature inside the test chamber is recorded with T-type thermocouples. Later, the same procedure is applied to back of the FR4 based LED light engine. An experimental system has been designed and manufactured for the current study. The setup is presented in Figure 15.

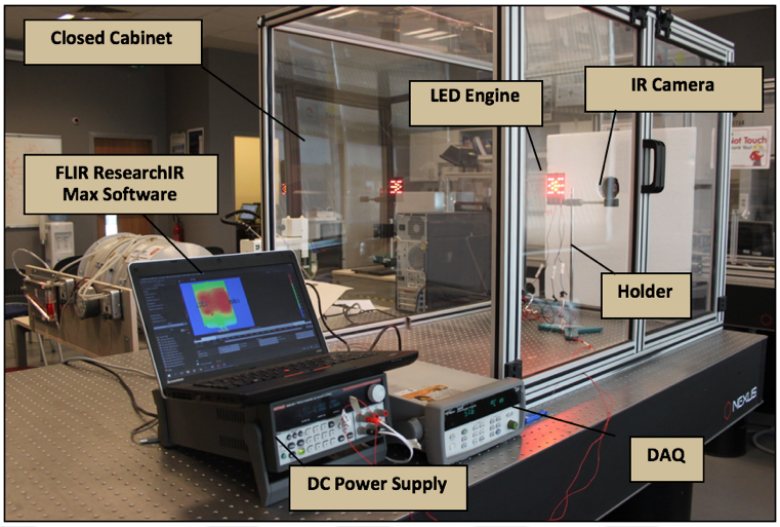

Figure 15: Thermal experimental setup

A Keithley 2230-30-1 Multi Channel DC power supply is used during the experiments. While voltage setting and voltage readback accuracy are 0.03%, basic current setting and readback accuracy is %0.1 [44]. A FLIR SC5000 IR camera with a wavelength range of 2.5 to 5.1 μm is used to measure surface temperatures of the LEDs. It can capture images with high sensitivity up to 20 mK. According to manufacturers specification, under 150°C, accuracy of the camera is $\pm$1% [45]. An Agilent 34972A LXI data acquisition with Omega T-type thermocouples are used in order to record temperature readings. Thermocouple probe accuracy is $\pm$1.0 while probe vendor accuracy is 0.4% [46]. Experiments are conducted for four different cases as given in Table 3. Each experimental case are shown in Figure 14. Power conditions for each case are mentioned in Table 3.

Experiments are also conducted to the Al and advanced heat spreader boards in the first set of LED light engines as well as second set of LED light engines.

2.3.2 Optical Experiments

In the study, optical experiments are conducted to understand effect of the thermal performance on the optical performance of LEDs. To evaluate optical performance of the LEDs, their radiometric and photometric properties are obtained via integrating sphere method. In this section, first of all, integrating sphere method will be briefly explained and then optical experimental procedure will be introduced.

2.3.2.1 Integrating Sphere Method

Integrating sphere method is most commonly used method to measure photometric and radiometric quantities of a light source [11][10]. Integrating spheres are spheres whose diameter is varies from couple of centimeters to couple of meters according to dimensions of the target light source. Integrating sphere should be coated with highly reflective material (¿98%). Working principle of the integrating sphere is that light rays coming from the source is reflected inside the sphere and collected in a detector [11][10]. The detector should not directly receive light rays so a baffle which prevents the direct light arrays is used in front of the detector as it is presented in Figure 17. Shadow that created by the baffle should be cover the collector. Therefore, during the measurement, place of the light source should be arranged accordingly [10].

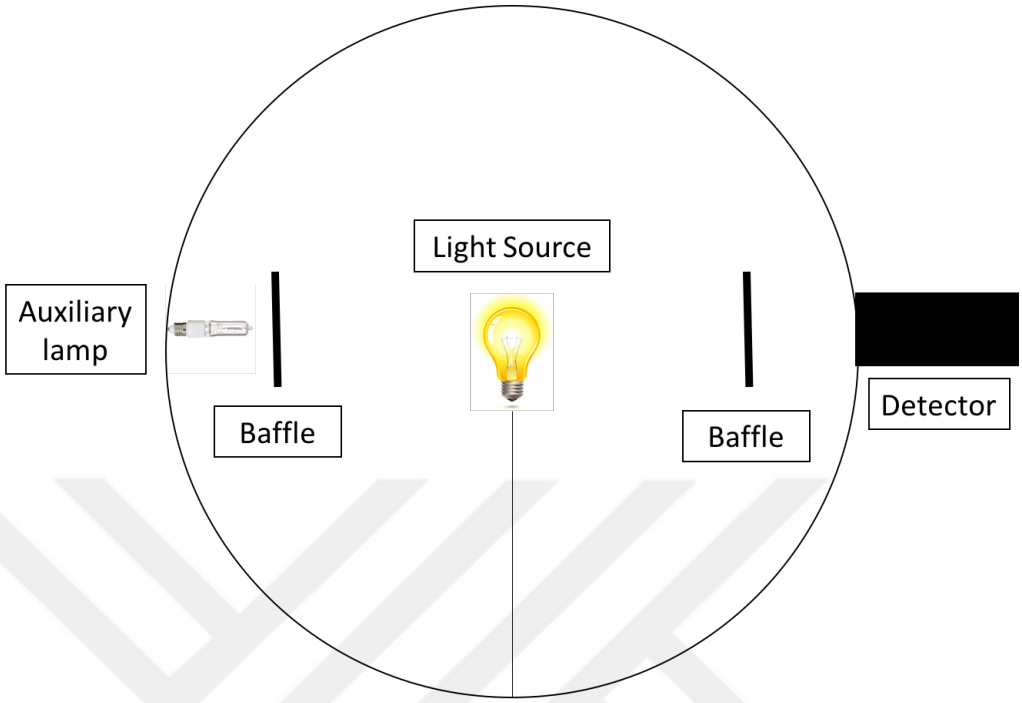

Figure 16: Schematic representation of the integrating sphere

In addition, surface of the light sources are not highly reflective so they can absorb some light and decrease accuracy of the measurement. Thus, an auxiliary lamp whose luminous flux is known is utilized for absorption correction [10].

As a detector, spectroradiometers are commonly used for integrating sphere systems. Spectroradiometers partitions the light by wavelength and calculate the amount of the light at every wavelength. As a result of this calculation, spectral distribution of the light source can be determined. According to the spectral distribution, CRI, CCT and chromacity diagrams can be obtained [10].

In the optical measurements, dimensions of the integrating sphere is also important for accurate measurements. One of the most significant criteria for dimensions of the sphere is that diameter of the light source should be four times smaller than the diameter of the sphere [10].

Consequently, with the integrating sphere system, radiometric quantities such

as radiant flux and photometric quantities such as luminous flux can be measured accurately.

2.3.2.2 Optical Experimental Procedure

In order to investigate the effect of elevated junction temperatures of LEDs on the optical performance [2][6], a set of optical experiments is conducted. An integrated sphere is utilized to measure radiometric and photometric quantities of each LED substrate such as luminous flux and radiant flux.

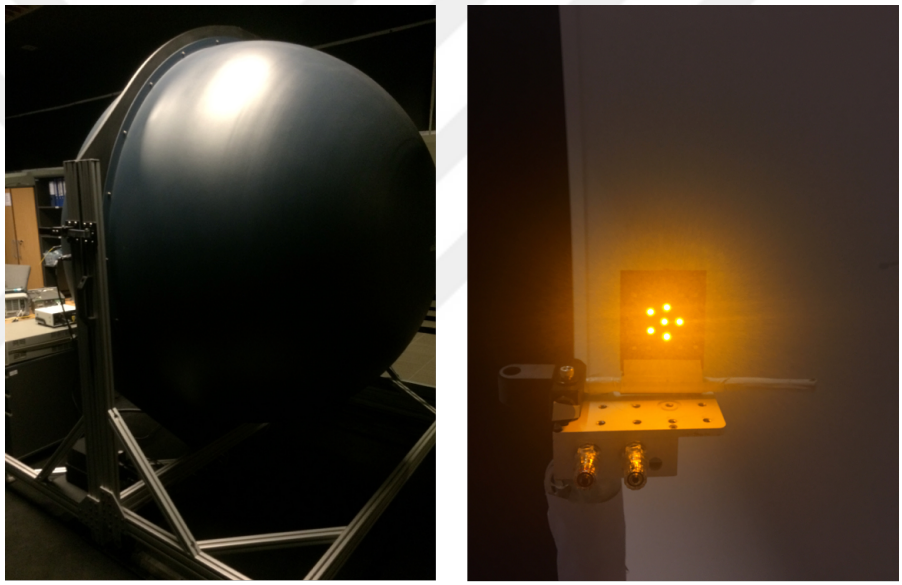

Figure 17: Optical experimental setup: (a) integrating sphere (b) LED light engine inside the sphere

Firstly, FR4 substrate is placed at the center of the sphere and placed by low conductive holder. Position of the substrate is arranged carefully. Spectrometer is left under the shadow of the buffer in order to block direct light rays. Then, electrical connections of the substrate are prepared. First calibration of the sphere with

auxiliary lamp is completed. Agilent power supply is used to drive LEDs. A computer with the LightMtrx software controls the system. A thermocouple is attached to the point on the LED light engine to determine that system comes to steady state or not. Luminous flux value is also checked for steady state decision. Steady state measurements have been performed. Then, radiometric and photometric values such as radiant power, optical spectrum and luminous flux are recorded for each substrate and each case which is demonstrated in 3.

2.3.3 Uncertainty Analysis for Thermal and Optical Experiments

During the thermal experiments, a Keithley 2230-30-1 Multi Channel DC power supply is used. While voltage setting and voltage readback accuracy are 0.03%, basic current setting and readback accuracy is %0.1 [44]. A FLIR SC5000 IR camera which is used to capture images has high sensitivity up to 20 mK. According to manufacturers specification, under 150°C, accuracy of the camera is ±1% [45]. An Agilent 34972A LXI data acquisition with Omega T-type thermocouples are used in order to record temperature readings. Thermocouple probe accuracy is ±1.0 while probe vendor accuracy is 0.4% [46]. Each thermal experiment are conducted twice and maximum standard deviation of the experiments is 0.21. Mean temperatures are used in the study. In addition, optical experiments are conducted twice, maximum calculated standard deviation of radiant flux, luminous flux and peak wavelength are 0.01, 0.92 and 0.07, respectively.

CHAPTER III

THERMAL PERFORMANCE INVESTIGATION OF LED BOARDS

Junction temperature of the LED chips depends on several physical properties of PCB [5], ambient conditions, and heat generation. Thus, understanding of the junction temperature is critical. The LED junction temperature is directly proportional to LED surface temperature, which can be recorded by infrared thermography technique. Dependency between junction and surface temperatures can be understood in detail [9].

$$T_j = T_s + R_{js}P \tag{13}$$

where T_j and T_s are surface and junction temperatures of LED, respectively, R_{js} is thermal resistance between junction point and LED surface and P is the input power of the LED. When surface temperature of an LED exceeds critical operating temperature (< 100), it can be inferred that junction temperature of that LED also exceeds the critical temperature. Therefore, in this study, surface temperatures of LEDs are determined by means of IR images.

3.1 Thermal Analysis for First Set of LED Light Engines

Firstly, IR imaging of conventional FR4 based PCB is recorded for four distinct cases mentioned in the experimental procedure. The Case-1 is the one in which LEDs are driven with minimum input power and moving to Case-4 input power is increasing from 288 mW to 5953 mW. As the input power increased, maximum temperatures on test vehicles also elevated. At the LEDs side of the FR4 based LED light engine,

maximum temperatures observed in each case are 34°C, 61.2°C, 92.8°C and 105°C, while temperature gradients over the board in each case are 5.3°C, 28.0°C, 56.3°C and 62.8°C, respectively. Temperature gradient is the difference between maximum surface temperature and minimum surface temperature occurred in front of the light engine. Additionally, at the back side of the FR4 based LED light engine, maximum temperatures are 41.0°C, 72.9°C, 90.4°C and 95.9°C, respectively, in each case while temperature gradients over back side of the light engine are calculated as 10.8°C, 44.4°C, 50.4°C and 53.7°C. In the first two experimental cases (Case-1 and Case-2), heat dissipation from electronics is found to be dominant due to lower power input of LEDs. Higher temperatures are observed on the electronics as it is shown in Figure 18 and 19.

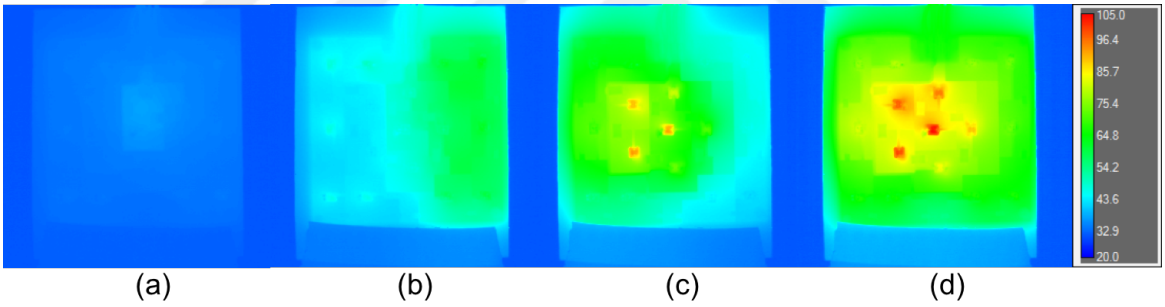

Figure 18: IR thermal images of LEDs' sides of the FR4 based light engine at (a) Case-1, (b) Case-2, (c) Case-3 and (d) Case-4

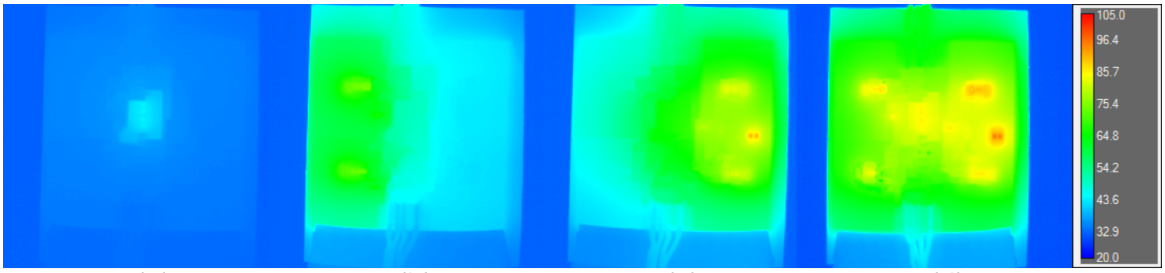

Figure 19: IR thermal images of electronics' sides of the FR4 based light engine at (a) Case-1, (b) Case-2, (c) Case-3 and (d) Case-4

Moreover, in Figure 18a and Figure 18b, heat flux densities from electronic components can be seen at LEDs side as well. Due to low thermal conductivity of FR4 substrate, a uniform temperature distribution is not observed in any experimental case; therefore, local hot spots occur in all the cases. In addition, the temperature gradient rises significantly with the increase of input power. Especially, maximum temperature experienced in Case-4 is close to critical junction temperature for LEDs (100°C) [2].

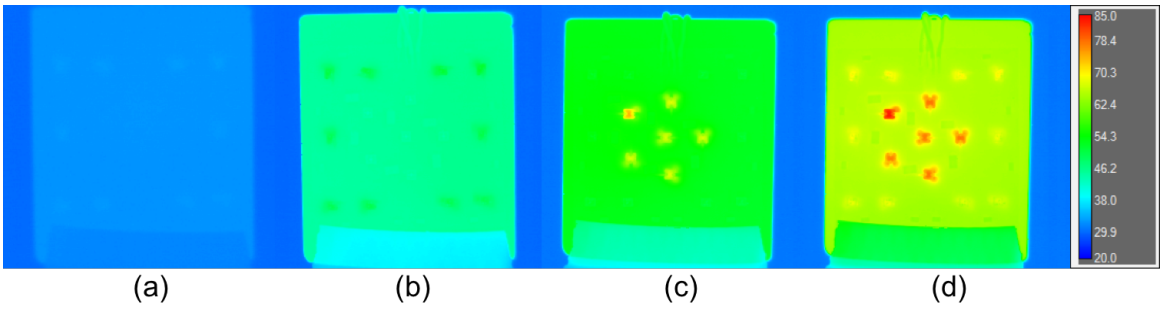

Figure 20: IR thermal images of LEDs' sides of the Al based light engine at (a) Case-1, (b) Case-2, (c) Case-3 and (d) Case-4

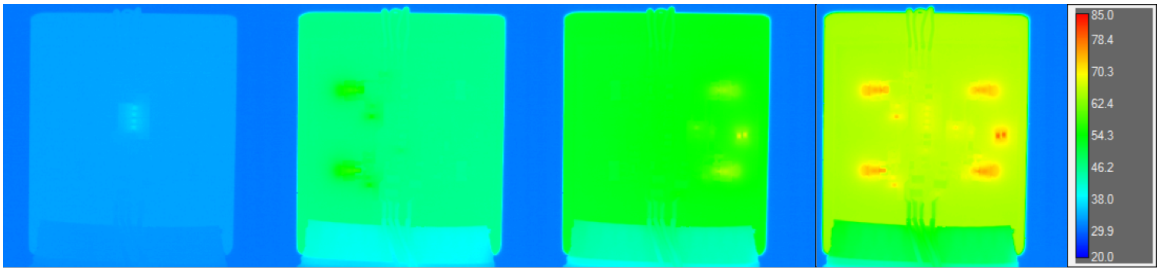

Figure 21: IR thermal images of electronics' sides of the Al based light engine at (a) Case-1, (b) Case-2, (c) Case-3 and (d) Case-4

As a second solution approach of using Al based board, experiments are conducted on Al board in order to observe its thermal performance under four different operating configurations. Due to the highest power supplied while the fourth experimental case is conducted, maximum temperature is observed as 84.1°C. According to Figure 22, at the LEDs (front) side of the board, maximum temperatures of each case are equal to 30.3°C, 49.9°C, 74.0°C and 84.1°C, respectively. In each case, temperature gradients over the electronics side of Al based board are obtained as 4.1°C, 13.1°C 17.4°C and 16.4°C, respectively. Due to the higher conductivity of Al substrate, the difference in temperature gradient between experimental cases is not high as much as the difference observed in FR4 board. Besides, uniform temperature distribution over board is observed during all experimental cases. Heat flux densities can be seen only on LEDs and electronic components.

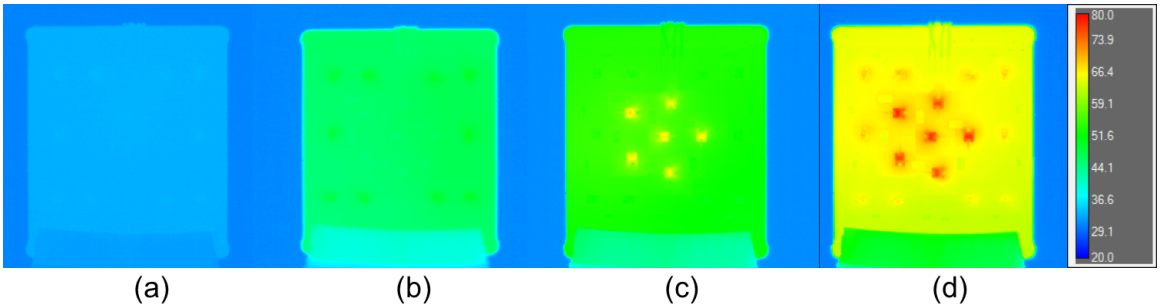

Figure 22: IR thermal images of LEDs' sides of the advanced heat spreader based light engine at (a) Case-1, (b) Case-2, (c) Case-3 and (d) Case-4

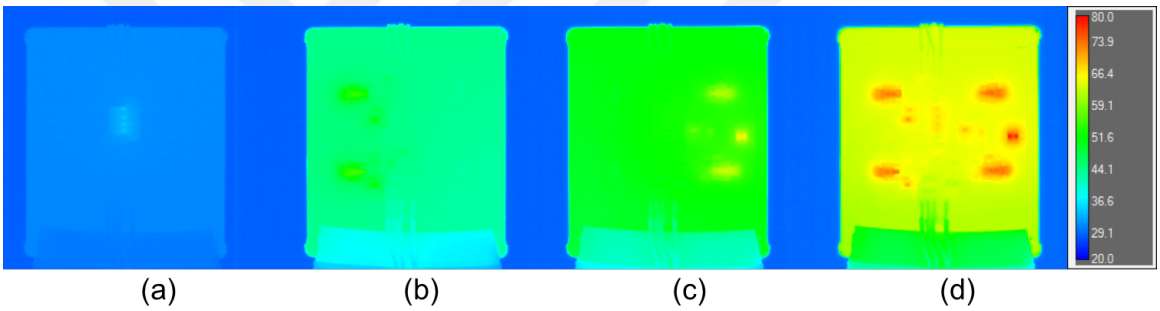

Figure 23: IR thermal images of electronics' sides of the advanced heat spreader based light engine at (a) Case-1, (b) Case-2, (c) Case-3 and (d) Case-4

Experimental investigation is continued with vapor chamber based advanced heat spreader board technology. Maximum temperatures at the LEDs side and the back side of advanced heat spreader board are experienced as 77.9°C and 79.4°C, respectively. When the vapor chamber based board is analyzed from Figure 22 and 23, maximum temperatures of each case are under the limits of junction temperature. Therefore, vapor chamber based board technology may be proposed as a novel technology for automotive exterior lighting.

All LEDs operated simultaneously (Case-4) is considered to be critical where the maximum input power. Therefore, maximum junction temperature is observed.

Fourth experimental case results are compared in Figure 25 and 26. From thermal images, it can be inferred that advanced heat spreader board shows the best performance among all three boards. While maximum LED surface temperatures of FR4 and Al based boards are recorded as 105°C and 84.1°C, respectively, maximum temperature of LED surfaces is 77.9°C at advanced heat spreader board.

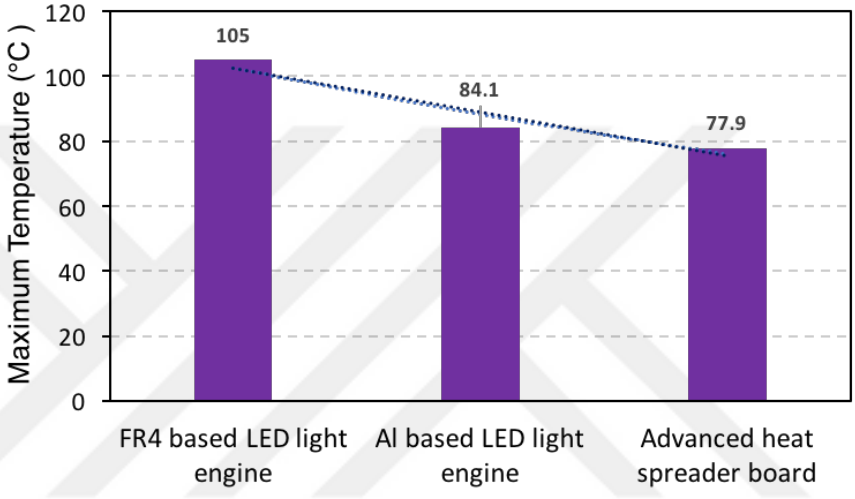

Figure 24: Comparison of LED light engines' maximum temperatures at the LEDs side of boards

In Figure 24, peak temperatures on the LED boards are presented. Maximum temperature that is observed on FR4 based board 105°C even at the room temperature. Although it is under a tolerable value (< 100°C), the ambient temperature in the automotive lighting system (> 45°C) can exceed the room temperature resulted in an increase of junction temperature of LEDs. Therefore, FR4 substrate is not sufficient for vehicles exterior lighting system.

According to Fourier law of conduction, one dimensional heat conduction is written as;

$$Q_{cond} = -kA\frac{dT}{dx} \tag{14}$$

where A is cross sectional area that heat is transferred, k is thermal conductivity

and T is temperature, x is the thickness and Q_{cond} is the rate of conduction heat transfer. Thermal resistance can be inferred from this formula as;

$$R = \frac{\Delta T}{Q_{cond}} = \frac{\Delta x}{kA} \tag{15}$$

Therefore, thermal resistance depends on thickness, thermal conductivity and cross sectional area of the material. In the current study, all board substrates have the same cross sectional area and thickness, therefore, difference in thermal resistance of different boards only depends on thermal conductivity of substrates. Copper-clad FR4 substrate has the lowest thermal conductivity which is about 1 W/m-K while vapor chamber substrate has the highest with thermal conductivity around 4000 W/m-K. In addition, thermal conductivity of the metal substrate is 167 W/m-K.

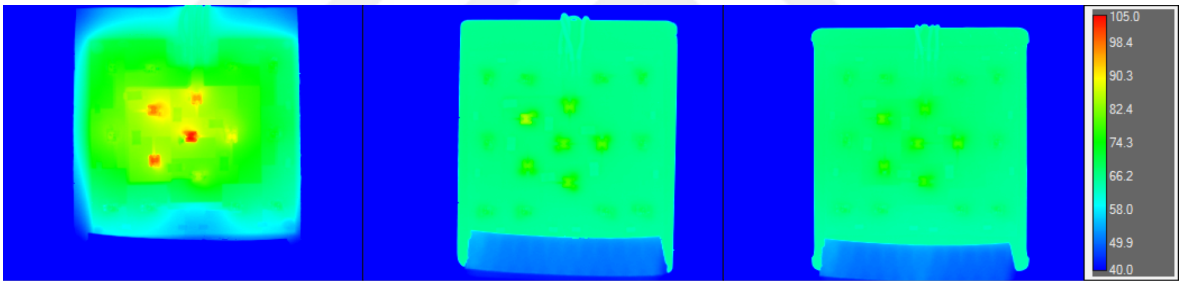

Figure 25: During Case-4, IR thermal images of LEDs' sides of based light engine at (a) FR4, (b) Al and (c) the advanced heat spreader based LED light engine

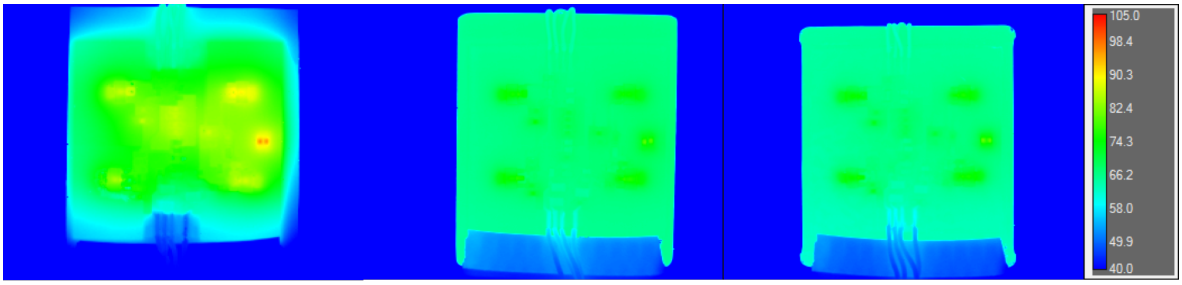

Figure 26: During Case-4, IR thermal images of electronics' sides of based light engine at (a) FR4, (b) Al and (c) the advanced heat spreader based LED light engine

Due to high thermal resistance of FR4 substrate, LEDs reach the maximum temperature leading to non-uniform temperature distribution with local hot spots [6]. However, Al and vapor chamber substrates tend to multi-dimensional heat transfer so heat can diffuse uniformly on these boards [6]. Thus, a higher temperature gradient is observed on FR4 based board. Moreover, temperature gradient at FR4 board increases rapidly than others due to high thermal spreading resistance of FR4 substrate. As presented in Figure 25 and 26, the uniform temperature distribution is observed over the vapor chamber based board while FR4 based board has a larger non-uniform thermal pattern.

3.2 Thermal Analysis for Second Set of LED Light Engines

Thermal performance of the first set of LED light engines which are made of FR4 flex PCB is open for improvement. Thermal resistance of the FR4 flex PCB forms significant amount of the total thermal resistance due to low thermal conductivity of the FR4 material. Therefore, in order to improve thermal performance of the LED engine, increase the thermal conductivity of the flex PCB is a reasonable solution for this case. Thus, second type of flex PCB (ceramic based flex PCB) which comprise of a copper foils, a white solder mask, a ceramic-polymer blend dielectric layer (Thermal

Clad HT 6), second copper foil and an adhesive layer (Bond-Ply) is produced in Bergquist Company. Because of ceramic and copper layers, thermal resistance of the ceramic based PCB is lower than the FR4 based PCB. Therefore, more uniform temperature distribution is observed over the LED light engines during the IR thermal experiments.

As first set of LED light engines are tested for different cases experimentally, the second set of LED engines are also tested for same experimental cases. Besides, as first set of LED light engines are consist of three LED light engines which are FR4, Al and advanced heat spreader based LED light engine, in second set of LED light engines are consist of identical three LED light engines.

Firstly, thermal experiments have been started with FR4 based LED engine with ceramic flex PCB at experimental case-1. Due to low power levels of Case-1, LED surface temperature increases by just 5°C while room temperature is 25 ± 0.5° C. There is also no significant temperature increase on surface temperature of electronics. Maximum temperature increase on electronics is 7°C at Case-1. At Case-2, maximum LED temperature reaches to 48.9°C and maximum electronic temperature reaches to 51.1°C. While minimum temperature observed over the board's LED side is 39.5°C, minimum temperature observed over the board's electronics side is 38.9°C. During the Case-2, uniform temperature distribution is observed over the both sides of the board. During the experimental Case-3, while amber LEDs are driven with 305 mW per LED, maximum LED temperature and electronic temperature are experienced as 67.4°C and 65.2°C, respectively. Maximum temperature difference over the LEDs' side and electronics' side of the LED light engine are 22°C and 20.1°C, respectively. In this case, amber LEDs and some of the electronic components form hot spots on the board as presented in Figure 27 c and Figure 28 c. In the last experimental case, all type of LEDs and electronic components operates simultaneously with the total power of 6143.2 mW. Due to high heat flux from the LEDs and components,

hot spots become more critical than hot spots formed in Case-3. Maximum LED surface temperature that is observed over the light engine is 76.9°C while minimum temperature that is observed over the LEDs' side of the light engine is 55.4°C. On the other side of the board, maximum surface temperature of the electronic components is 74.8°C while minimum temperature that is observed over this side of the board is 54.5°C. Although there are hot spots over the some of LEDs and electronic components, heat is spreading uniformly over the board especially in first three experimental cases. Temperature increase on the LED light engine while input power increasing in experimental cases 1 to 4 can bee seen from the Figure 27.

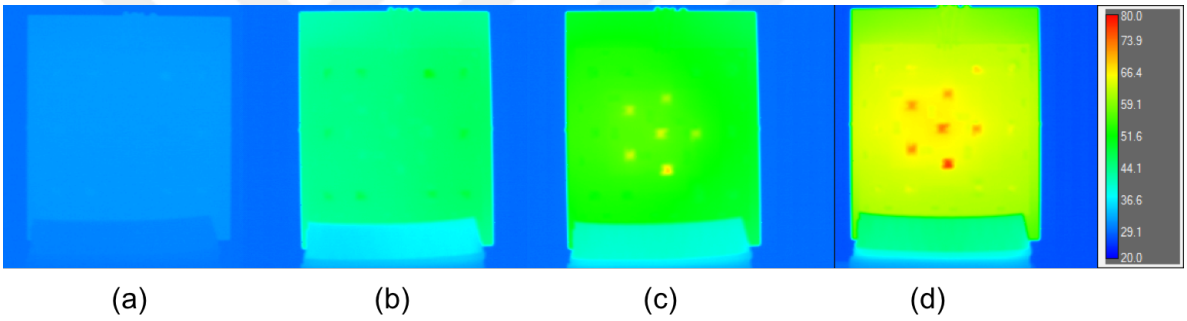

Figure 27: IR thermal images of LEDs' sides of the FR4 based light engine with ceramic flex PCB at (a) Case-1, (b) Case-2, (c) Case-3 and (d) Case-4

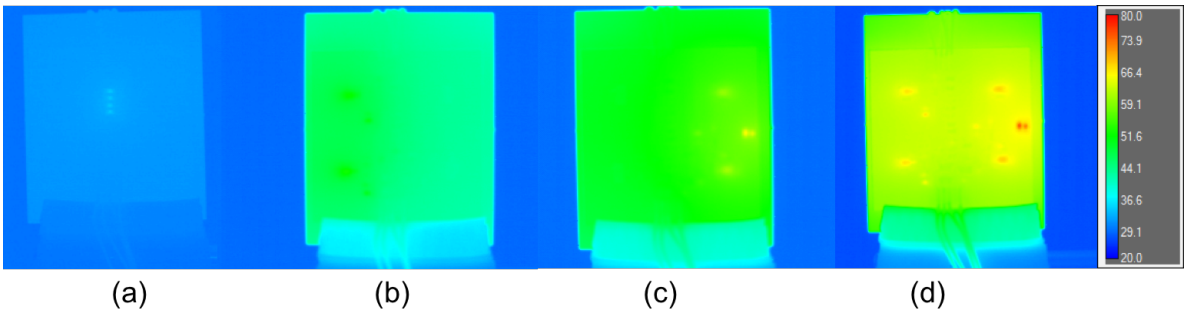

Figure 28: IR thermal images of electronics' sides of the FR4 based light engine with ceramic flex PCB at (a) Case-1, (b) Case-2, (c) Case-3 and (d) Case-4

Secondly, Al based LED light engine with ceramic flex PCB is tested under four experimental cases. In the Case-1, because of low input power, maximum temperature increase of the LEDs and electronics are just 2.7°C and 4.8°C, respectively while ambient temperature is 25 ± 0.5°C. During the Case-1, R1, R2, R3, R4, D1, D2, D3, D6 and C1 are working among the electronics. By reason of the fact that only R1, R2, R3 and R4 consume considerable amount of power compared to other electronics and produce heat, hot spots occur on these resistors which is presented in Figure 30a. In the second case, again 10 red LEDs are operated with 110 mW per LED for representing stop function of the lighting system. Due to power increase compared to first case, maximum LED temperatures also increase to 45.9°C. In addition, maximum temperature of the electronics increased to 47.9°C. While temperature difference that is experienced over the LEDs' side of the light engine is 6.3°C, temperature difference that is experienced over the electronics' side of the light engine is 8.4°C. At the Case-3, only signal LEDs are working with 305 mW per LED for signal function. In Figure 29 c, hot spots which are caused by heat flux from the signal LEDs can be seen. At the other side of the light engine, resistors R17 and R19 consumes 224 mW power per resistor which is the highest consumption amount among the all electronics. Therefore, hot spots occur on these resistors. Maximum LED temperature and electronic temperature reach to 59.1°C and 63.0°C during Case-3. Minimum board temperature on the LEDs' side and electronics' of the light engine is both 45.7°C. At the forth case, as it is presented in the Figure 29d and Figure 30d, several hot spots forms on the LEDs and electronics due to high power consumption because of the fact that all LEDs and electronics are operated. During the Case-4, maximum LED and electronic temperature are experienced as 71.1°C and 74.1°C, respectively which are under the critical junction temperature of LEDs and electronics [2]. Maximum temperature difference over the LEDs' side of the Al light engine is 14.7°C and 17.7°C, respectively.

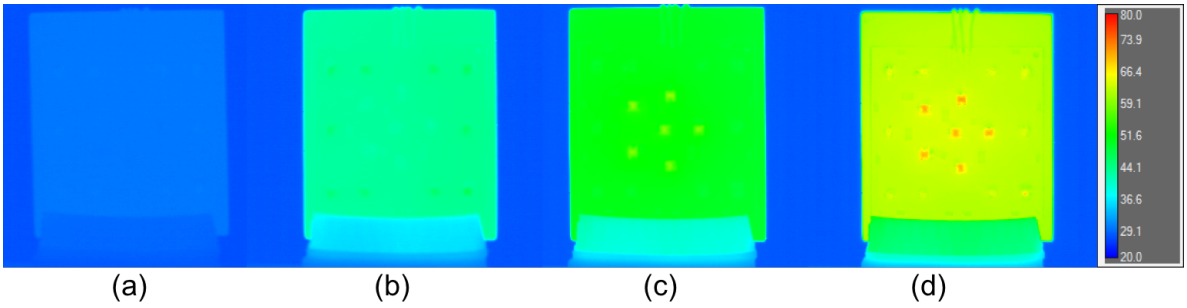

Figure 29: IR thermal images of LEDs' sides of the aluminum based light engine with ceramic flex PCB at (a) Case-1, (b) Case-2, (c) Case-3 and (d) Case-4

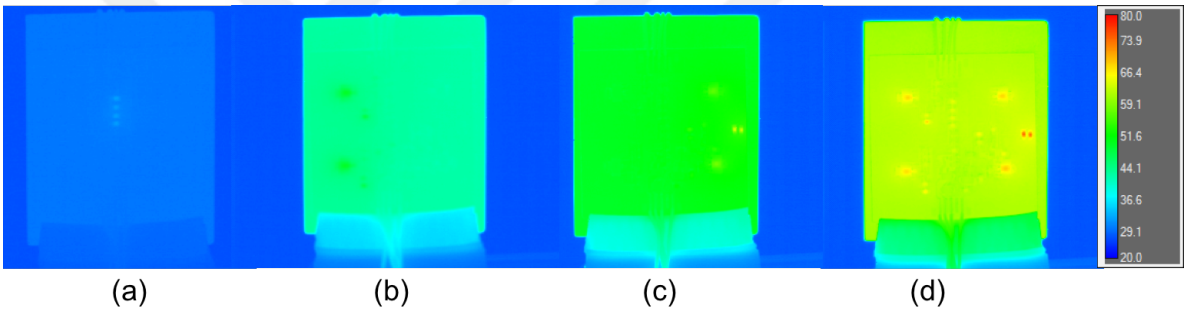

Figure 30: IR thermal images of electronics' sides of the aluminum based light engine with ceramic flex PCB at (a) Case-1, (b) Case-2, (c) Case-3 and (d) Case-4

Advanced heat spreader substrate is also assembled with ceramic flex PCB and IR thermal tests are applied on it. The previous experiments were conducted while the ambient temperature was 25 ± 0.5°C. However, experiments with the advanced heat spreader LED light engine with ceramic flex PCB is conducted while the ambient temperature is 27.5 ± 0.5°C. At the first experimental case, maximum LED temperature reaches to 32.7°C while minimum temperature is observed over the LEDs' side of the board is 31.8°C. On the electronics' side of the LED engine, maximum electronic temperature is 34.3°C, while minimum temperature is observed over the board is 31.6°C. At Case-2, maximum LED and electronic surface temperature reach

to 46.7°C and 49.5°C, respectively. Minimum board temperature over the LEDs' and electronics' sides are 41.5°C and 41.9°C, respectively. During the signal LEDs are operating at the Case-3, maximum LED surface temperature is experienced as 63.2°C while minimum board temperature is experienced as 48.5°C. At the other side of the LED light engine, maximum electronic surface temperature is experienced as 66.7°C while minimum board temperature is experienced as 48.5°C. At the Case-3, over the LEDs' side of the engine, hot spots over the signal LEDs: LED 11, 12, 13, 14 and 15 are observed in Figure 31c and hot spots over electronics: Q5, Q6, R17 and R19 are presented in Figure 32c. During the Case-4, maximum LED and electronics surface temperatures are 73.3°C and 77.7°C, respectively. While maximum temperature difference observed on LEDs' side is 13.2°C, maximum temperature difference observed on electronics' side is 16.7°C. The highest amount of input power is consumed at this case so the most critical hot spots observed at this case over signal LEDs, transistors and resistor 17 and 19.

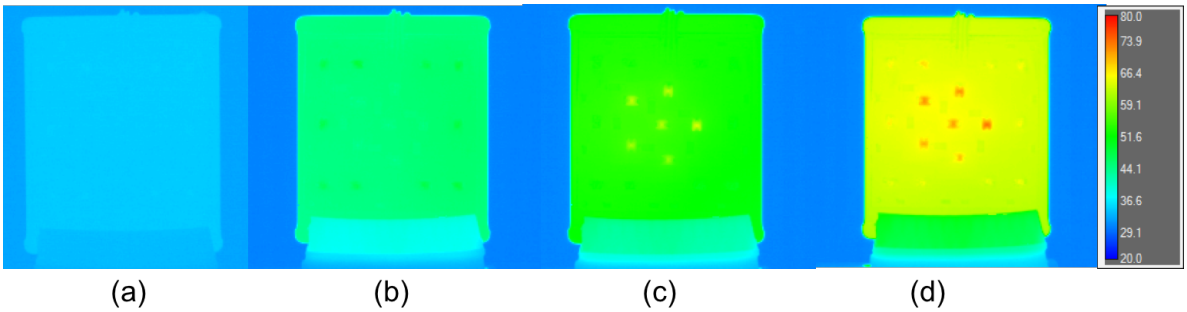

Figure 31: IR thermal images of LEDs' sides of the advanced heat spreader based light engine with ceramic flex PCB at (a) Case-1, (b) Case-2, (c) Case-3 and (d) Case-4

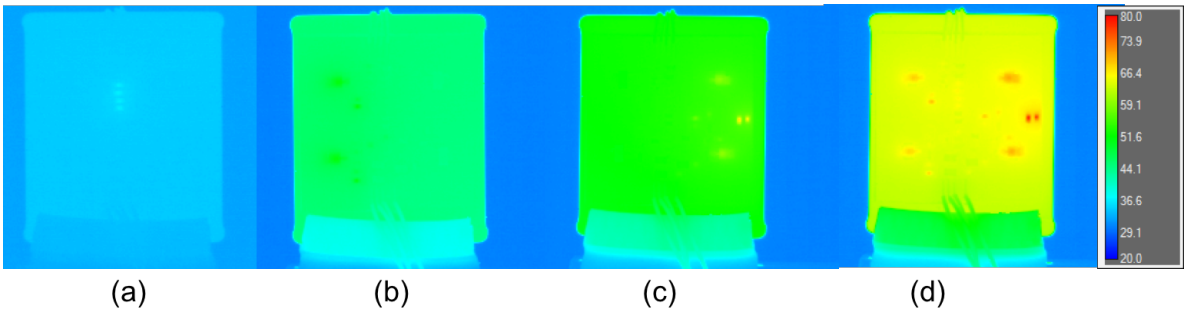

Figure 32: IR thermal images of electronics' sides of the advanced heat spreader based light engine with ceramic flex PCB at (a) Case-1, (b) Case-2, (c) Case-3 and (d) Case-4

Because of the fact that the most critical case for automotive exterior lighting in terms of thermal limitations is Case-4, thermal performance of the three LED light engines are compared at this case. Firstly, IR thermography results of LEDs' side of the LED light engines are compared. As it is presented in Figure 33, heat distribution is more uniform in Al based and advanced heat spreader based LED light engine than FR4 based LED light engine due to the lower thermal conductivity of the FR4 material. While, over the flex PCB, heat distributes uniformly, at least 2°C temperature difference forms between the substrate and the flex PCB at top and bottom side of the FR4 based LED light engine. However, at the Al and advanced heat spreader based PCBs, this distinction between substrate and flex PCB can not be realized because of the uniform temperature distribution. Although there is difference in temperature distribution over the board changes by the substrate of the LED light engine, maximum temperatures which are observed over the LEDs are not changes as much as the first set of LED engines.

If FR4 based LED engine is taken as baseline, Al based LED light engine performs 11.2% better than FR4 based LED light engine. On the other hand, advanced heat spreader based LED light engine performs 11.7% better than FR4 based LED light

engine. As it can be seen from Figure 33, behaviors of the advanced heat spreader and Al based LED light engines under the conditions of Case-4 are very similar. Advanced heat spreader based LED light engine shows only 0.7 % better performance than Al based LED light engine. Due to the inconsiderable performance difference of advanced heat spreader and Al based LED light engines, Al based LED light engine with ceramic based flex PCB can be used instead of advanced heat spreader based light engine for this kind of applications due to its higher manufacturability and low cost. Furthermore, maximum LED surface temperature is not close to the critical LED temperature (100°C) and its performance is close to the performances of other light engines. Therefore, for this application FR4 based LED light engine can be used with ceramic flex PCB as profitable solution.

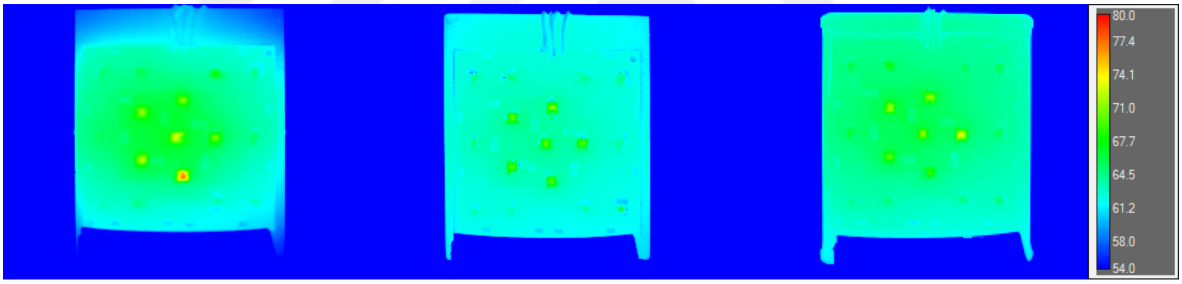

Figure 33: During the Case-4, IR thermal images of LEDs' sides of based light engine at (a) FR4, (b) Al and (c) the advanced heat spreader based LED light engine with ceramic flex PCB

Comparison of the thermal performance of the LED light engine continues with IR thermography of electronics side of the LED light engines. As LEDs' side of the engine, electronics' side of the engine has the distinction between FR4 substrate and flex PCB in terms of temperature which can be observed in Figure 34. Differently from the LEDs' side, at the electronics side maximum LED surface temperature is experienced over the advanced heat spreader LED light engine and FR4 based

light engine follows it. While aluminum based LED light engine have 1.4% better performance than FR4 based LED light engine. Advanced heat spreader based LED light engine performs 0.8% worse than FR4 and 2.2% worse than aluminum based LED light engine. Although the performance differences of the engine are quite low, it was expected that advanced heat spreader board will have the highest performance among the FR4 and aluminum based LED light engines due to its higher thermal conductivity. Advanced heat spreader substrate benefits form phase change heat transfer, therefore it is highly thermally conductivity. However, phase change can not be occurred efficiently at low temperatures so maybe advanced heat spreader board's performance is not efficient in that temperature.

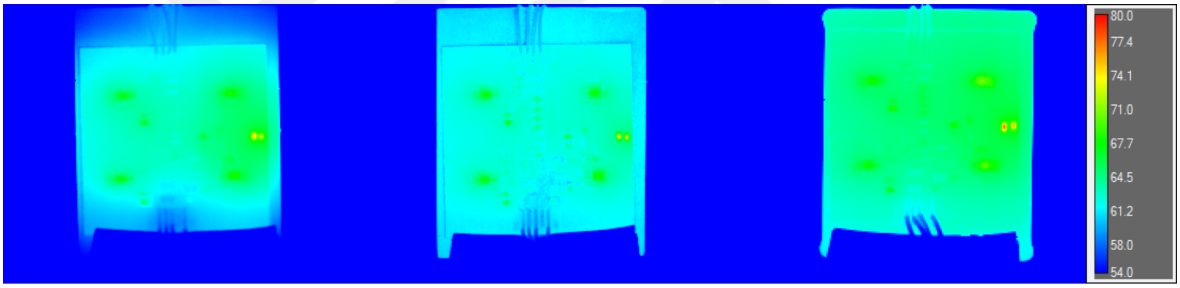

Figure 34: During Case-4, IR thermal images of electronics' sides of based light engine at (a) FR4, (b) Al and (c) the advanced heat spreader based LED light engine with ceramic flex PCB

3.3 Thermal Performance Comparison of First and Second Set of LED Light Engines

To enhance thermal performance of the LED light engines, in the second set of LED light engines, ceramic based multilayer flex PCB is used as an alternative for FR4 flex PCB. Due to the lower thermal resistance of the ceramic based flex PCB, more uniform temperature distribution and lower surface temperature over the LED and

electronic components are experienced at the second set of LED light engines. Experimental results of first and second set of boards at Case-4 will be discussed in following for each type of board substrate separately.

When FR4 based LED light engine with FR4 flex PCB is operated at Case-4, maximum LED temperature reaches to 105°C which is very close to critical LED temperature. Therefore, FR4 substrate is not usable with flex FR4 PCB for 3-purpose automotive exterior lighting applications. However, when FR4 substrate is assembled with multilayer ceramic flex PCB for LED light engine, maximum LED temperature is experienced as just 76.9°C. Besides, more critical hot spots forms over signal LEDs and some of the transistors and resistors on the FR4 based LED light engine with FR4 flex PCB. In addition, as it is presented in Figure 35 and Figure 36, more uniform temperature distribution pattern is experienced at the FR4 based LED light engine with ceramic based flex PCB due to its higher thermal conductivity. Consequently, thermal performance of the FR4 based LED light engine is enhanced 26.8 % in terms of maximum surface temperature of the LEDs when ceramic based flex PCB is used instead of FR4 based flex PCB.

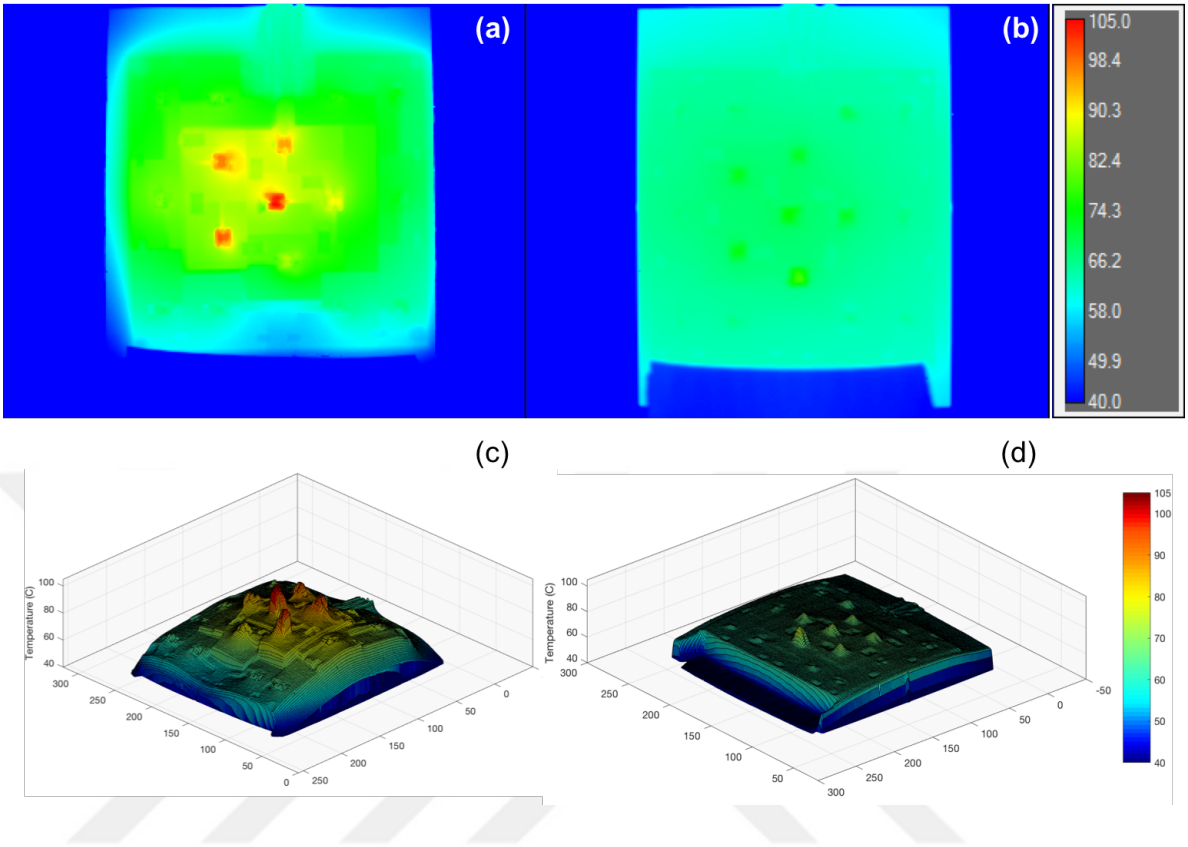

Figure 35: IR thermography images of LEDs side of (a) FR4 based LED light engine with the FR4 flex PCB, (b) FR4 based LED light engine with the multilayer ceramic flex PCB, 3-D contour plots of (c) FR4 based LED light engine with the FR4 flex PCB, (d) FR4 based LED light engine with the multilayer ceramic flex PCB

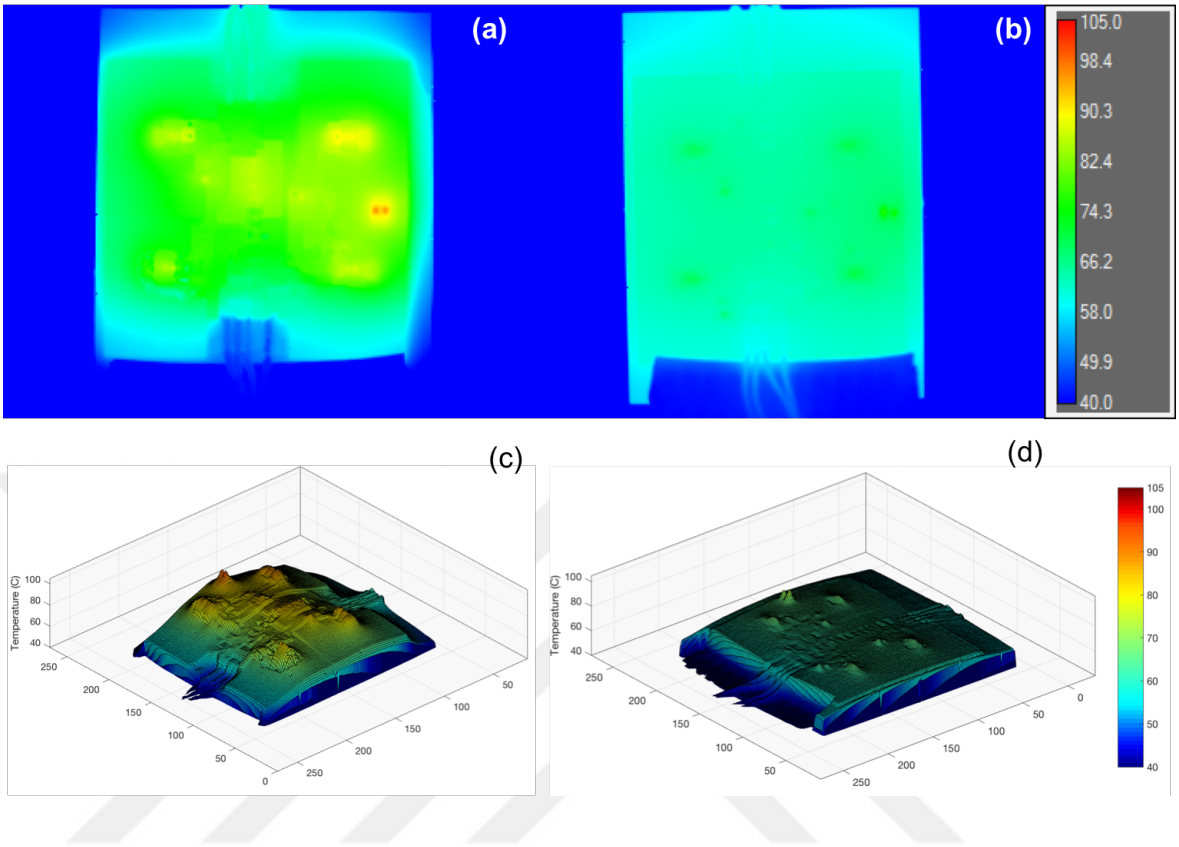

Figure 36: IR thermography images of electronics side of (a) FR4 based LED light engine with the FR4 flex PCB, (b) FR4 based LED light engine with the multilayer ceramic flex PCB, 3-D contour plots of (c) FR4 based LED light engine with the FR4 flex PCB, (d) FR4 based LED light engine with the multilayer ceramic flex PCB

Aluminum based LED light engine with FR4 flex PCB enhances the thermal performance compared to that of FR4 based LED light engine. Furthermore, performance of the Al substrate is improved by 15.5 % when it is using with the ceramic flex PCB. Although hot spots over LEDs and some of the electronics are experienced in two type of the LED light engines, hot spots occurred on aluminum based LED light engine with FR4 flex PCB is more explicit than hot spots occurred on aluminum based LED light engine with ceramic flex PCB. Besides, on the LED 16 of the first set of board, there is accumulation of heat. The reason behind this can be mounting defect or manufacturing defect of the LED.

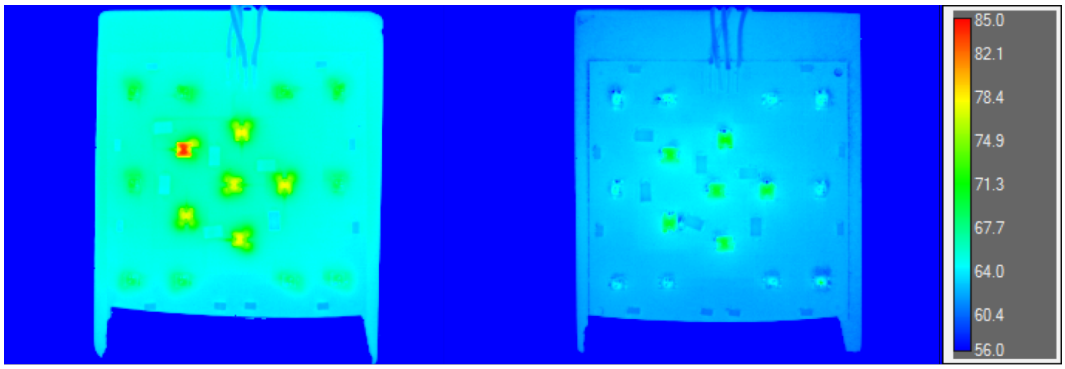

Figure 37: Comparison between thermal performances of Aluminum based LED light engine with FR4 flex PCB and ceramic flex PCB (LEDs' side)

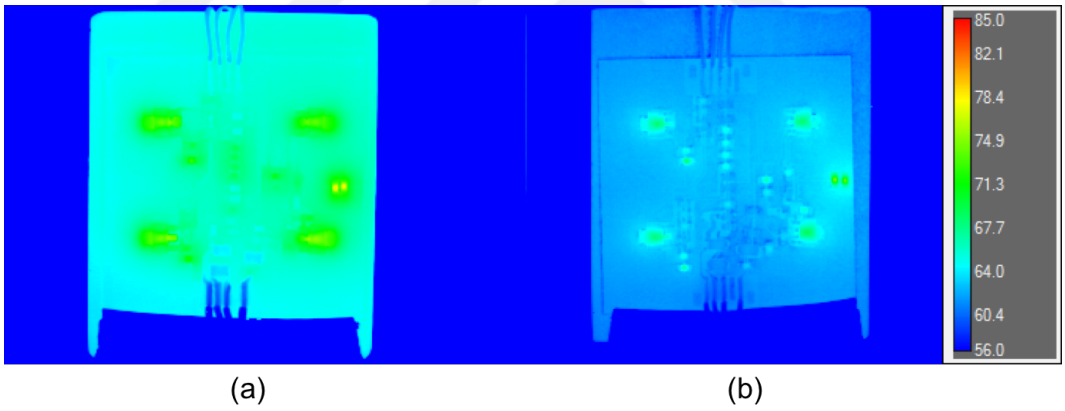

Figure 38: Comparison between thermal performances of Aluminum based LED light engine with FR4 flex PCB and ceramic flex PCB (electronics' side)

Minimum enhancement with 9.1% is observed in advanced heat spreader LED light engine when ceramic flex PCB is used instead of FR4 flex PCB. It can be inferred from the Figure 39 that heat distributes more uniformly over the advanced heat spreader LED light engine with the ceramic flex PCB. Especially, more critical hot spots formed over the amber LEDs, R17 and R19 on the advanced heat spreader

LED light engine with the FR4 flex PCB.

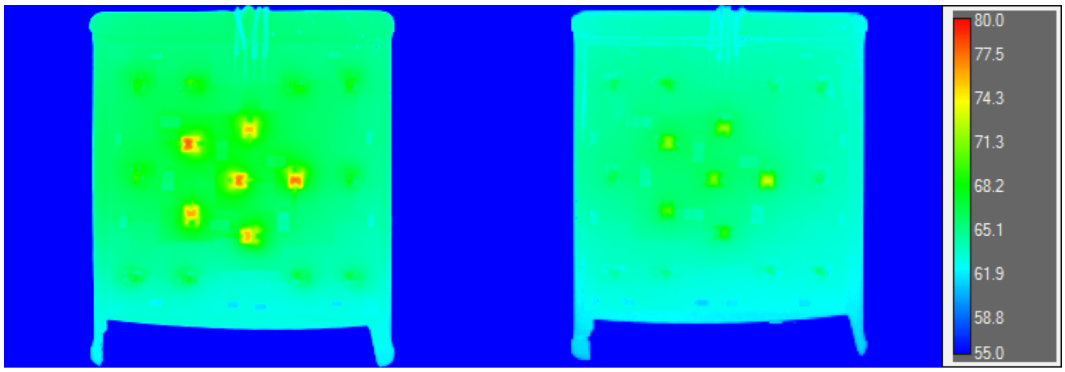

Figure 39: Comparison between thermal performances of advanced heat spreader based LED light engine with FR4 flex PCB and ceramic flex PCB (LEDs' side)

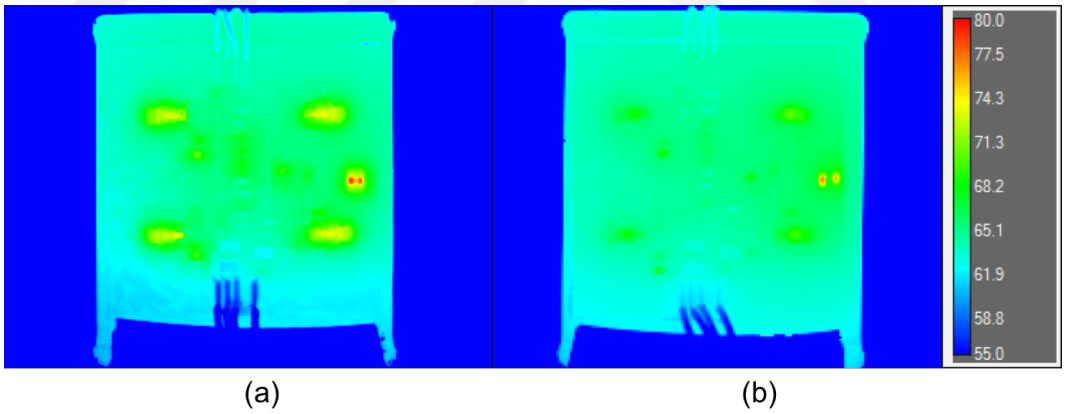

Figure 40: Comparison between thermal performances of advanced heat spreader based LED light engine with FR4 flex PCB and ceramic flex PCB (Electronics' side)

CHAPTER IV

OPTICAL PERFORMANCE INVESTIGATION OF LED BOARDS

Thermal management design of the LED lighting systems have significant effect on optical output of the system. Therefore, optical measurements should be done for performance analysis of the LED systems. In this chapter, optical performance of the first and second set of the boards are obtained with integrated sphere under the four experimental conditions. Then, the results will be discussed.

4.1 Optical Analysis for First Set of LED Light Engines

One of the most important parameter to understand performance of an LED lighting system is optical spectrum [10]. Therefore, first of all, optical spectrum of the first LED light engines are analyzed. Then, radiometric and photometric quantities of the each engine are investigated.

Investigation begins with FR4 based LED light engine. Spectral power distribution of the engine is demonstrated in Figure 41. One of the most important parameter in the spectral curve of the LEDs is the peak wavelength shift because it is the function of junction temperature of AlGaInP LEDs [47]. While, the junction temperature of an LED increases, peak wavelength of the LED shifts toward infrared region. According to the Figure 41, there is 4nm peak wavelength shift between Case-1 and Case-2 since the junction temperature of the LEDs increases at Case-2. Even at Case-4, peak wavelength in the red region shifts by 8nm compared to Case-1 and in the amber region, it shifts by 3 nm compared to Case-3 due to the fact that at Case-4, input power and junction temperature reach to the highest value among the other

cases.

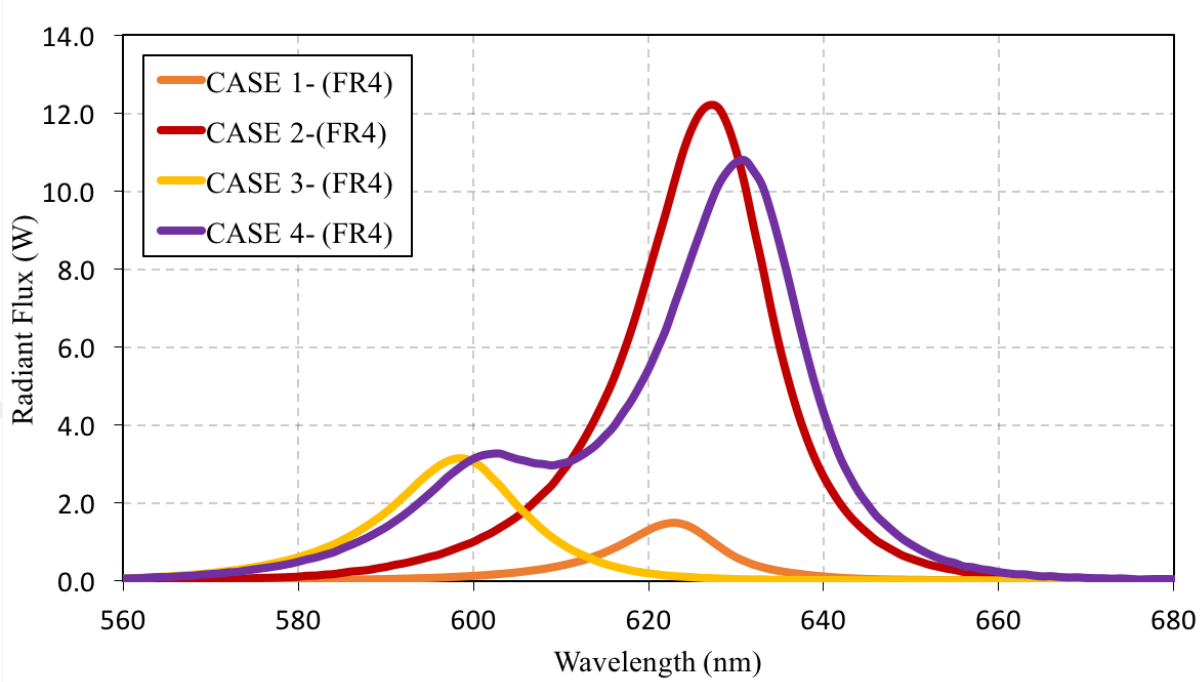

Figure 41: Spectral flux distribution of the FR4 based board during Case-1, Case-2, Case-3 and Case-4

Another key parameter to determine performance of the electrical system is efficiency which is the ratio of output power to input power. However, different from electronic systems, in LED lighting systems, the output of the system is light [10]. In addition, useful part of the light is the light perceived by the human eye that is called luminous flux. Therefore, conversion ratio of the lighting system which is called efficacy is calculated by division of luminous flux over input power of the system [10]. Efficacy of the FR4 based LED light engine is 69.8 lm/W at the Case-1, but it decreases by 8.1 lm/W at the Case-2 because of the elevated junction temperature of the LEDs. At Case-3, only amber LEDs operate while at Case-1 and Case-2 only red LEDs operate. Therefore, although, at Case-3, efficacy drops 17.5 lm/W, efficacy of different color LEDs can not be compared due to their different light emitting [10].

Radiant power, luminous power, CCT, CRI and overall efficacy of the FR4 based LED light engine at four different cases is presented in Table 4.

Table 4: Optical measurement results of the FR4 based light engine

Case	*Total Input Power*(mW)	*Input Powerof LEDs*(mW)	*Radiant Power* (mW)	*Luminous Flux* (lm)	*CCT*	*CRI*	*Overall Efficacy* (lm/W)
Case-1	288.0	100.0	37.2	7.0	1000	23.1	69.8
Case-2	2423.9	1000.0	370.8	61.7	1000	28.7	61.7
Case-3	3360.0	1830.0	111.2	32.0	1481	-13.5	17.5
Case-4	5711.8	2930.0	411.0	75.7	1000	43.7	25.8

Investigation continues with the aluminum based LED light engine with the FR4 flex PCB. As it is demonstrated at Figure 42, peak wavelength of the red LEDs shifts by 5nm and 3nm from Case-1 to Case-2 and from Case-2 to Case-4, respectively. When spectral distribution of amber LEDs at Case-3 and Case-4 is analyzed, peak wavelength shift from 597 nm to 599 nm can be seen.

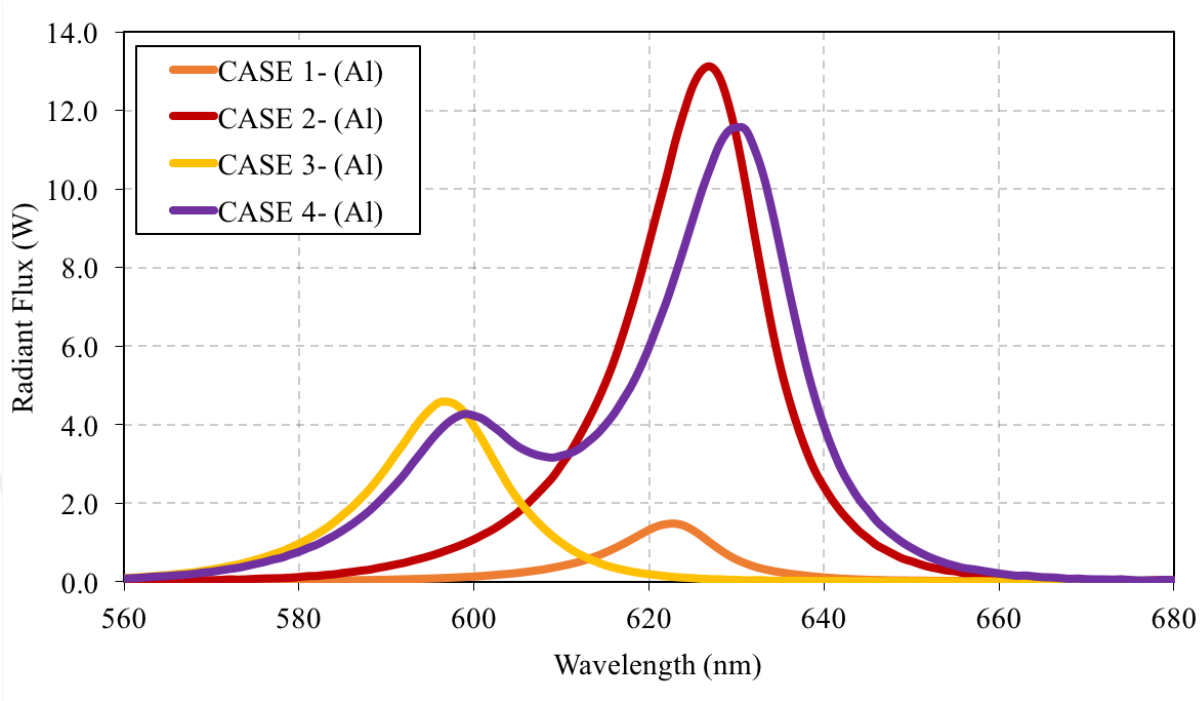

Figure 42: Spectral flux distribution of the Aluminum based board during Case-1, Case-2, Case-3 and Case-4

Photometric and radiometric quantities of the aluminum based LED light engine is presented in Table 5. According to the table, overall efficacy of the light engine is decreased by 4.5 lm/W from Case-1 to Case-2.

Table 5: Optical measurement results of the Aluminum based light engine

Case	*Total Input Power*(mW)	*Input Powerof LEDs*(mW)	*Radiant Power* (mW)	*Luminous Flux* (lm)	*CCT*	*CRI*	*Overall Efficacy* (lm/W)
Case-1	288.0	100.0	35.4	6.9	1000	22.2	69.7
Case-2	2519.8	1000.0	392.9	65.2	1000	28.2	65.2
Case-3	3599.7	1830.0	145.1	45.5	1547	-17.8	24.9
Case-4	6047.5	2930.0	440.2	90.3	1000	43.6	30.8

Lastly, advanced heat spreader based LED light engine is analyzed in terms of optical performance. While peak wavelength is experienced at 623 nm during Case-1, it reaches 627 nm during the Case-2. Peak wavelength of the amber LEDs at Case-3 is 596 nm while it shifts 3nm at Case-4 because of the junction temperature increase.

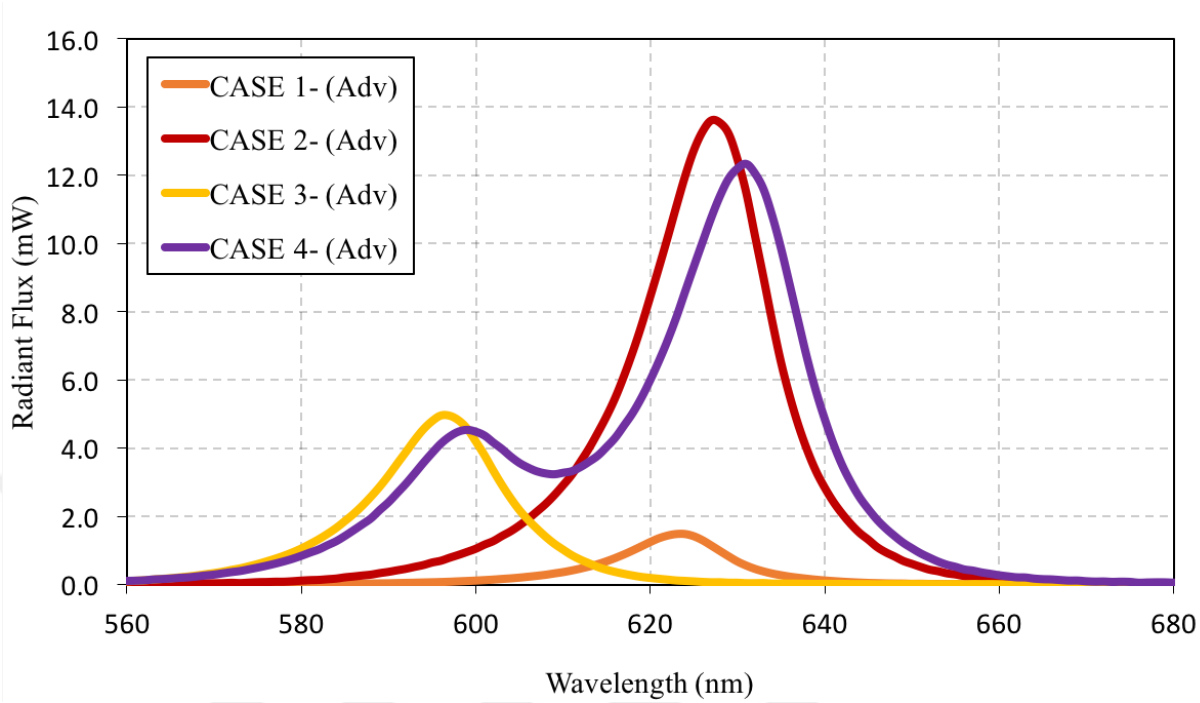

Figure 43: Spectral flux distribution of the advanced heat spreader based board during Case-1, Case-2, Case-3 and Case-4

Photometric and radiometric quantities of the advanced heat spreader based LED light engine is presented in Table 7. When photometric and radiometric results of the LED light engine is investigated, overall efficacy is decreased by 3.8 lm/W from Case-1 to Case-2.

Table 6: Optical measurement results of the advanced heat spreader based light engine

Case	*Total Input Power*(mW)	*Input Powerof LEDs*(mW)	*Radiant Power* (mW)	*Luminous Flux* (lm)	*CCT*	*CRI*	*Overall Efficacy* (lm/W)
Case-1	288.0	100.0	38.7	6.9	1000	24.1	69.4
Case-2	2495.8	1000.0	394.7	66.6	1000	27.6	66.6
Case-3	3599.6	1830.0	155.8	49.1	1553	-18.3	26.8
Case-4	6047.2	2930.0	478.0	95.4	1000	45.0	32.6

In order to understand the optical performance of the advanced heat spreader board, it is compared with FR4 based and aluminum based boards for each four different experimental cases. Firstly, spectral power distributions of the LED light engines compared for different cases to obtain possible wavelength shifts.

During the first case, as it is presented in Figure 44, peak wavelength of the all three LED light engines are really similar, the difference is less than 1 nm. This can be attributed that LEDs on all three LED light engines have close junction temperatures at the first experimental case. During this case, maximum temperature of the LEDs increase by just 9°C, 5.39°C and 6.2°C while ambient temperature is 25 ± 0.5°C because input power supplied by power supply is low as 288 mW.

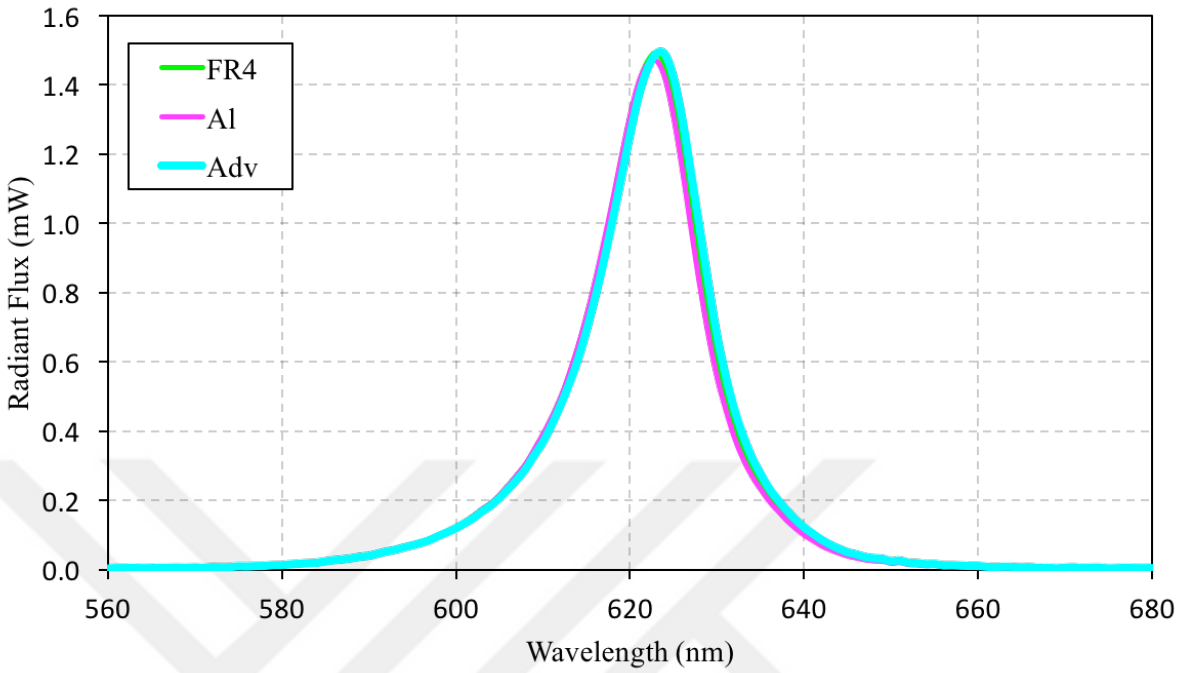

Figure 44: Spectral flux distribution comparison of FR4, Aluminum and advanced heat spreader based LED light engines at Case-1

When spectral power distribution of LED light engines during second experimental case, slight wavelength shift which is lower than 1 nm can be seen. Although peak wavelength of the LED light engines are same, relative spectral power corresponding peak wavelength of advance heat spreader LED light engine is the highest among the three LED light engines. This is because junction temperature of the LEDs are lowest at advance heat spreader LED light engine.

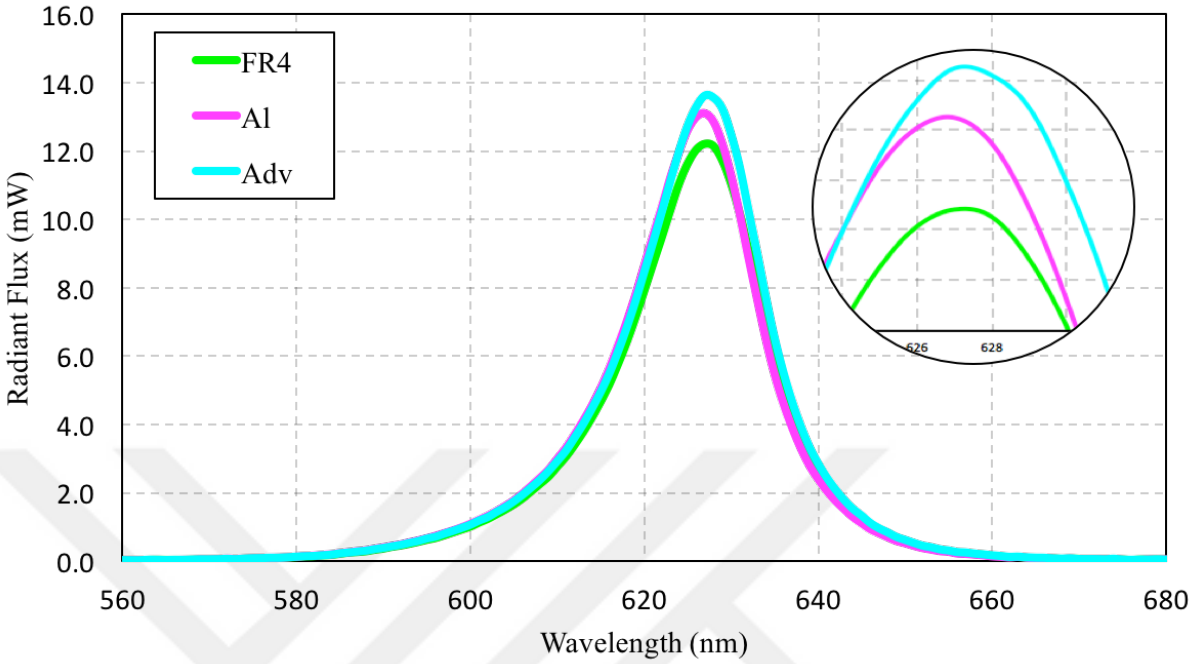

Figure 45: Spectral flux distribution comparison of FR4, Aluminum and advanced heat spreader based LED light engines at Case-2

While input power of the engines increases, at Case-3, the most distinct wavelength shift can be observed between spectral distributions of LED light engines. While junction temperature increases from advanced heat spreader based LED light engine to FR4 based LED light engine, peak wavelength shifted from 596 nm to 599 nm. In addition, there is approximately 2 mW difference between relative spectral powers correspond to peak wavelength of the LEDs of advanced heat spreader and FR4 based LED light engines.

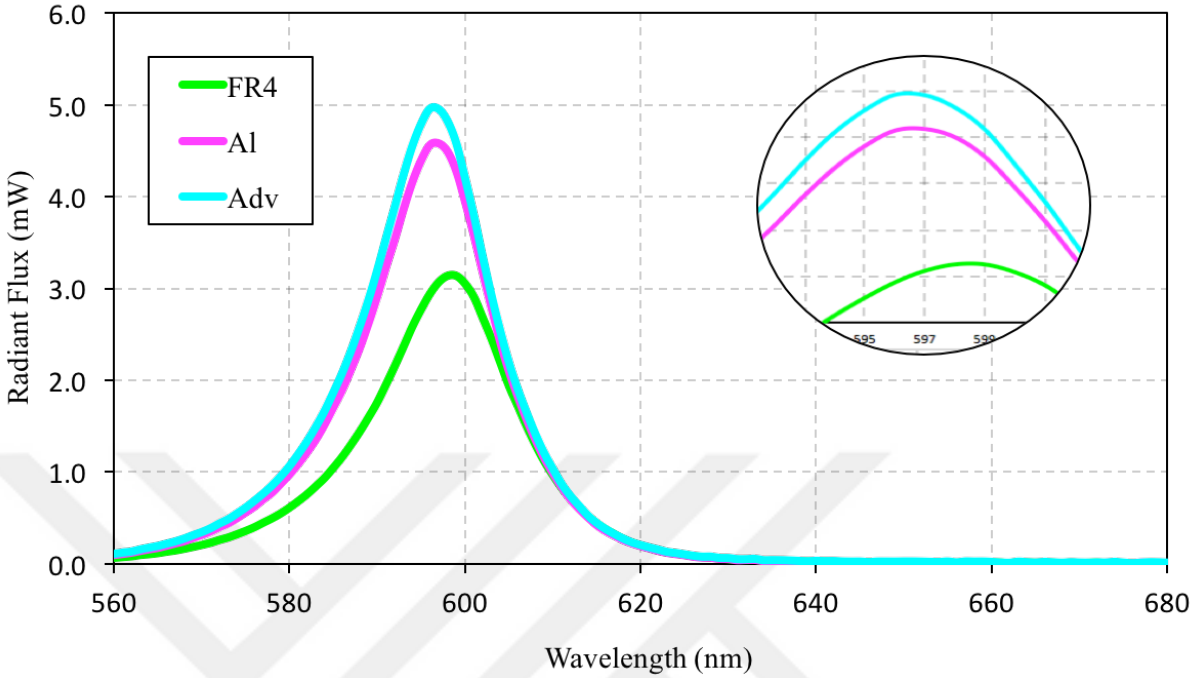

Figure 46: Spectral flux distribution comparison of FR4, Aluminum and advanced heat spreader based LED light engines at Case-3

At Case-4, both amber and red LEDs operate simultaneously so at the spectral flux distribution, spectrum of these two colors forms together. Although peak wavelengths of three light engines at the red region are really similar, at the amber region, while peak wavelength of the advanced heat spreader and aluminum based LED light engines are really close and 599 nm, peak wavelength of the FR4 based LED light engines is 2 nm higher than the others. Also, relative power correspond to peak wavelength of advanced heat spreader based LED light engine is greatest as it is indicated in Figure 47.

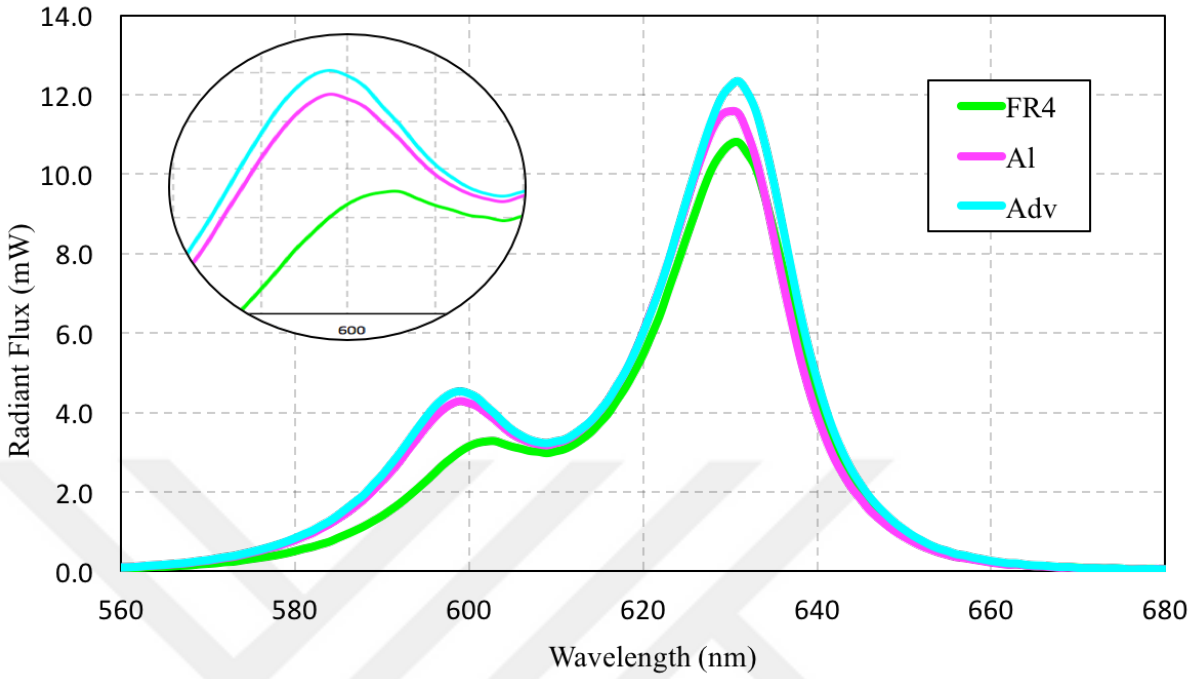

Figure 47: Spectral flux distribution comparison of FR4, Aluminum and advanced heat spreader based LED light engines at Case-4

LEDs emit photons as a result of electron hole recombination. Probability of the recombination is inversely proportional to temperature [14]. Therefore, while junction temperature of LEDs elevates, probability of the recombination gets lower and radiant flux of the LEDs decreases [20]. Figure 48 demonstrates radiant flux difference of FR4, aluminum and advanced heat spreader LED light engine at four experimental cases. Radiant flux of the FR4, aluminum and advanced heat spreader LED light engines are approximately identical at the first experimental case because their junction temperatures are very similar. At Case-2, radiant flux of aluminum and advanced heat spreader based light engine are 6.0% and 6.5% greater than that of radiant flux of the FR4 based light engine while maximum LED surface temperature observed on aluminum and advanced heat spreader based light engine are 18.5% and 20.6% less than that of maximum LED surface temperature of the FR4 based

light engine, respectively. At Case-3, total radiant flux of the amber LEDs 30.5% and 40.1% enhance when aluminum and advanced heat spreader based LED light engines are used instead of that of FR4 based LED light engine, respectively. At Case-4, aluminum and advanced heat spreader based LED light engines show 7.1% and 16.3% better performance in terms of radiant flux, respectively.

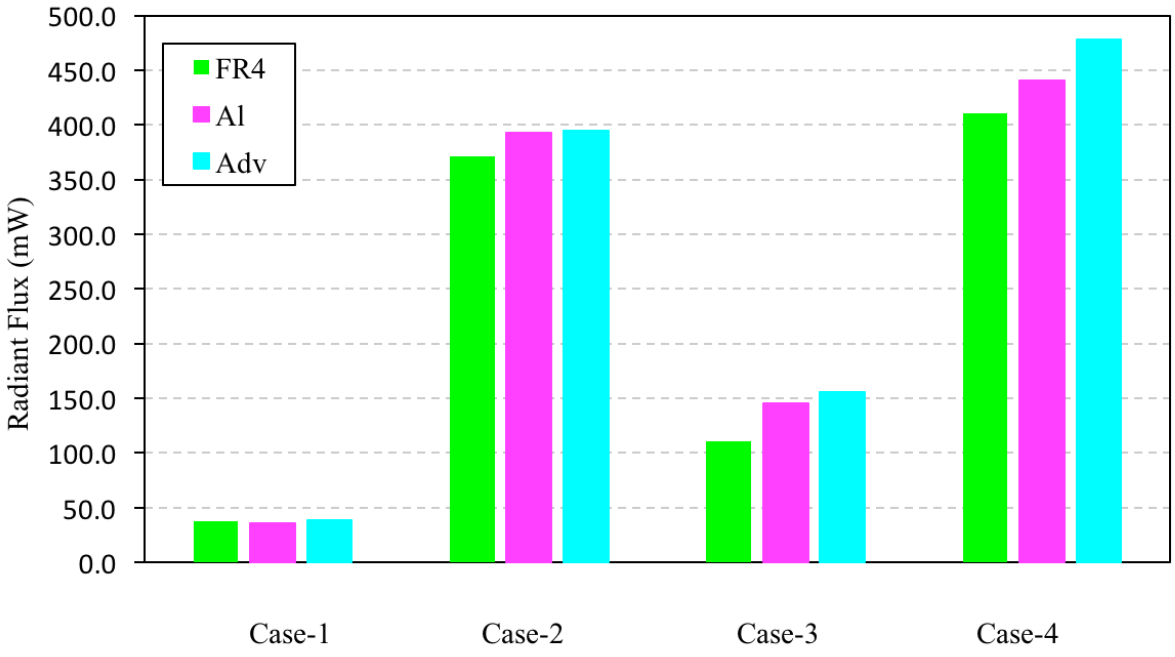

Figure 48: Radiant flux of the three different LED light engines at Case-1, Case-2, Case-3 and Case-4

Luminous flux is another important performance indicator for our problem. While radiant flux is radiometric quantity, luminous flux is a photometric quantity which is derived by weighed the radiant flux by the spectral response of the human eye. Therefore, similar trend is experienced in Figure 48 and 49. At the first experimental case, luminous flux of the FR4, aluminum and advanced heat spreader LED light engines are approximately identical because their junction temperatures are also very similar at this case. At the second case, luminous flux of aluminum and advanced

heat spreader based light engine are 5.7% and 7.9% greater than that of luminous flux of the FR4 based light engine, respectively. Effect of elevated junction temperature is more explicit on optical output of the LEDs at Case-3. Total luminous flux of the amber LEDs enhances by 42.4% and 53.4% when aluminum and advanced heat spreader based LED light engines are used instead of that of FR4 based LED light engine, respectively. Similar trend with Case-2 and Case-3 is also observed at Case-4.

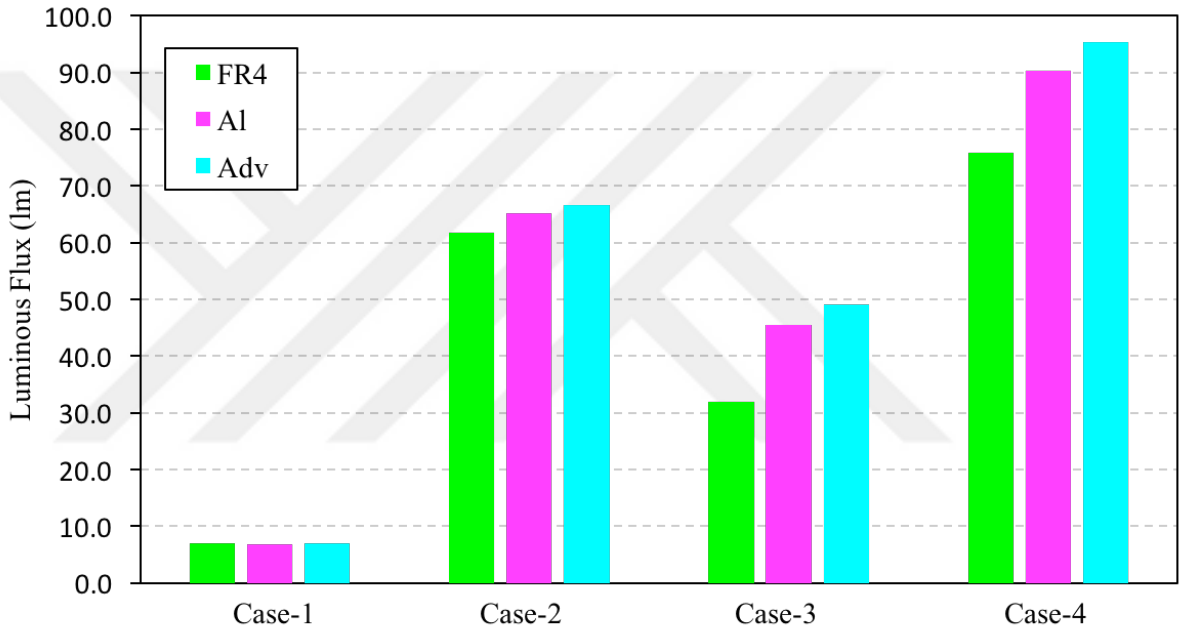

Figure 49: Luminous flux of the three different LED light engines at Case-1, Case-2, Case-3 and Case-4

Relation between maximum LED surface temperature and total luminous flux can be analyzed from Figure 50. There is inverse proportion between them. While advanced heat spreader based LED light engine has highest luminous flux and minimum LED surface temperature, FR4 based LED light engine has minimum luminous flux and maximum LED surface temperature.

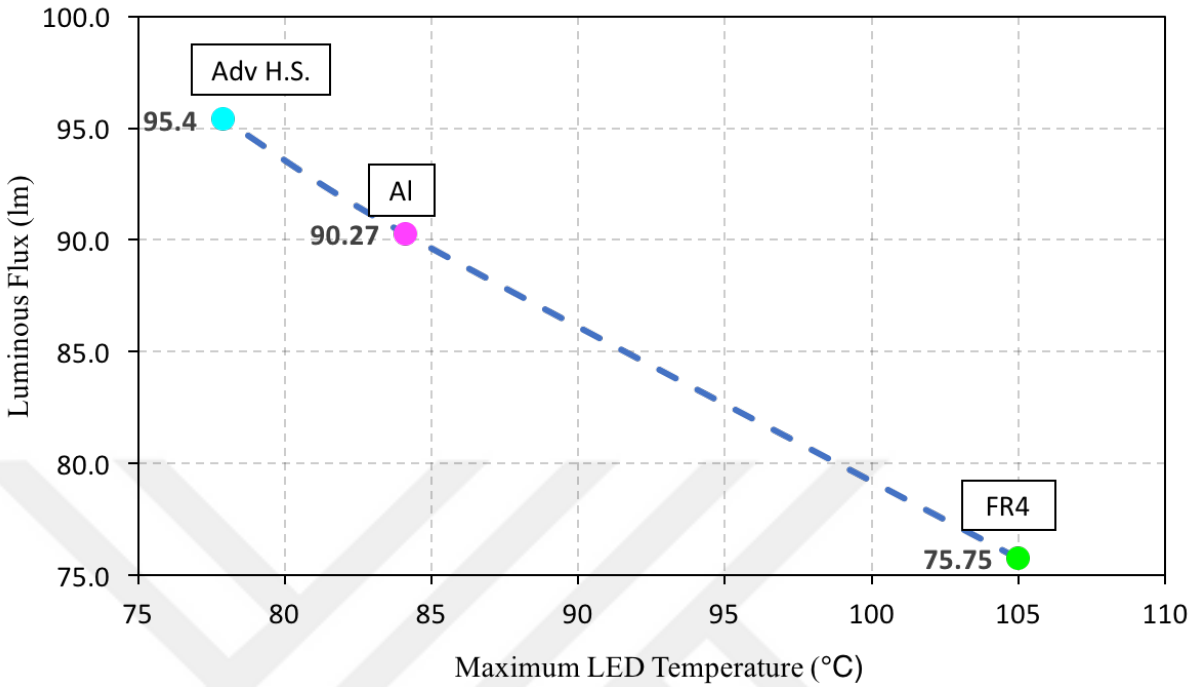

Figure 50: Luminous flux comparison of the three different LED light engines at Case-4

Figure 51 shows that when advanced heat spreader board base used instead of FR4 board base, luminous efficacy can be improved by 25.9%. This improvement originates from better thermal management of the advanced heat spreader based LED light engine.

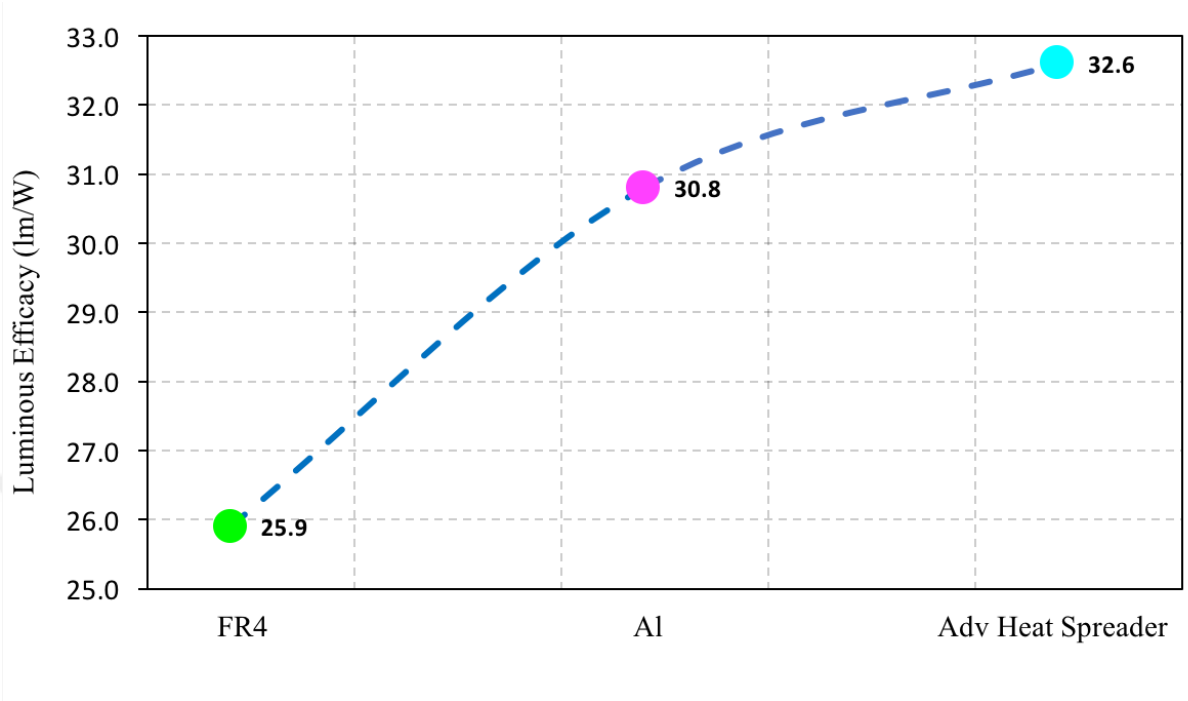

Figure 51: Luminous efficacy comparison of the three different LED light engines at Case-4

4.2 Optical Analysis for Second Set of LED Light Engines

After optical experiments of the first set of LED light engines were complicated, optical experiments of the second set of LED light engines conducted. However, optical experiments are conducted only on FR4 based LED light engine at Case-4 among LED light engines of the second set.

Spectral power distribution of the FR4 based LED light engine with ceramic flex PCB can be seen from Figure 52. The peak wavelength at the amber region of the spectrum is 599 nm while the corresponding relative power is 4.3 mW. The peak wavelength at the red region of the spectrum is 631 nm while corresponding relative power is 11.1 mW.

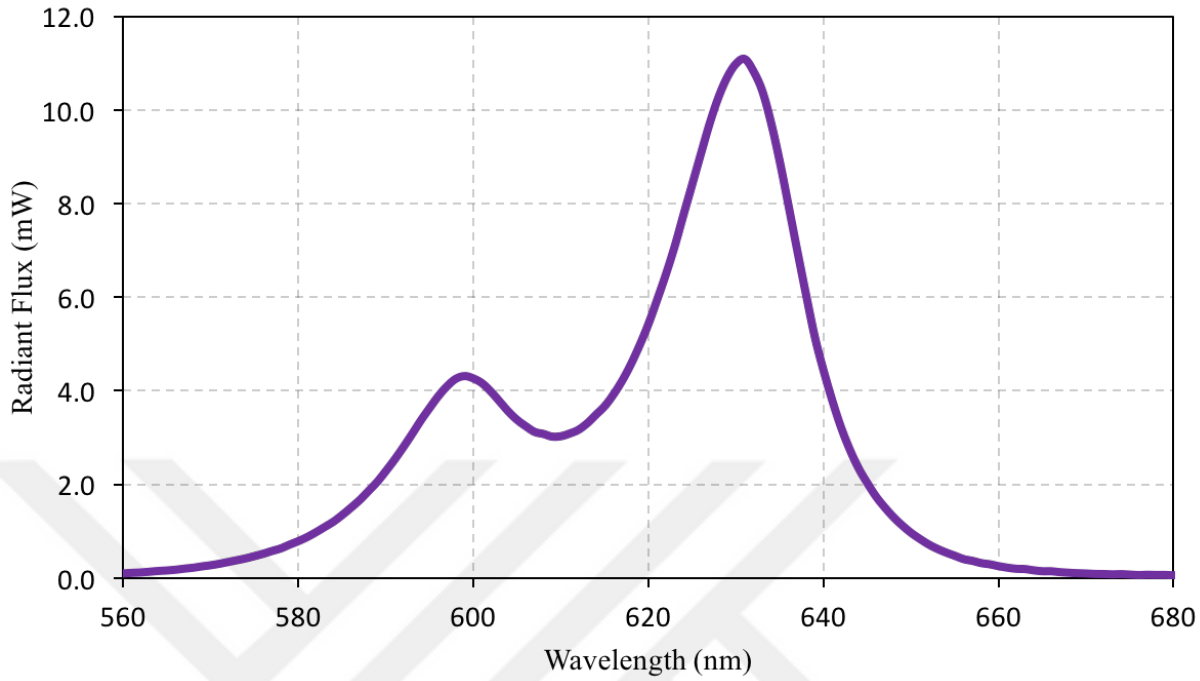

Figure 52: Spectral flux distribution of FR4 based light engine with ceramic flex PCB at Case-4

Radiometric and photometric quantities of the LED light engine is presented in Table 7. According to the table, radiant flux, luminous flux and luminous efficacy of the LED light engine are 474.1 mW, 88.6 lm and 30.2 lm/W, respectively while total input power of the LEDs is 2930 mW.

Table 7: Optical results of the advanced heat spreader based light engine

Case	*Total Input Power*(mW)	*Input Powerof LEDs*(mW)	*Radiant Power* (mW)	*Luminous Flux* (lm)	*CCT*	*CRI*	*Overall Efficacy* (lm/W)
Case-4	6192	2930.0	474.1	88.6	1000	45.7	30.2

Spectral distribution of FR4 based board with FR4 flex PCB and FR4 based board with ceramic flex PCB are compared in Figure 53. As it is presented in Figure 53, peak wavelength at the amber region is shifted 3nm when FR4 flex PCB is used instead of ceramic flex PCB with the FR4 board base. Furthermore, relative power corresponding the peak wavelength is enhanced 13.9% via FR4 based LED light engine with ceramic flex PCB.

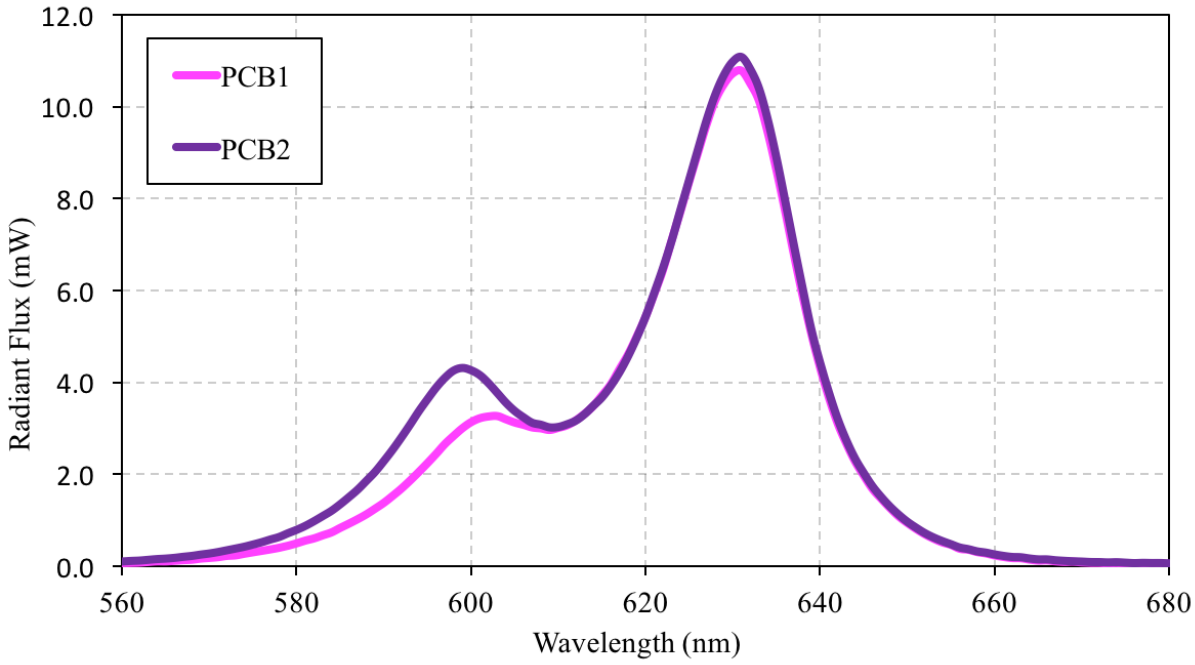

Figure 53: Flux spectrum comparison of FR4 based light engine with FR4 flex PCB and with ceramic based PCB at Case-4

According to Figure 54, there is inverse relationship between luminous flux and maximum LED surface temperature. While junction temperature of the LED increase, optical output of the LED decreases. Maximum temperature observed over the LEDs on the light engine is 36.5% greater at the FR4 based light engine with FR4 flex PCB than that of engine with ceramic flex PCB. This temperature elevation led to 14.6% decrease in the lumen output of the light engine.

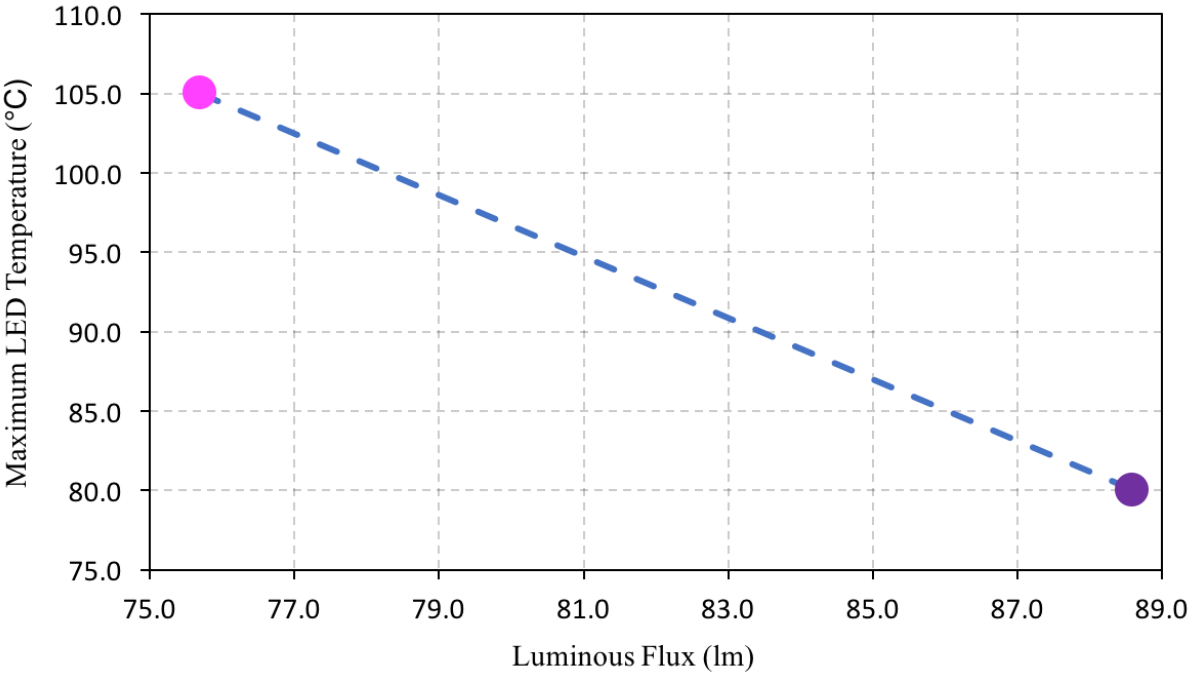

Figure 54: Relationship between maximum LED temperature and luminous flux of FR4 based LED light engine with FR4 flex PCB and ceramic flex PCB

Similar relationship between luminous flux and maximum LED surface temperature can also be observed between radiant flux and maximum LED surface temperature. While the maximum LED temperature decreases by 28.1°C, radiant flux of the LED light engine degrades by 13.3%.

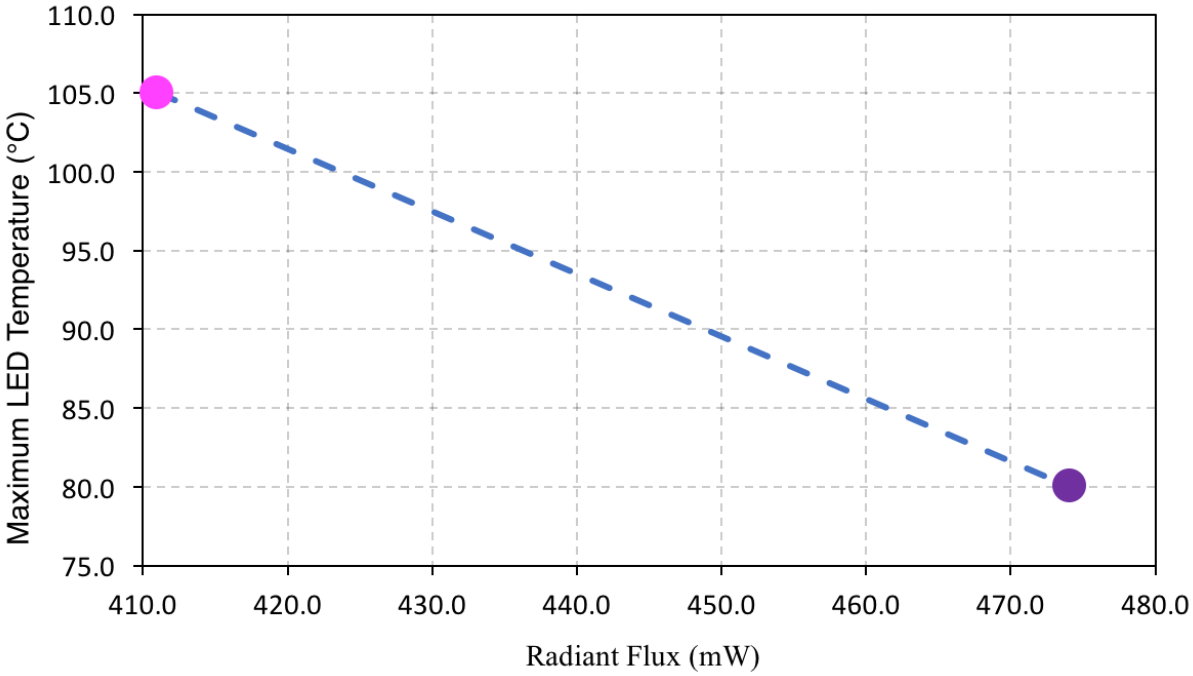

Figure 55: Relationship between maximum LED temperature and radiant flux of FR4 based LED light engine with FR4 flex PCB and ceramic flex PCB

CHAPTER V

RELATIONSHIP BETWEEN THERMAL AND OPTICAL PERFORMANCE OF LEDS

Photometric, electrical and thermal properties of LEDs are highly dependent with each other. Luminous efficacy of the LED systems is highly sensitive to junction temperature of the LEDs because optical output of the LEDs is changing with temperature. Therefore, designers should be consider the dependency between electrical, photometric and thermal quantities to achieve optimal performance. In this chapter, dependency between photometric, electrical and thermal parameters of the FR4 LED light engine with FR4 flex PCB is investigated.

5.1 Measurement of Electrical Power of LEDs

To understand thermal and optical performance relation, FR4 based LED light engines (with FR4 flex PCB) are driven at 6 different power levels. Firstly, only red LEDs are driven by six different input electrical power of 0.5W, 1W, 1.5W, 2W, 2.5W and 3W. Then, only amber LEDs are driven by these six input electrical powers. Total electrical power which is given by power supply to the LED light engine during the thermal and optical experiments is known. However, both electronic components and LED chips are consumed the total electrical power so portion of this total power which is supplied for only LEDs is not known. Therefore, total input power supplied for LEDs is measured by Keysight DSO-X3024 Oscilloscope. Details of the electrical measurements for amber and red LEDs can be seen in following subsections.

5.1.1 Red LEDs

There are 10 red LED chips on the light engine.In this case, to understand thermal and optical behavior relation of red chips, only red chips are operated. For optical and thermal experiments, the LED light engine is driven by 0.5W, 1W, 1.5W, 2W, 2.5W and 3W, in total. In order to measure the input power of the LEDs, electrical measurements are conducted with digital oscilloscope.

In the LED light engine, there are 2 branches which are connected in parallel. As it is presented in Figure 56, in every branches, there are 5 LED chips which are connected in series. First branch is called as PO/STOP_1 and the second is called as PO/STOP_2.

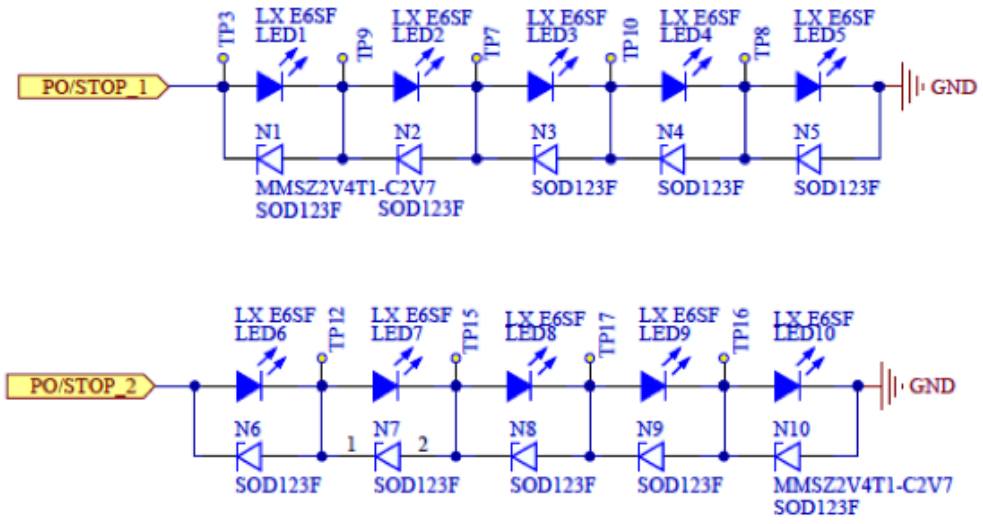

Figure 56: Schematic of electrical circuit of red LEDs

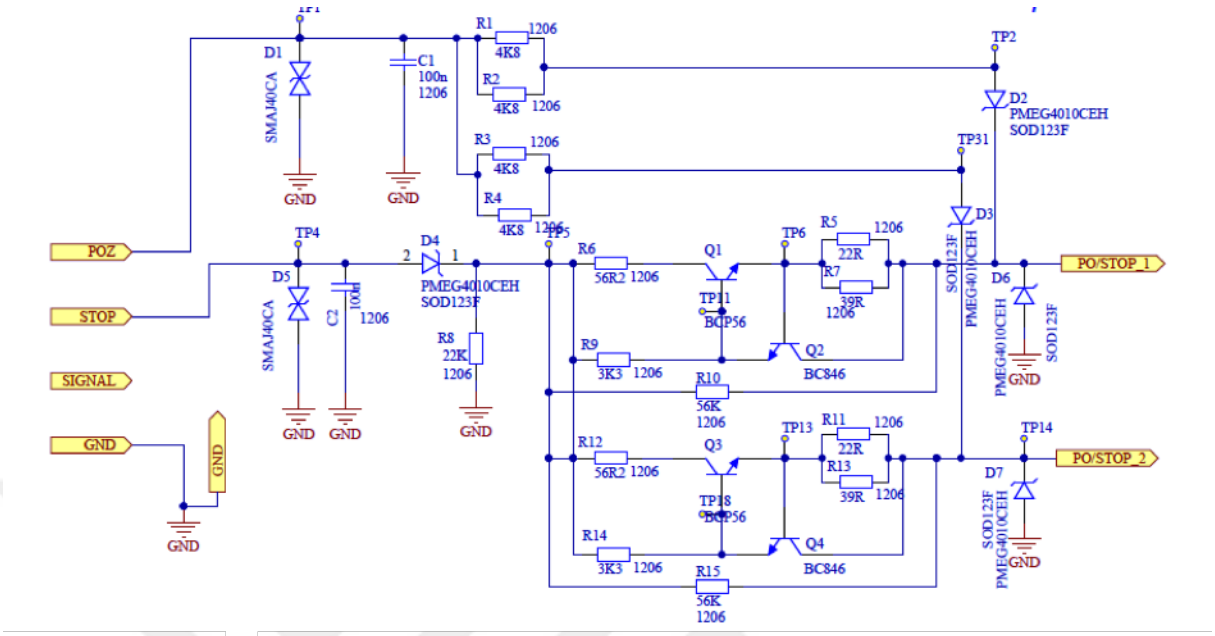

Figure 57: Schematic of electrical circuit of electronic components which are in charge of driving red LEDs

Due to the fact that there are two parallel branches, firstly, voltage difference across one of the branches and electrical current passed through that branch are measured. In the beginning of the measurement, FR4 based LED light engine is connected to Agilent DC power supply with position, stop and ground cables. In this case, power is supplied for 10 red LEDs and electronic components which are represented in Figure 57. A differential probe Keysight N2791 A is used to measure voltage difference. Positive tip of the differential probe is attached to the PO/STOP_1 cable between electronics and LEDs as shown in Figure 58. Negative tip of the differential probe is attached to the ground cable between electronics and LEDs as shown in Figure 58. Also, a current probe Keysight N2893A is utilized to measure electrical current pass through the circuit. The current probe is clamp-on current probe whose working principle is based on detecting the magnetic field caused by current flow through Hall effect element [48]. According to direction of current flow,

the current probe is connected to the PO/STOP_1 cable between electronics and LEDs. Both the differential and the current probes are connected to DSO-X3024A Oscilloscope to forward the acquired signal. After the system reaches to steady state, the voltage and current values are measured by the scope.

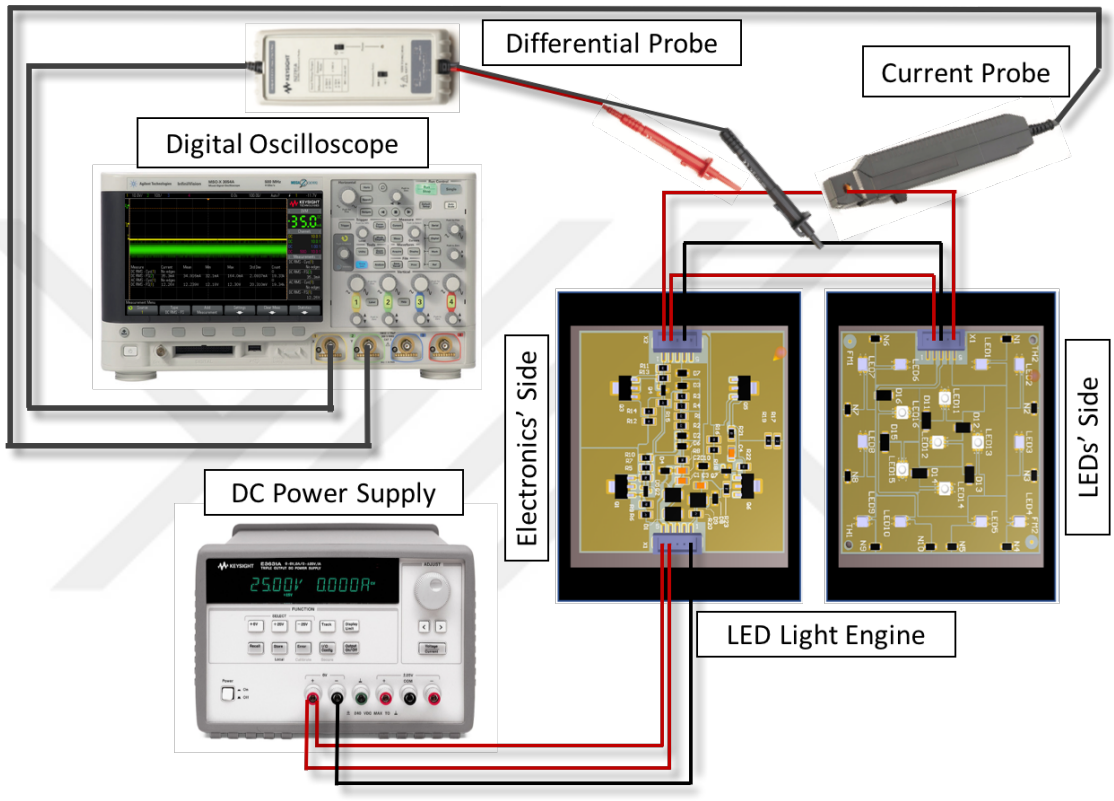

Figure 58: Setup of electrical measurement of red LEDs

According to Ohm's Law, product of measured voltage difference and current gives the total electrical power of the branch. Then, voltage difference and electrical current of the other branch PO/STOP_2 are measured with the same method. To find the total input power that is supplied to red LEDs, measured powers for each branch are summed.

As it is mentioned previously, red chips of the FR4 based LED light engine is driven by 6 different power levels, 0.5W, 1W, 1.5W, 2W, 2.5W and 3W, approximately. Therefore, the measurement is repeated for every power levels. Total input electrical

power of the board and measured input electrical power that is supplied to LEDs is presented in Table 8 for each six cases.

Table 8: Results of electrical measurements of red LEDs

Supplied to All Components			Supplied to Only Red LEDs		
$Voltage$ (V)	$Current$ (mA)	$TotalPower$ (mW)	$Voltage$ (V)	$Current$ (mA)	$TotalPower$ (mW)
11.5	43	494.5	9.1	43.6	395.5
13.0	76	991.3	9.4	78.6	737.3
16.00	93	1488.1	9.5	92.6	878.8
20.2	98	1980.2	9.5	98.0	931.0
24.0	102	2448.4	9.5	102.0	968.0
28.3	105	2971.7	9.5	105.0	996.5

Ratio of the power which is supplied to LEDs to total input power decreases while total input power increases. In the first case, while total electrical input power is 494.5 mW, 80% of the total power is supplied to red LEDs but at the final case, 33.5% of the input power is supplied to LEDs. From Figure 59, it can be also inferred that input electrical power of the red LEDs is decreasingly growing while total electrical power of the engine is increasing linearly.

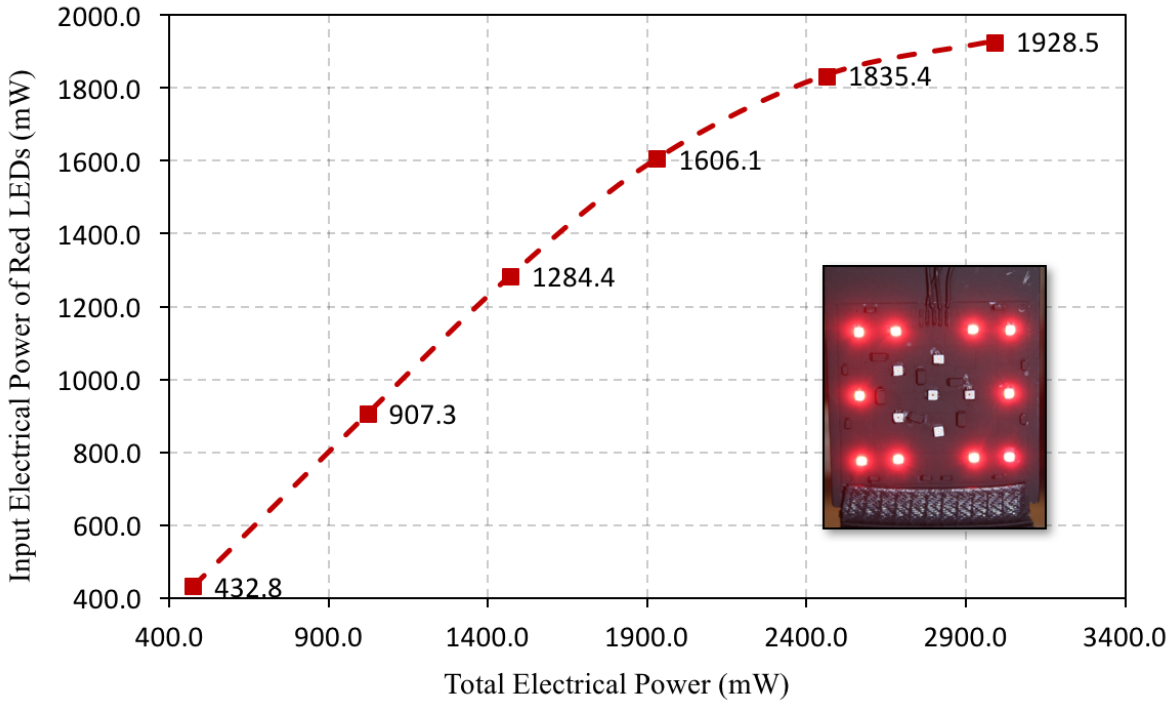

Figure 59: Change in input electrical power of red LEDs while total electrical power increases from 396 mW to 997 mW

5.1.2 Amber LEDs

There are 6 amber LED chips on the light engine. In this case, to understand thermal and optical behavior relation of the amber chips, only amber chips are operated. For optical and thermal experiments, the LED light engines are driven by 0.5W, 1W, 1.5W, 2W, 2.5W and 3W, in total. In order to measure the input power of amber LEDs, electrical measurements are conducted with digital oscilloscope.

In the LED light engine, amber LEDs are connected in series. As it is demonstrated in Figure 60, the SIGNAL branch consists of these 6 amber LEDs.

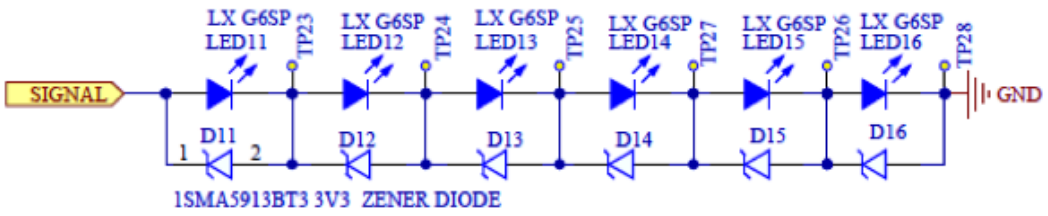

Figure 60: Schematic of electrical circuit of amber LEDs

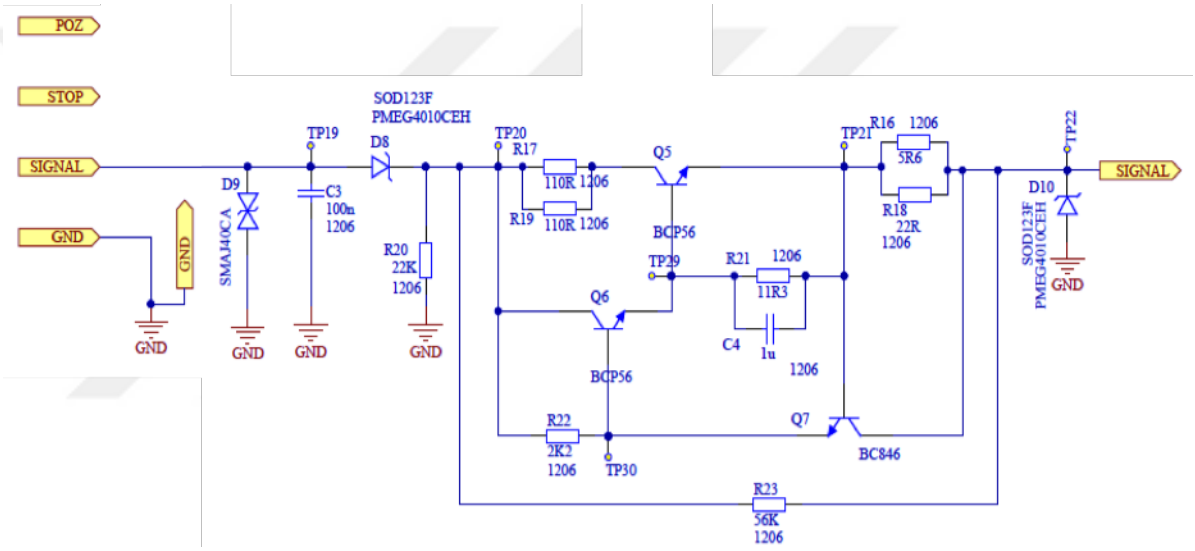

Figure 61: Schematic of electrical circuit of electronic components which are in charge of driving amber LEDs

Input power which is supplied to the amber LEDs is obtained via same method with red LEDs'. Firstly, FR4 based LED light engine is connected to DC power supply. In this case, power is supplied for only amber LEDs and electronic components which are presented in Figure 61.

Positive tip of the differential probe is attached to the SIGNAL cable between electronics and LEDs. Negative tip of the differential probe is attached to the ground cable between electronics and LEDs. According to direction of current flow, the current probe is connected to the SIGNAL cable between electronics and LEDs. Both

the differential and the current probes are connected to the oscilloscope. After the system reaches to steady state, the voltage and current values are measured by the scope. According to Ohm's Law, product of measured voltage difference and current gives the total input power that is supplied to red LEDs.

As it is done for red LEDs, amber chips of the FR4 based LED light engine is driven by 6 different power levels, 0.5W, 1W, 1.5W, 2W, 2.5W and 3W. Total input electrical power of the board and measured input electrical power that is supplied to LEDs is presented in Table 9 for each six case.

Table 9: Results of electrical measurements of amber LEDs

Supplied to All Components			Supplied to Only Amber LEDs		
$Voltage$ (V)	$Current$ (mA)	$TotalPower$ (mW)	$Voltage$ (V)	$Current$ (mA)	$TotalPower$ (mW)
13.55	35	474.3	12.3	35.3	432.8
14.61	70	1022.8	12.7	71.5	907.3
15.15	97	1469.7	13.0	98.8	1284.4
15.95	121	1930.1	13.1	122.6	1606.1
18.10	136	2461.6	13.3	138.0	1835.4
21.20	141	2989.3	13.3	145.0	1928.5

Ratio of the power which is supplied to LEDs to total input power decreases while total input power increases. In the first case, while total electrical input power is 474.3 mW, 91.2% of the total power is supplied to red LEDs but at the final case, 64.5% of the input power is supplied to LEDs. From Figure 62, it can also be inferred that input electrical power of amber LEDs is decreasingly growing while total electrical power of the engine is increasing linearly.

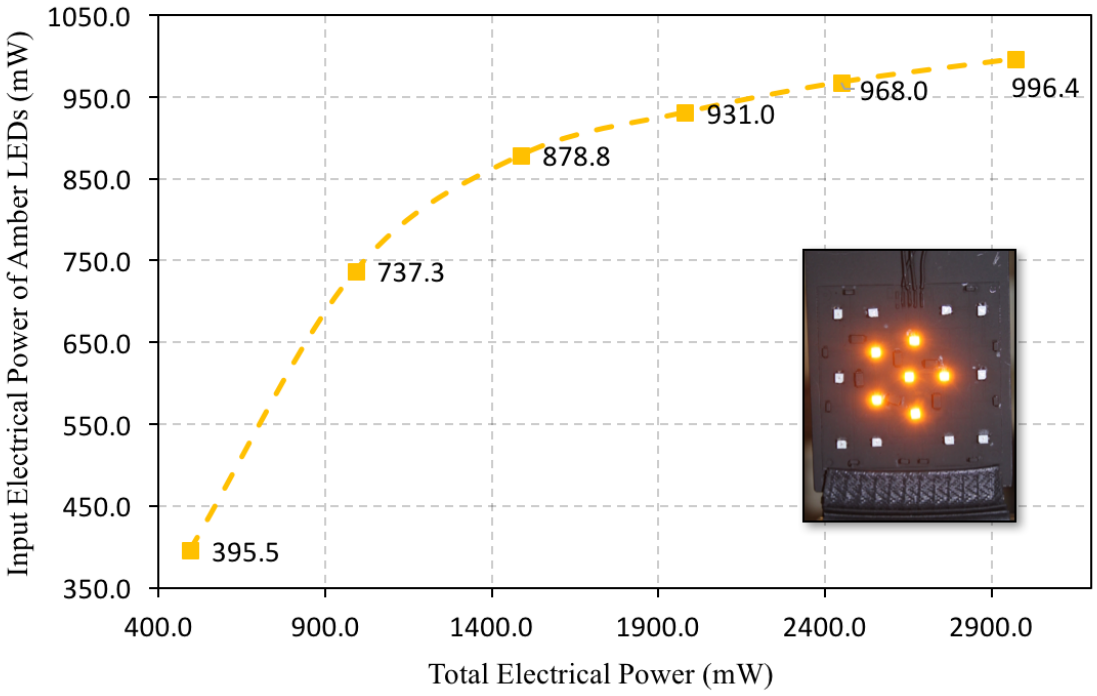

Figure 62: Change in input electrical power of amber LEDs while total electrical power increases from 433 mW to 1929 mW

5.2 Thermal Measurements of Red and Amber LEDs at 6 Different Power Levels

As it is mentioned in previous section, red and amber LEDs are operated separately for six different power conditions. For each LED color and power condition, thermal experiments are conducted to observe change on thermal characteristics of the LED light engine. Thermal experiment are conducted according to experimental procedure which is explained in Chapter II. Firstly, thermal experiment results of the red LEDs were shared and discussed, and then, results of amber LEDs will be analyzed.

5.2.1 Red LEDs

Thermal tests are conducted on FR4 based LED light engine with FR4 PCB when only red LEDs were operated during six different power conditions. At these six

thermal experiments, while total input powers supplied to the LED light engine are 500 mW, 1000 mW, 1500 mW, 2000 mW, 2500 mW and 3000 mW, total input power supplied to red LEDs are 396 mW, 737 mW, 879 mW, 931 mW, 968 mW and 997 mW.

As it is indicated in Figure 63, hot spots over the red LEDs become more critical while input power increases. The electronics that are operated to drive red LEDs are located behind the LED1, LED2, LED3, LED4 and LED5. Therefore, at Figure 63c, d, e, and f, temperature of the right-hand side of the LED light engine which LED1, LED2, LED3, LED4 and LED5 are placed is higher and several local hot spots are observed over these LEDs. Thus, nonuniform temperature distribution is experienced over the LED light engine.

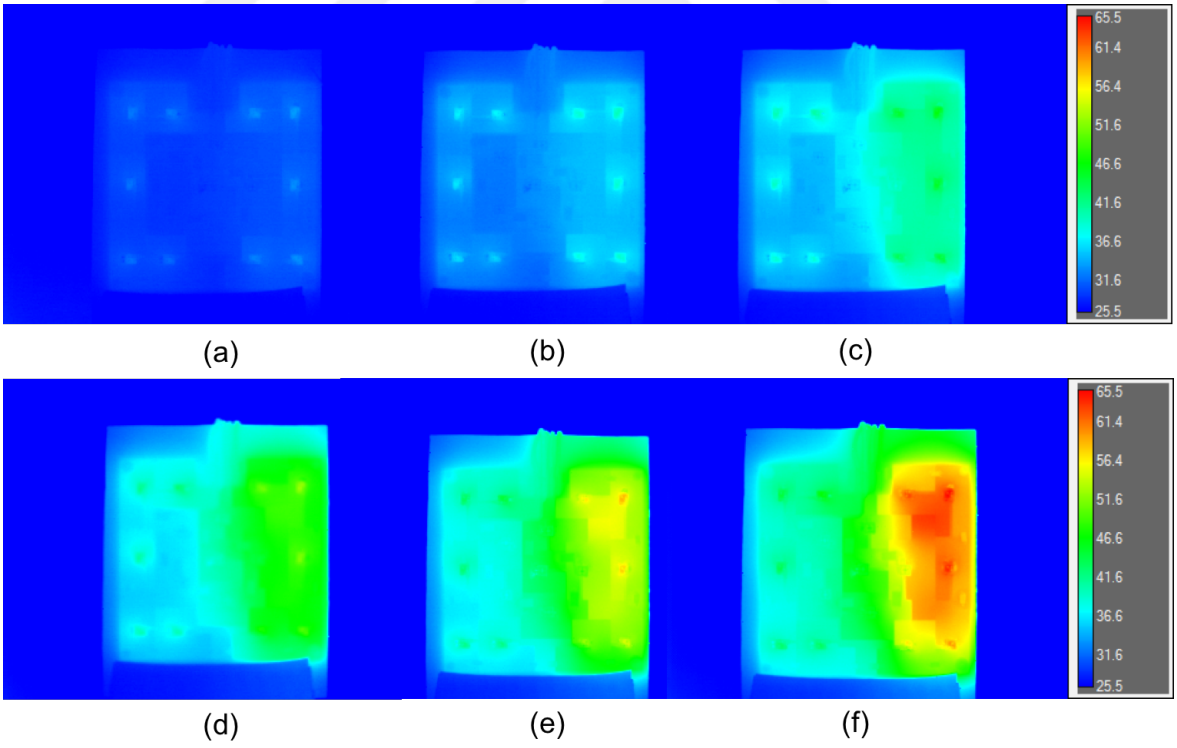

Figure 63: IR thermal images of the LED light engines while input electrical power of red LEDs is (a) 396 mW, (b) 737 mW, (c) 879 mW, (d) 931 mW, (e) 968 mW and (f) 997 mW

Maximum temperatures of the LED 6, 7, 8, 9 and 10 increase linearly with increasing input power as presented in Figure 64. However, maximum temperatures of the LED 1, 2, 3, 4 and 5 increase sharply after the second input power level because of the the heat dissipation from the electronics at the back side. In the graph, slope of the first 5 LED is approximately twice of the slope of the other 5 LEDs.

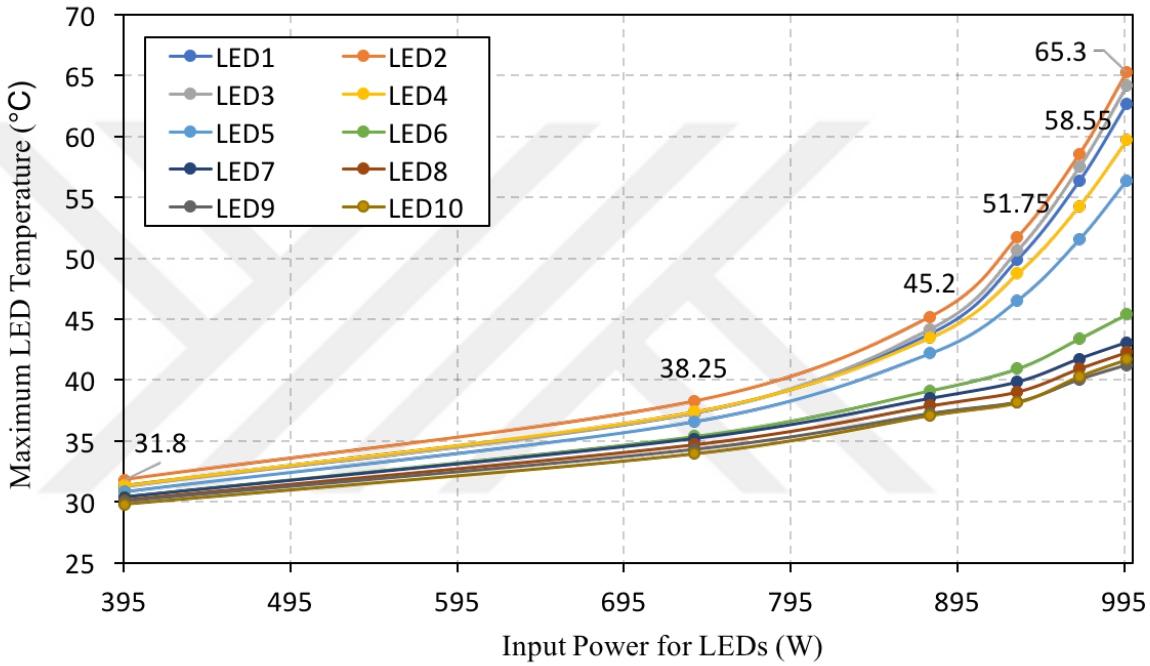

Figure 64: Temperatures of each red LEDs at 6 different power inputs

Figure 65 shows maximum red LED temperature during 6 different experimental conditions. While x-axis shows total heat generation of 10 red LEDs which is calculated from difference of total input power of the LEDs and total radiant flux of the LEDs, y-axis shows temperature of the LED2 which reaches highest surface temperature among the ten LEDs. In addition to input LED power, heat conduction from operated electronics also led to temperature rise of the LED 2. Therefore, increasing rate of the maximum LED temperature is more than increasing rate of the total heat generation.

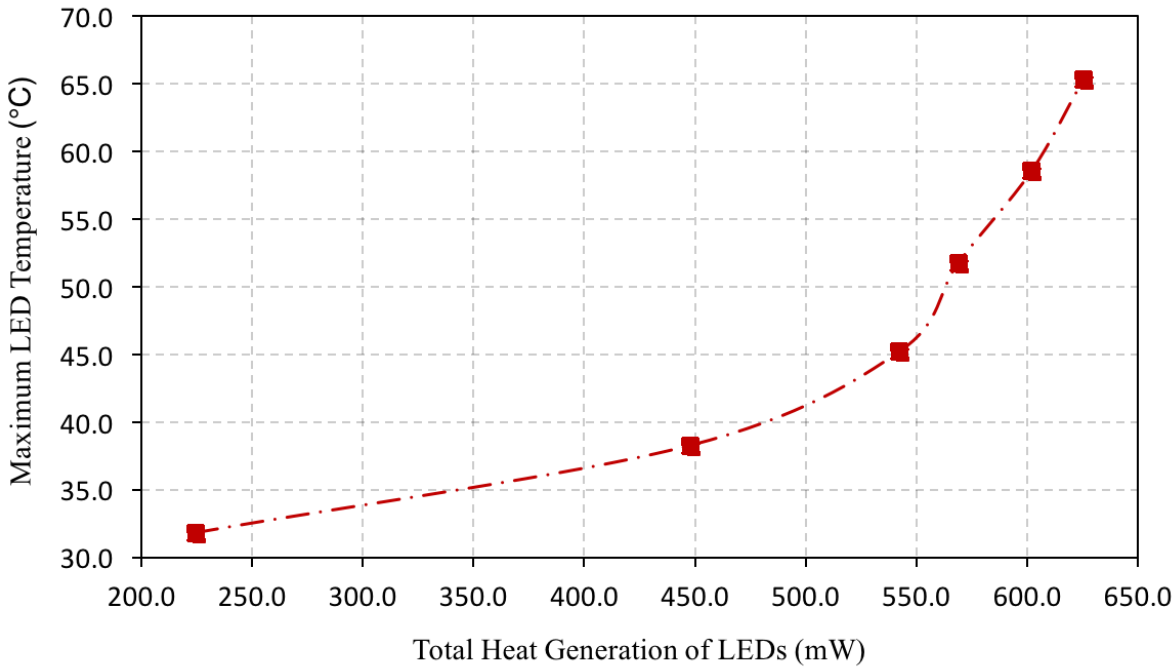

Figure 65: Maximum LED temperature with respect to total heat generation of red LEDs

5.2.2 Amber LEDs

Thermal tests are continued with FR4 based LED light engine with FR4 PCB when only amber LEDs were operated during six different power conditions. At these six thermal experiments, while total input powers supplied to the LED light engine are 500 mW, 1000 mW, 1500 mW, 2000 mW, 2500 mW and 3000 mW, total input power supplied to the amber LEDs are 433 mW, 907 mW, 1284 mW, 1606 mW, 1835 mW and 1929 mW.

Infrared thermal images of the FR4 based LED light engine at different input power levels are presented in Figure 66. It can be inferred from the Figure that local hot spot firstly forms around amber LEDs. Then, while input power starts to increase, hot spots expand to surrounding of these LEDs. Electronics that in charge of driving amber LEDs are located on right-hand side of the electronics side of the engine which

is correspond to left-hand side of the LEDs' side of the engine. Therefore, at last two experiments, temperature of the left hand side becomes higher and local hot spots become more explicit over LEDs 12, 15 and 16.

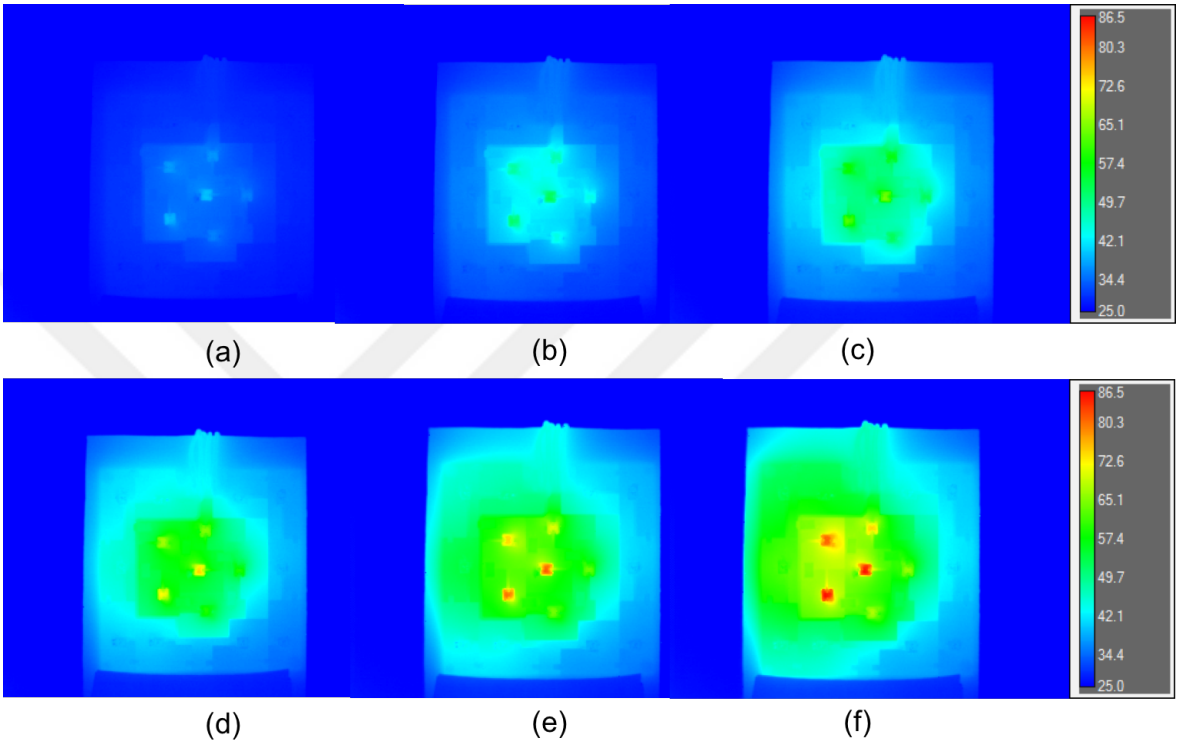

Figure 66: IR thermal images of the LED light engines while input electrical power of amber LEDs (a) 433 mW, (b) 907 mW, (c) 1284 mW, (d) 1606 mW, (e) 1835 mW and (f) 1929 mW

Maximum temperatures of the LEDs increase linearly with increasing input power as presented in Figure 67. However, maximum temperatures of the LED 12, 15 and 16 increase sharply when input power is 1929 mW because of the heat dissipation from the electronics at the back side. LED 12 has the highest temperature as 86.05°Cduring all experimental conditions.

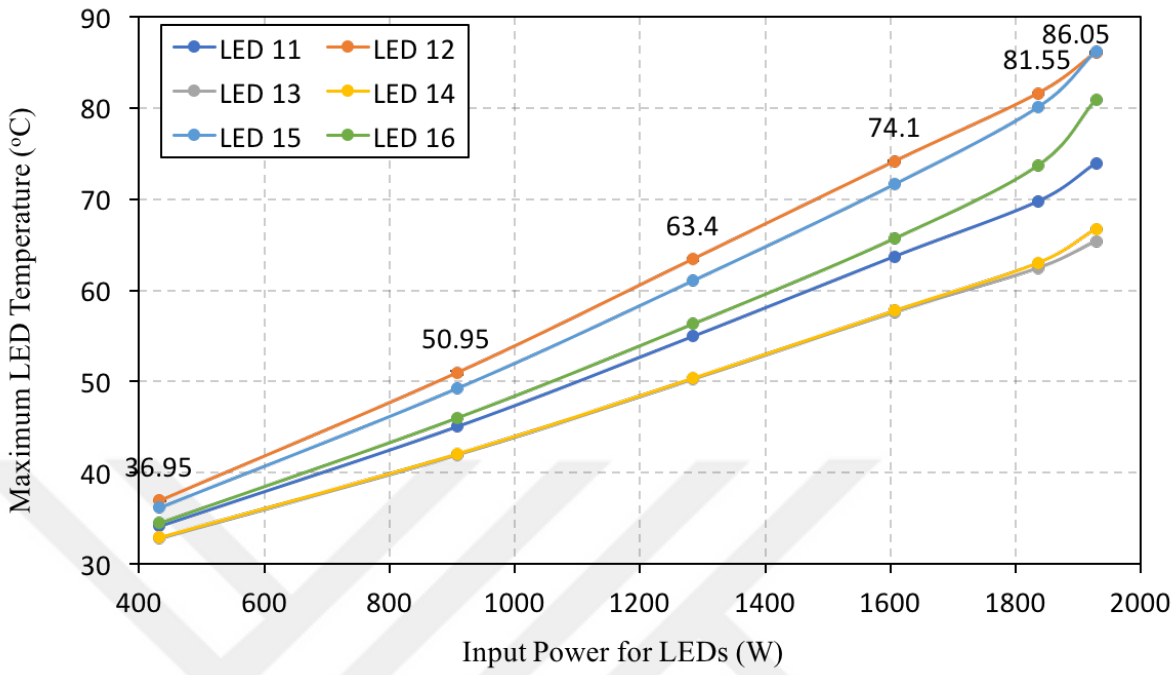

Figure 67: Temperatures of each amber LEDs at 6 different power inputs

Figure 68 shows maximum amber LED temperature during 6 different experimental conditions. While x-axis shows total heat generation of 10 amber LEDs which is calculated from difference of total input power of the LEDs and total radiant flux of the LEDs, y-axis shows temperature of the LED12 which reaches highest surface temperature among the six amber LEDs. In addition to input LED power, heat conduction from operated electronics also led to temperature rise of the LED 12. Therefore, increasing rate of the maximum LED temperature is more than increasing rate of the total heat generation.

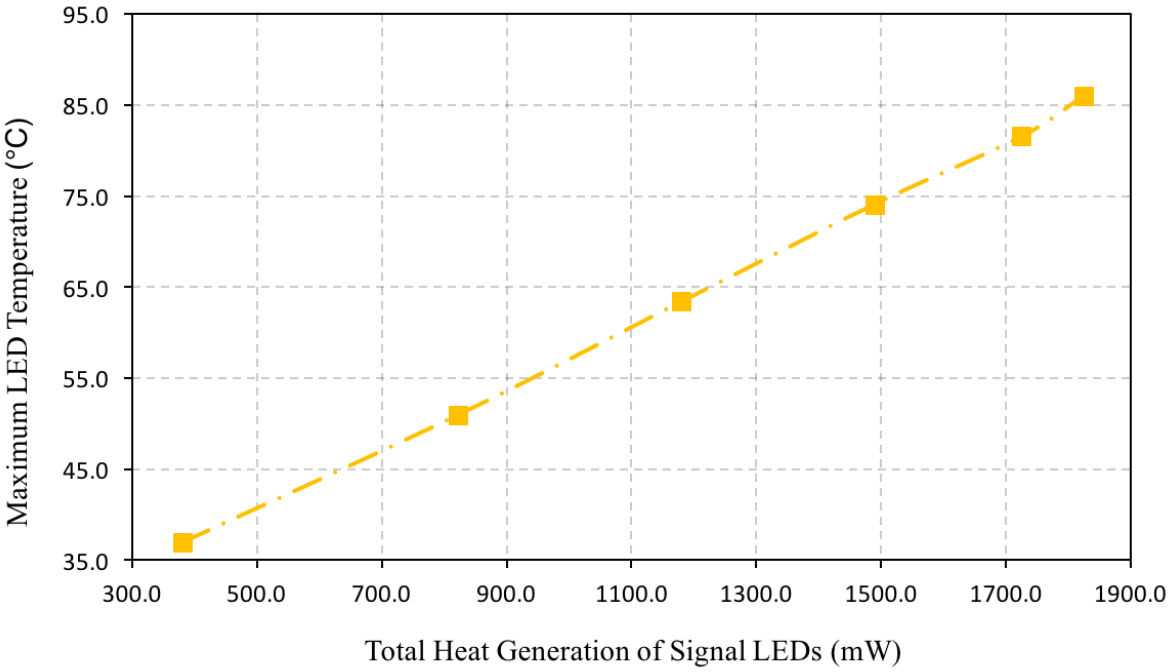

Figure 68: Maximum LED temperature with respect to total heat generation of amber LEDs

5.3 Optical Measurement of Red and Amber LEDs at 6 Different Power Levels

After electrical and thermal experiments, optical experiments are conducted on the same LED light engine to determine photometric and radiometric characteristic of the light engine during six different power conditions. The optical experiments are conducted according to experimental procedure that is explained in Chapter II. First of all, the light engine is tested to understand optical performance change of the red LEDs during input power increases. Then, the light engine is tested to observe optical performance change of the amber LEDs during input power increases.

5.3.1 Red LEDs

Optical experiments conducted on FR4 based LED light engine with FR4 flex PCB while only 10 red LEDs operated under six different power conditions. Optical characteristic differentiation while driven by different input powers are analyzed in this section.

First of all, optical spectrum of the red LEDs at different power conditions are analyzed in Figure 69. As a result of input power of the LEDs increase, peak wavelength shifts towards to right-hand side. While total input power supplied to LED light engine is elevated by 2.5 W, peak wavelength shifts by 4nm. Reason of the peak wavelength shift is energy bandgap shrinking. Bandgap energy is temperature dependent because of electron-phonon interactions and lattice vibrations [15].

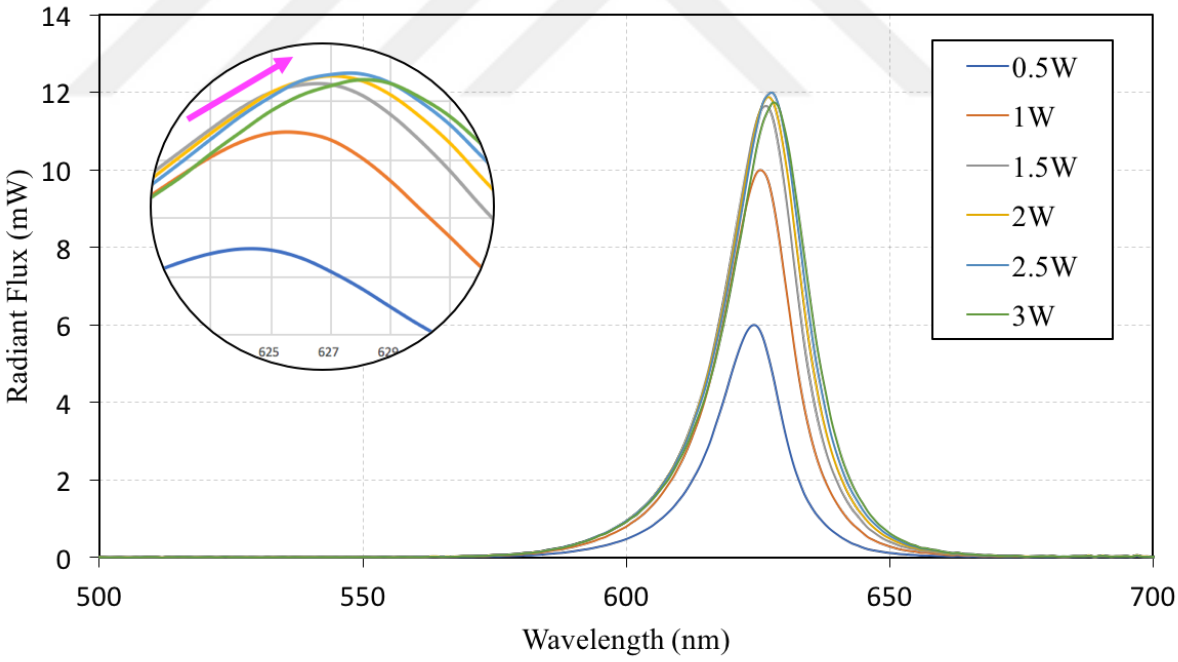

Figure 69: Flux spectrum of red LEDs during six power conditions

Figure 70 demonstrates peak wavelength increment respect to input electrical power of the red LEDs in detail. Peak wavelength raise of the red LEDs accelerates

after third power condition due to junction temperature elevation.

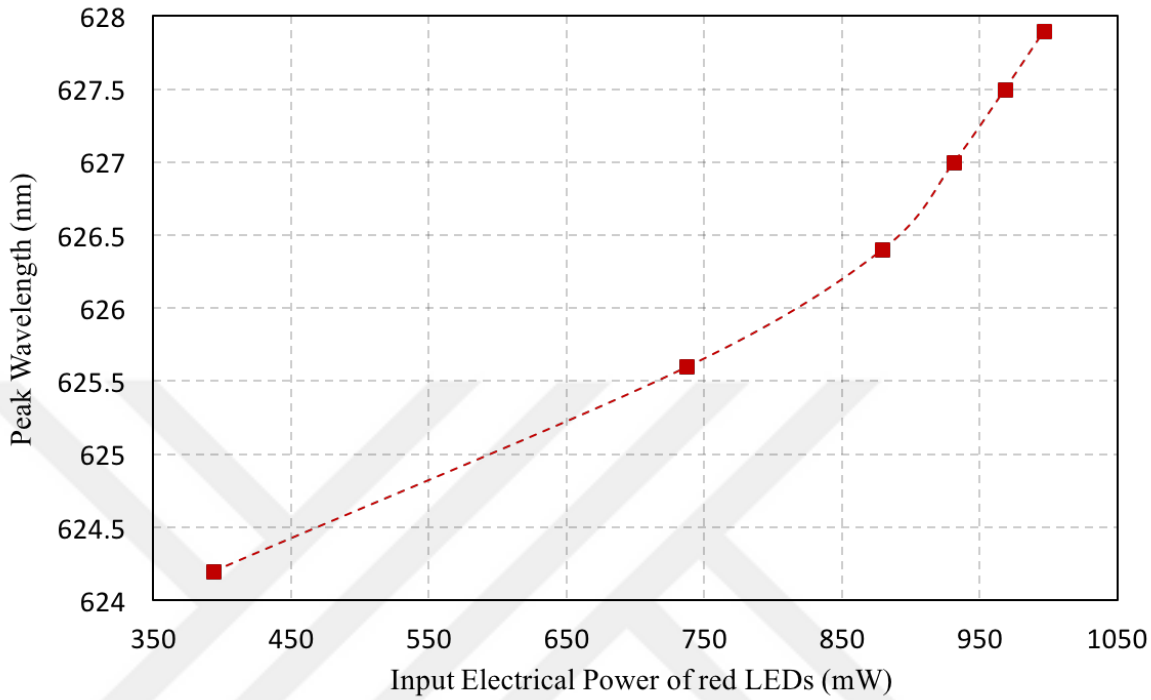

Figure 70: Peak wavelength change while input electrical power of red LEDs increasing from 396 mW to 997 mW

Table 10 presents input electrical power, radiant power, heat generations and luminous flux of the LEDs during six different power conditions.

Table 10: Optical measurement results of red LEDs on the FR4 based LED light engine at 6 different power levels

$InputElectrical\ Powerof Red\ LEDs(mW)$	$Radiant\ Power\ (mW)$	$Heat\ Generation\ (mW)$	$Luminous\ Flux\ (lm)$
395.5	170.9	224.6	28.5
737.3	289.5	447.8	48.6
878.8	336.4	542.4	57.0
931.0	362.1	569.0	58.5
968.0	366.0	602.0	59.4
996.5	371.1	625.4	58.4

Radiant power change respect to input power of the LEDs are presented in Figure 71. Although there is linear relation between radiant flux and input power, at last three power conditions, while input power increases by 7%, radiant flux increases by 2.5%.

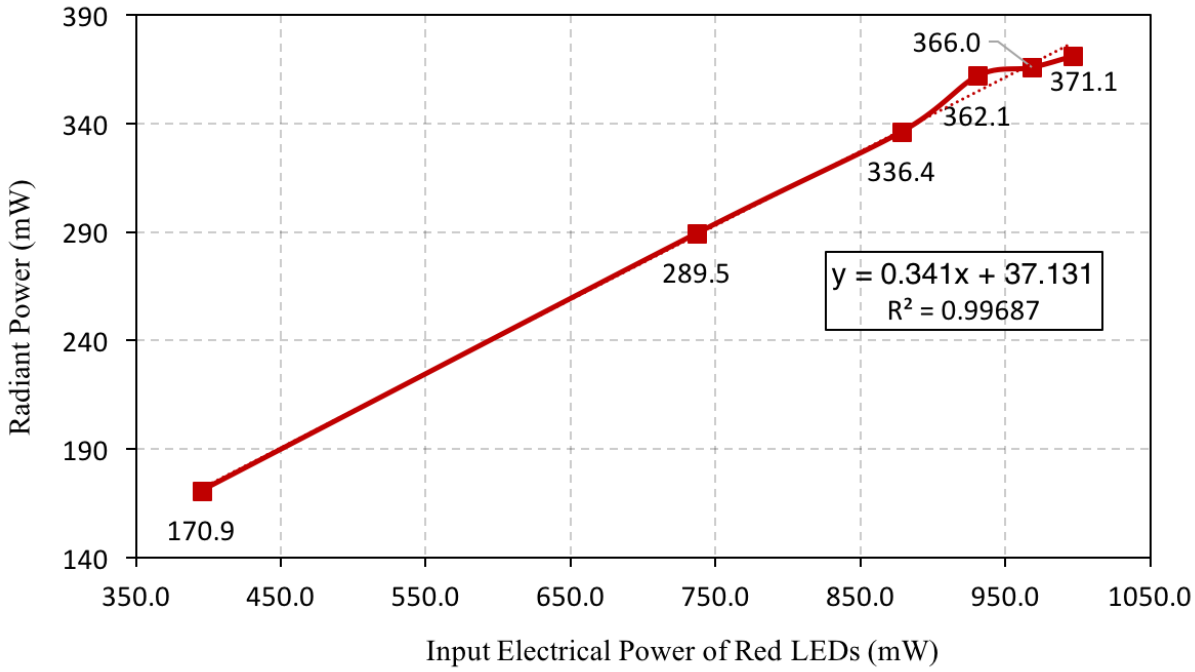

Figure 71: Radiant power change while input electrical power of red LEDs increasing from 396 mW to 997 mW

According to Figure 72, as input power increases from 395.5 mW to 996.5 mW, luminous efficacy decreases by 13.6 lm/W. Sharp fall in luminous efficacy is experienced at last case compared to the first five cases because of the fact that junction temperature of the LEDs increase at most in this case.

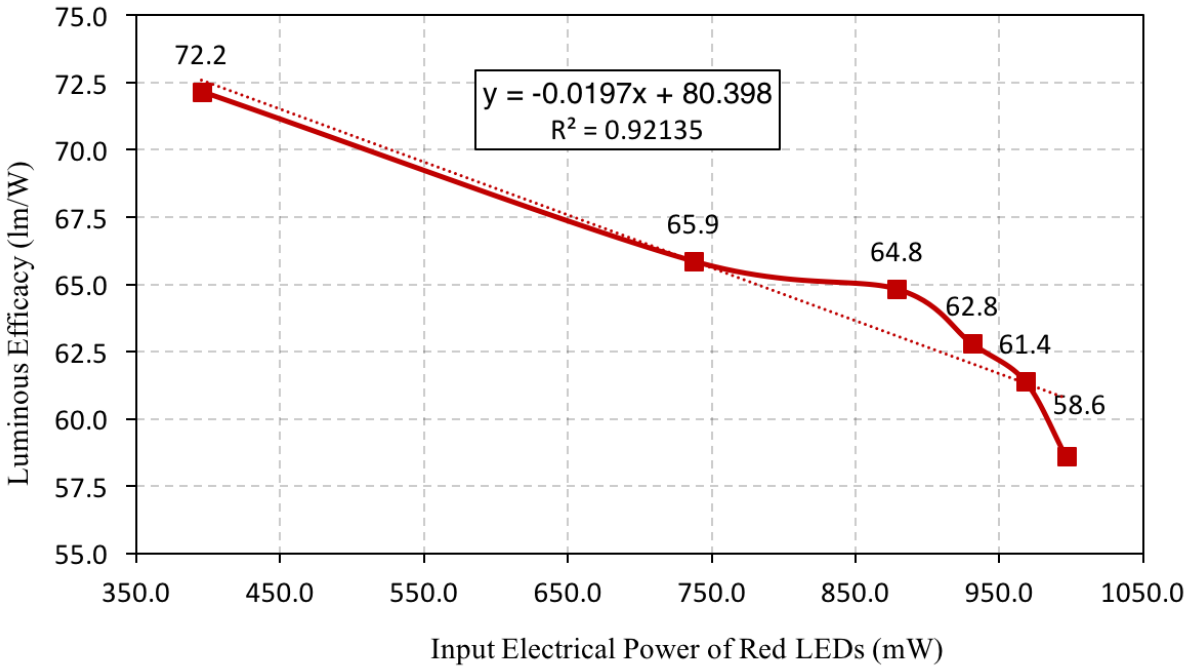

Figure 72: Luminous efficacy change while input electrical power of red LEDs increasing from 396 mW to 997 mW

5.3.2 Amber LEDs

Optical experiments conducted on FR4 based LED light engine with FR4 flex PCB while only 6 amber LEDs operated under six different power conditions. Optical characteristic differentiation of the amber LEDs while driven by different input powers are analyzed in this section.

First of all, optical spectrum of the amber LEDs at different power conditions are analyzed in Figure 73. According to the graph, while input power increases from 0.5 W to 2 W in total, peak wavelength shifts right by 6 nm and radiant flux at peak wavelength increases by 1.7 mW. However, while input power increases from 2 W to 4 W in total, peak wavelength shifts right by 3 nm and radiant flux at peak wavelength decreases by 0.8 mW. Therefore, efficiency decrease can be inferred from relative radiant flux decrease.

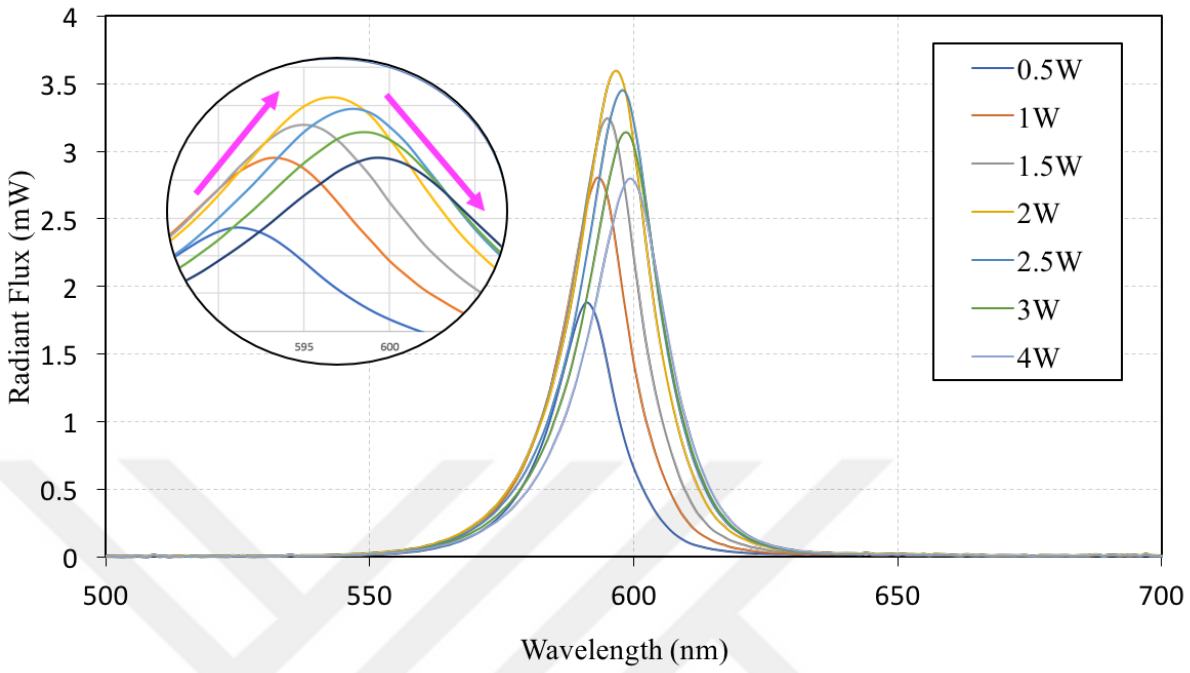

Figure 73: Flux spectrum of amber LEDs

Figure 74 demonstrates peak wavelength increment respect to input electrical power of the amber LEDs in detail. Peak wavelength raise of the amber LEDs accelerates at the last power condition due to junction temperature elevation.

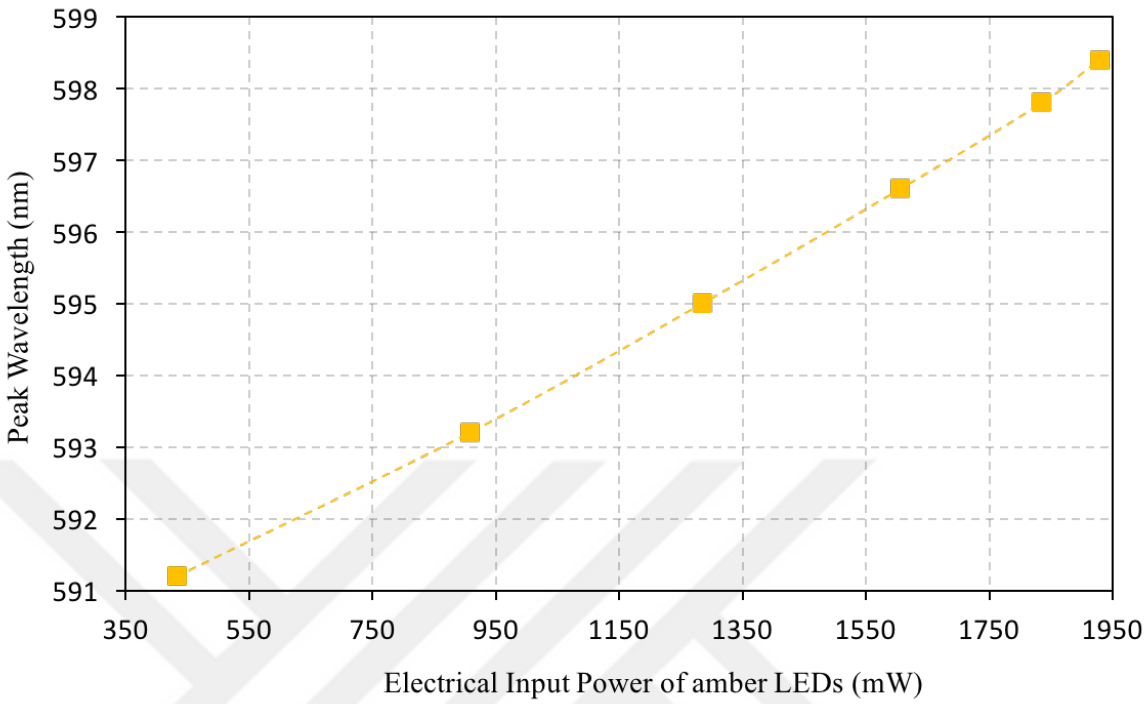

Figure 74: Peak wavelength change while input electrical power of amber LEDs increasing from 433 mW to 1928.5 mW

Table 11 presents input electrical power, radiant power, heat generations and luminous flux of the amber LEDs during six different power conditions.

Table 11: Optical measurement results of amber LEDs on the FR4 based LED light engine at 6 different power levels

$Input Electrical\ Power of Red\ LEDs (mW)$	$Radiant\ Power\ (mW)$	$Heat\ Generation\ (mW)$	$Luminous\ Flux\ (lm)$
432.8	52.7	380.0	17.6
907.3	85.7	821.7	26.9
1284.4	104.8	1179.7	31.5
1606.1	117.0	1489.1	35.4
1835.4	110.8	1724.6	34.1
1928.5	103.0	1825.6	31.1

Radiant power change respect to input power of the LEDs are presented in Figure 71. Radiant flux of the amber LEDs increases until input power reaches to 1606.1 mW. However, after this point radiant flux starts to decrease although input power increases. While input power of the LEDs increasing, junction temperature of the LEDs also increasing due to the ineffective thermal management of FR4 based LED light engine. As a result of the junction temperature elevation, optical output of the LED decreases as in our case. Therefore, increasing input power after 1606.1 mW is not effective to increase radiant flux. Thus, for this case, drive LEDs with around 1600 mW is optimum power level in order to reach maximum radiant flux.

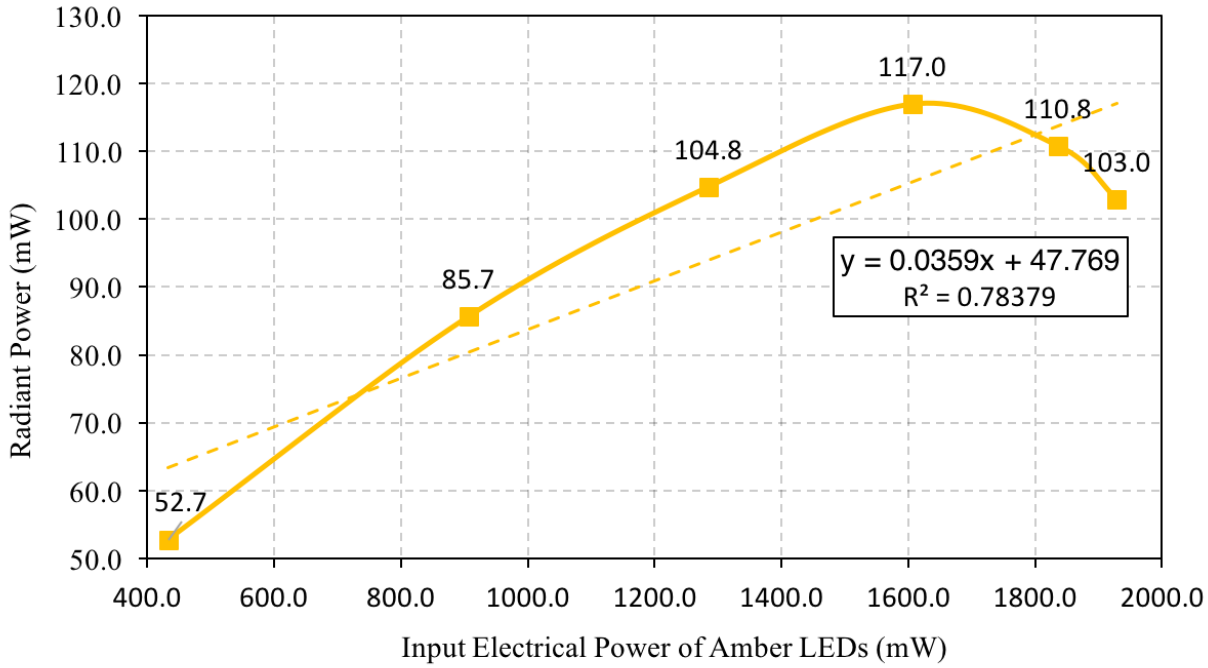

Figure 75: Radiant power change while input electrical power of amber LEDs increasing from 433 mW to 1928.5 mW

According to Figure 76, as input power increases from 432.8 mW to 1928.5 mW, luminous efficacy decreases by 24.6 lm/W. Until forth experimental case, luminous efficacy increases slowly, after that it starts to decrease with positive acceleration. Decreasing in luminous flux causes this luminous efficacy decrease. As a result, power level of 1600 mW is critical for amber LEDs in this study.

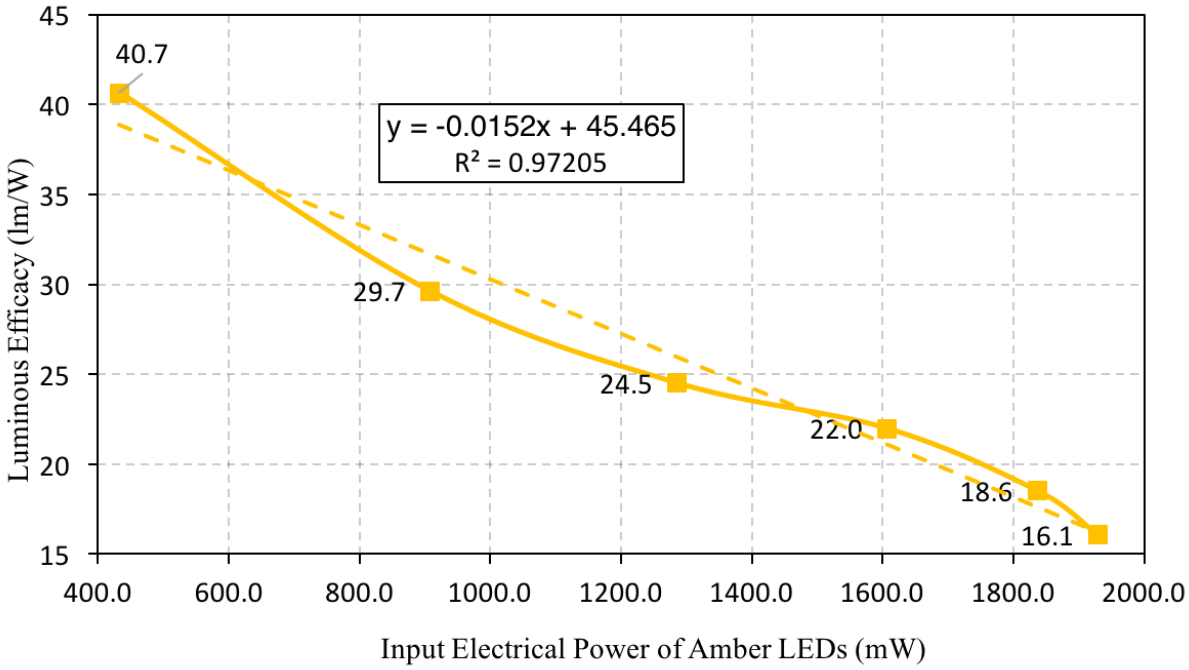

Figure 76: Luminous efficacy change while input electrical power of amber LEDs increasing from 433 mW to 1928.5 mW

5.4 Discussion for Thermal and Optical Performance Relation of LEDs

In this section, thermal and optical experimental results were analyzed to understand the relation between them. Thermo-electro-photometric relation is developed for red and amber LEDs. Discussion for thermo-electro-photometric relation begins with red LEDs and then, it continues with the amber LEDs.

5.4.1 Red LEDs

First of all, relation between thermal and optical performance of the red LEDs that are placed to FR4 based LED light engine is discussed.

As it is represented in Figure 77, heat generation of LEDs increases linearly with

increasing input LED power. However, due to the additional effect of the heat generation of the electronics, maximum LED temperature increase growingly.

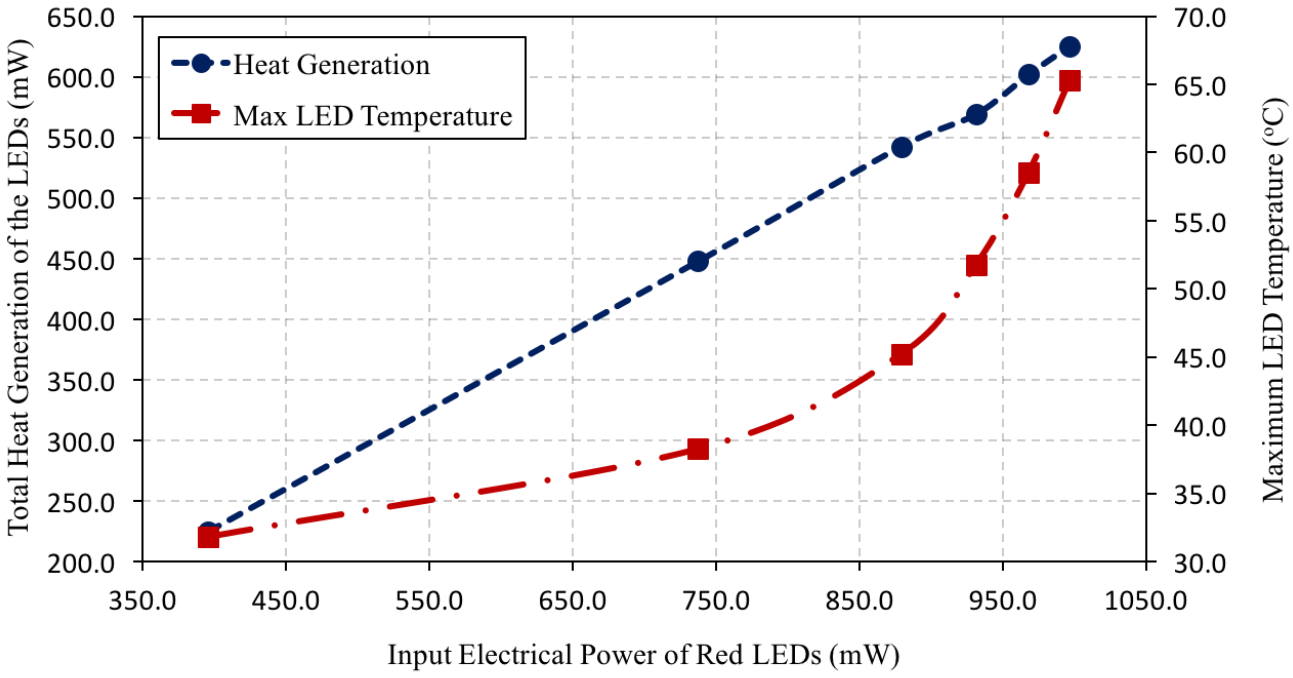

Figure 77: Change in total heat generation and maximum LED temperature with respect to input electrical power of red LEDs

The graph in Figure 78 shows that luminous flux of the red LEDs does not change significantly after input LED power exceeds 879 mW. Thus, driving LEDs with the input power higher than 879 mW is ineffective for this lighting system. As it is represented in the graph, after 879 mW input power, increasing rate of the maximum temperature rises. Therefore, inverse relationship between junction temperature and luminous flux can be inferred from the graph.

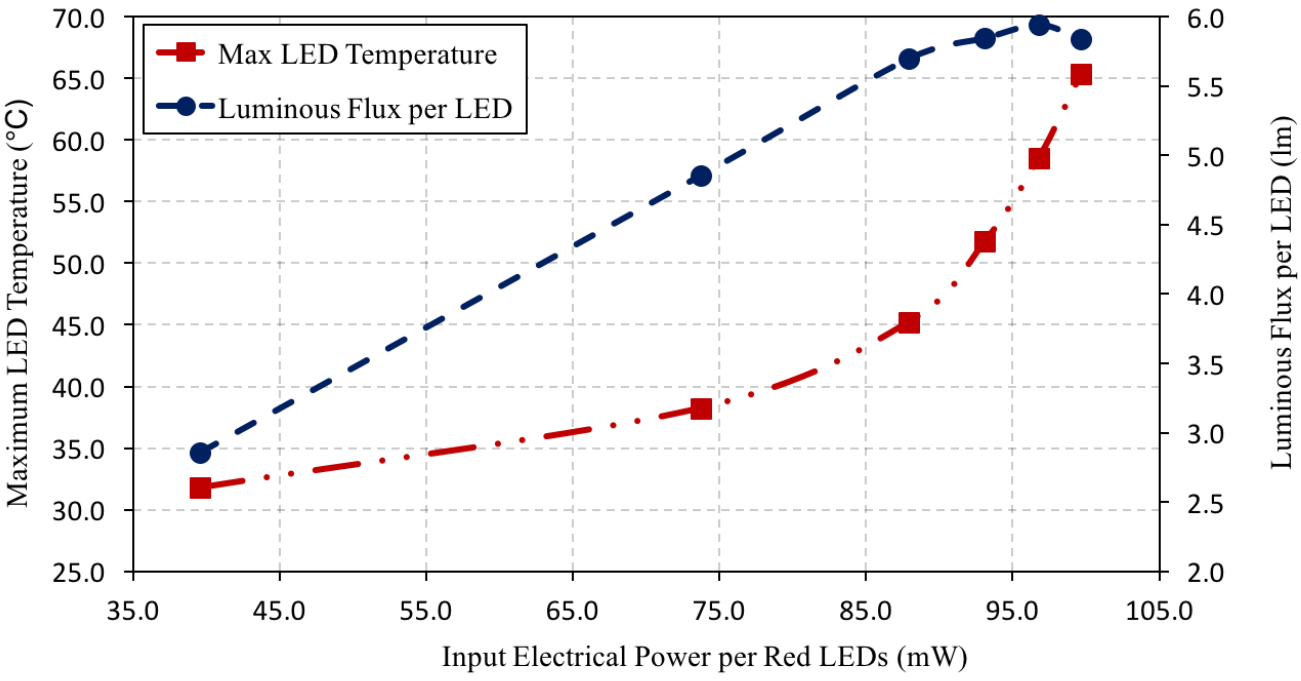

Figure 78: Change in luminous flux per LED and maximum LED temperature with respect to input electrical power of red LEDs

Input electronic power transforms into radiant flux and heat. The amount of the heat generation alters according to performance of the cooling technologies in lighting systems. The bar chart in Figure 85 indicates the portion of the radiant flux and heat generation of the red LEDs. While input power of the red LEDs is 395.5 mW, 43% of the electrical power turns into radiant flux. However, as input power of the red LEDs is 996.5 mW, 37% of the electrical power turns into radiant flux. Consequently, conversion rate of the red LEDs decreases 6% because of junction temperature increase.

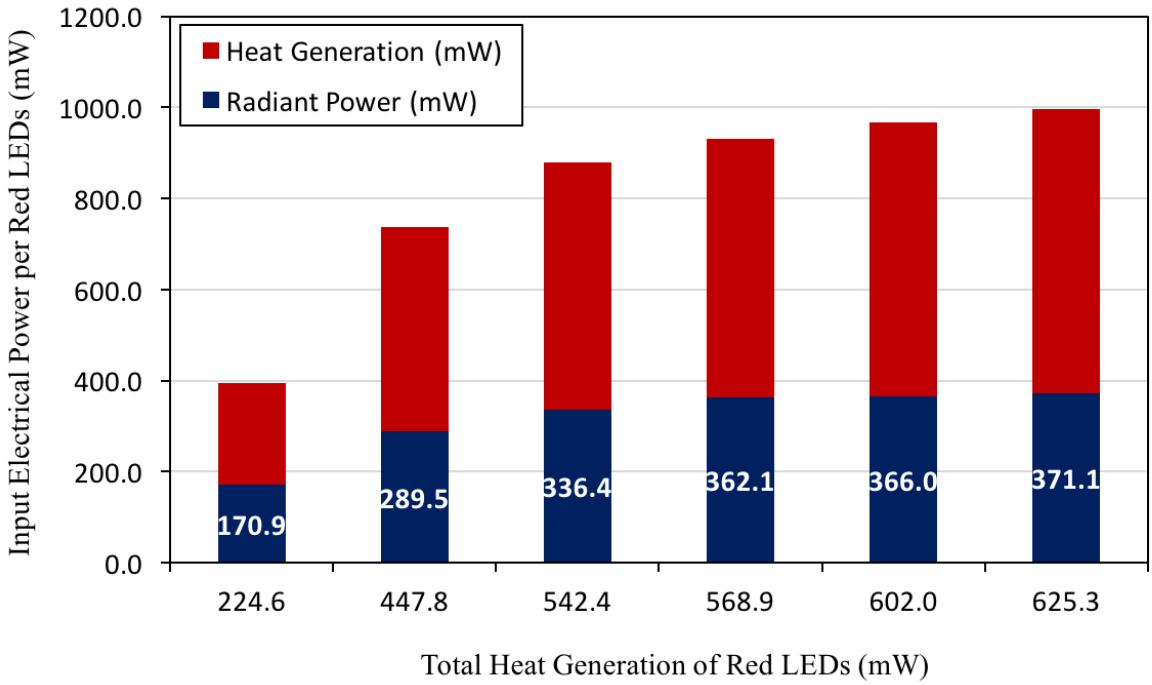

Figure 79: Amount of heat generation and radiant flux of the red LEDs in six different experimental conditions

As mentioned in literature review, LEDs can convert more amount of power to radiant flux than conventional lighting fixtures. Although LEDs can transform 20% of the electrical input power to radiant flux in average, this value can vary by color and junction temperature of the LED. Therefore, in this study, conversion rate of the LED at different junction temperatures for both red and amber LEDs were obtained. Conversion rate measures that a LED can turn what percentage of the electrical input power into radiant flux. It is calculated by radiant flux of the LED divided by input power of the LED and multiply the answer by 100 as represented in equation below.

$$Conversion\ rate\ (\%) = \frac{Radiant\ flux}{Input\ power} \times 100 \tag{16}$$

Conversion rate is plotted with respect to maximum LED temperature at six different power levels. From the relation between maximum surface temperature of the

LED and conversion rate, a correlation is developed. While maximum temperature increases, conversion rate of the LED decreases. This correlation enables to determine radiant flux of the red LED whose maximum surface temperature and input power are known. While this correlation is generated, multi-chip LED board is used and it is assumed that all LEDs have identical radiant power and LED temperature. However, due to nonuniform heat distribution, LEDs have different radiant flux and temperatures. Therefore, it should be considered that this assumption led to some uncertainties.

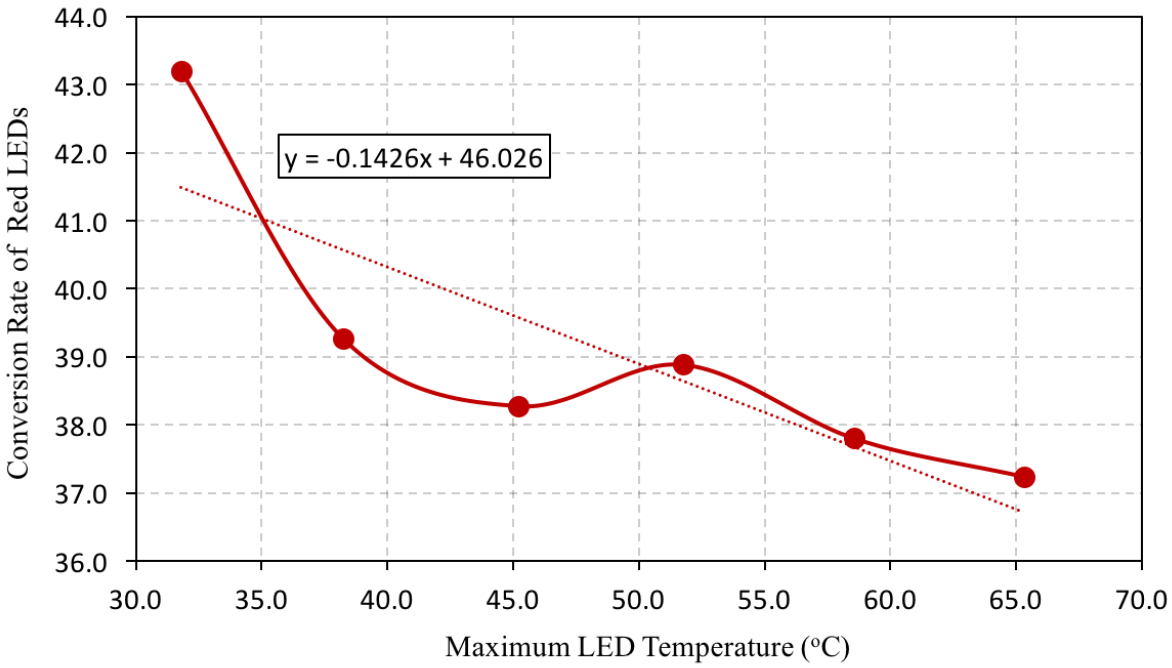

Figure 80: Relation between maximum LED temperature and conversion rate of red LEDs

5.4.2 Amber LEDs

Secondly, relation between thermal and optical performance of the amber LEDs that are placed to FR4 based LED light engine is discussed.

As it is demonstrated in Figure 77, heat generation of LEDs increases linearly with

increasing input LED power. In addition, maximum LED temperature also increases linearly with increasing input LED power.

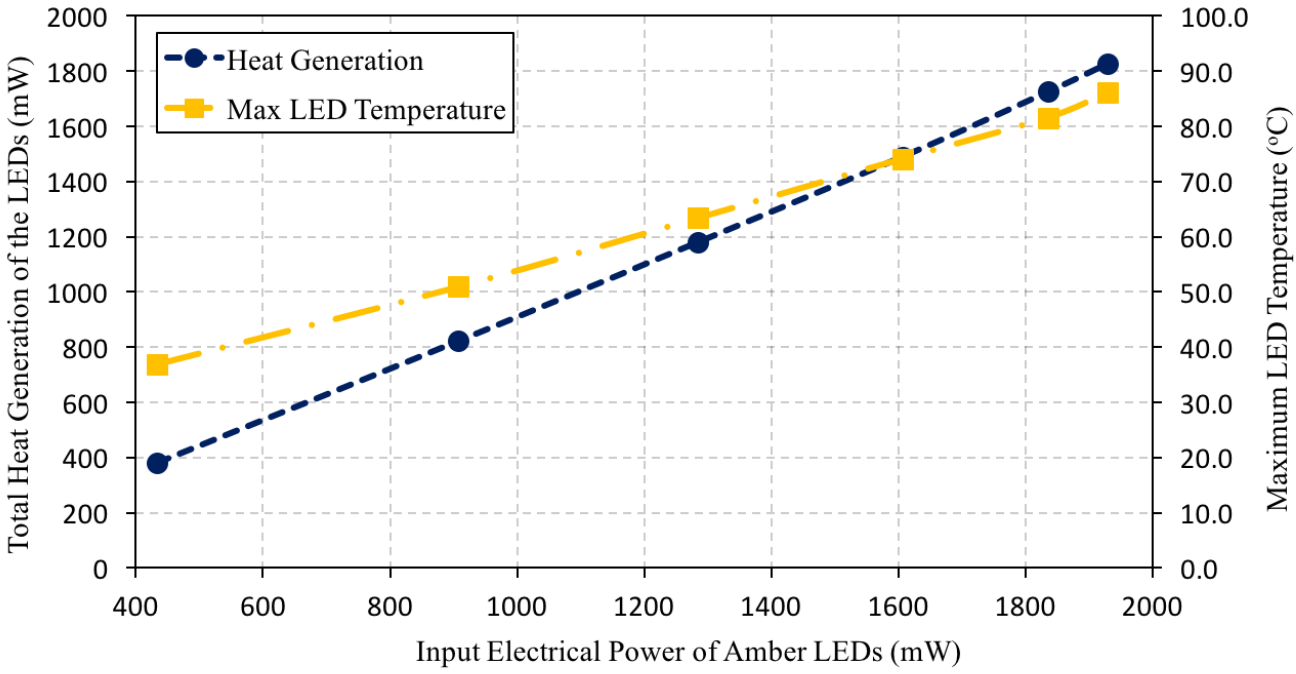

Figure 81: Change in total heat generation and maximum LED temperature with respect to input electrical power of amber LEDs

Similar trend of red LEDs for change of luminous flux and maximum LED temperature with respect to input LED power is also observed for amber LEDs. The graph in Figure 82 shows that luminous flux of the amber LEDs starts to decrease after input LED power exceeds 1606.1 mW. Thus, driving LEDs with the input power higher than 1606.1 mW is ineffective for this lighting system. As it is represented in the graph, at last power condition, increasing rate of the maximum temperature slightly rises.

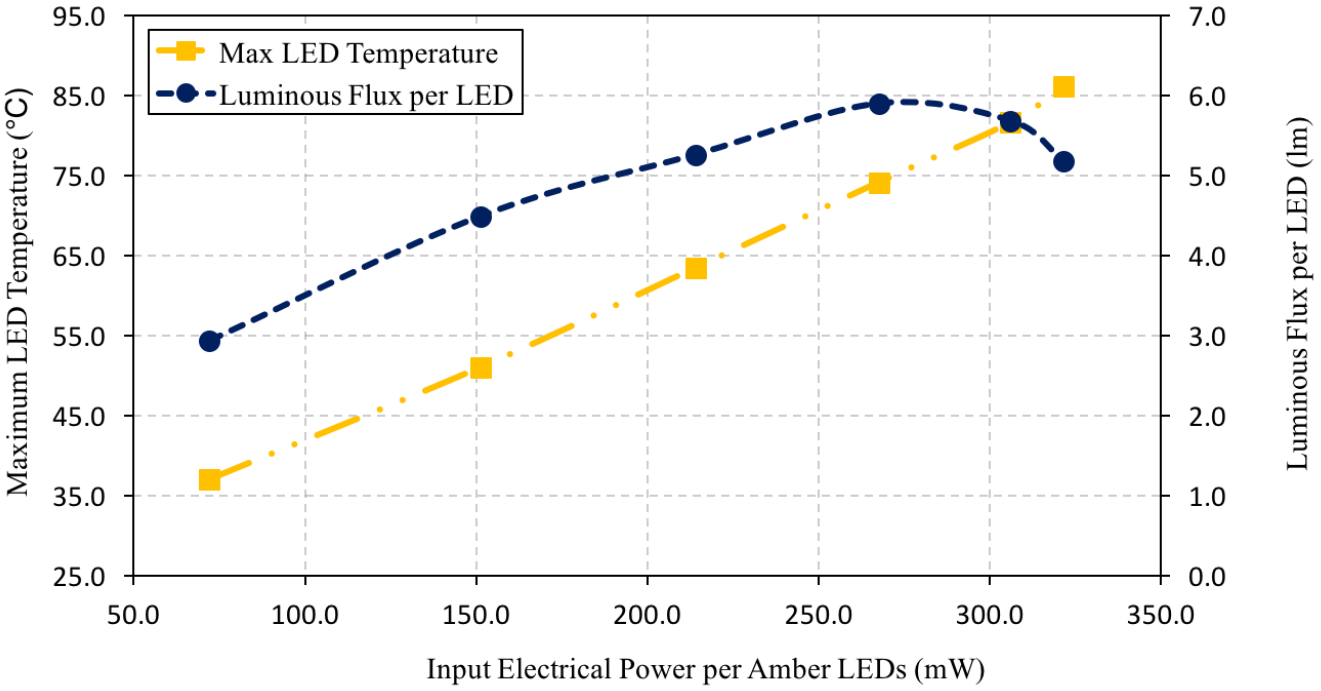

Figure 82: Change in luminous flux per LED and maximum LED temperature with respect to input electrical power of amber LEDs

While heat generation increase linearly with increasing input power, radiant flux decreases after 1606.1 mW input power. Effect of the heat dissipation from the electronics may cause more elevation on junction temperature of the LEDs so optical efficiency of the LEDs drops significantly. Overall, inverse relationship between junction temperature and radiant flux can be understood from the graph.

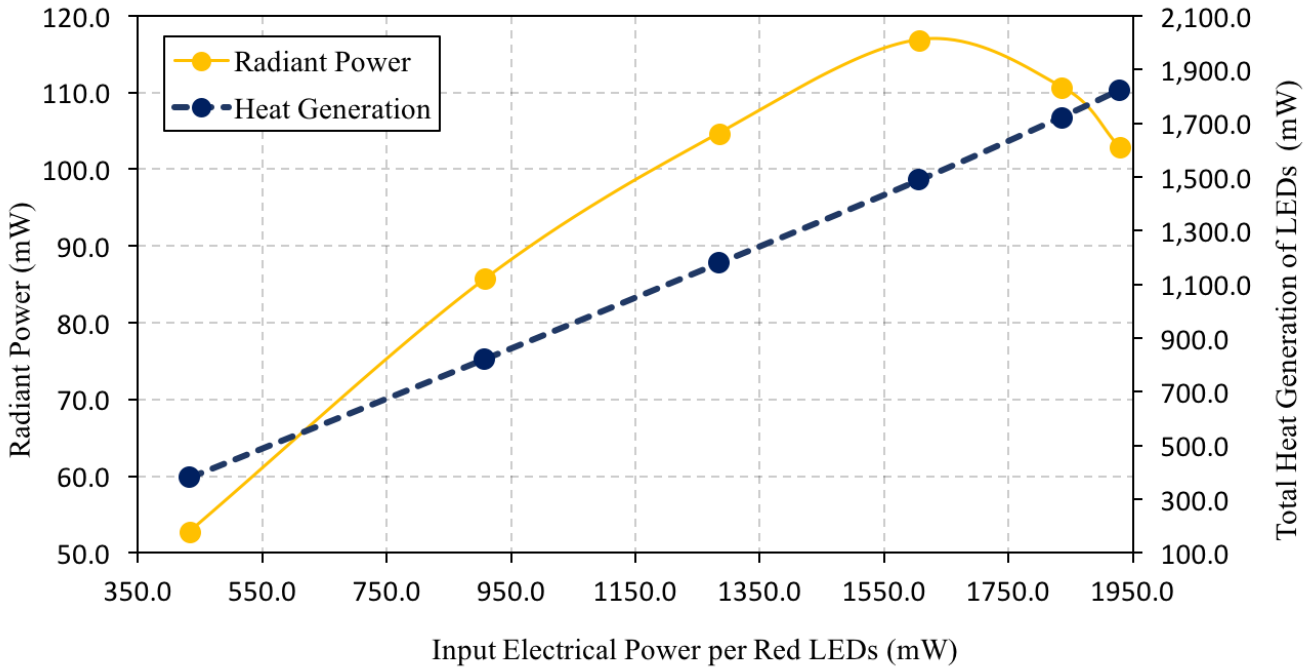

Figure 83: Change in radiant power and total heat generation with respect to input electrical power of amber LEDs

The bar chart in Figure 84 shows the portion the radiant flux and heat generation of the amber LEDs. While input power of the amber LEDs is 432.8 mW, 12% of the electrical power turns into radiant flux. However, as input power of the amber LEDs is 1928.5 mW, 5% of the electrical power turns into radiant flux. Consequently, conversion rate of the amber LEDs decreases 7% because of junction temperature increase.

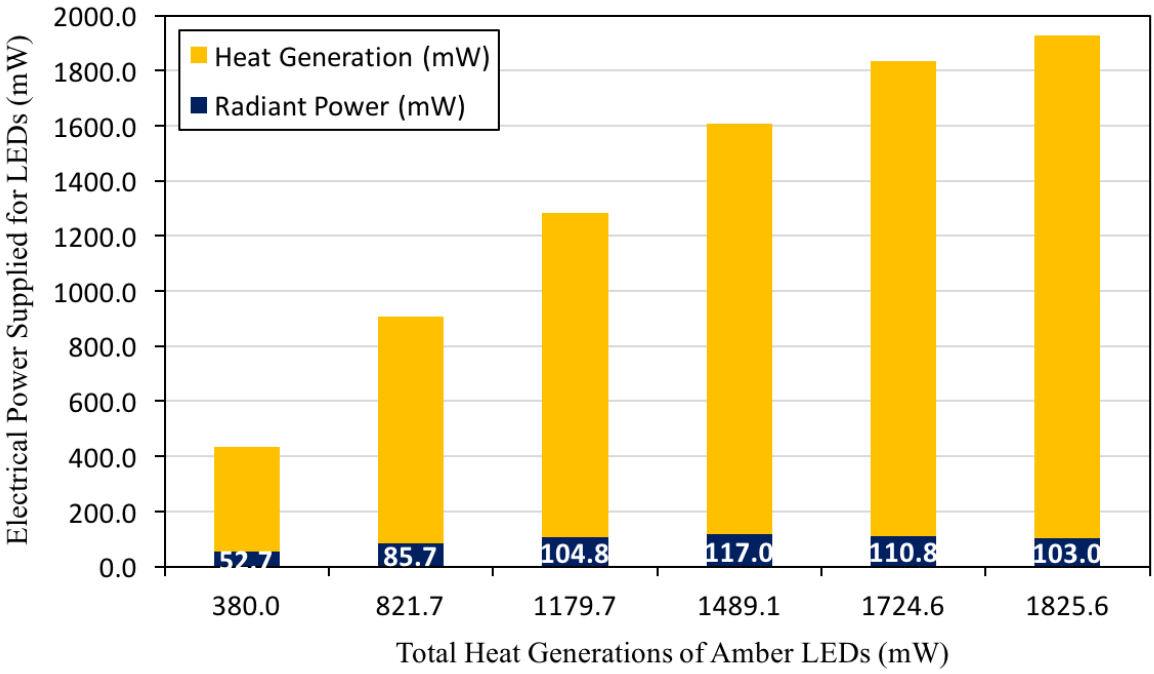

Figure 84: Amount of heat generation and radiant flux of the amber LEDs in six different experimental conditions

Figure 85 reveals that there is inverse proportion between conversion rate and maximum LED temperature of the amber LEDs. As maximum temperature rises, conversion rate of the amber LEDs decreases. It can be said that a downward trend of the conversion rate is quite linear.

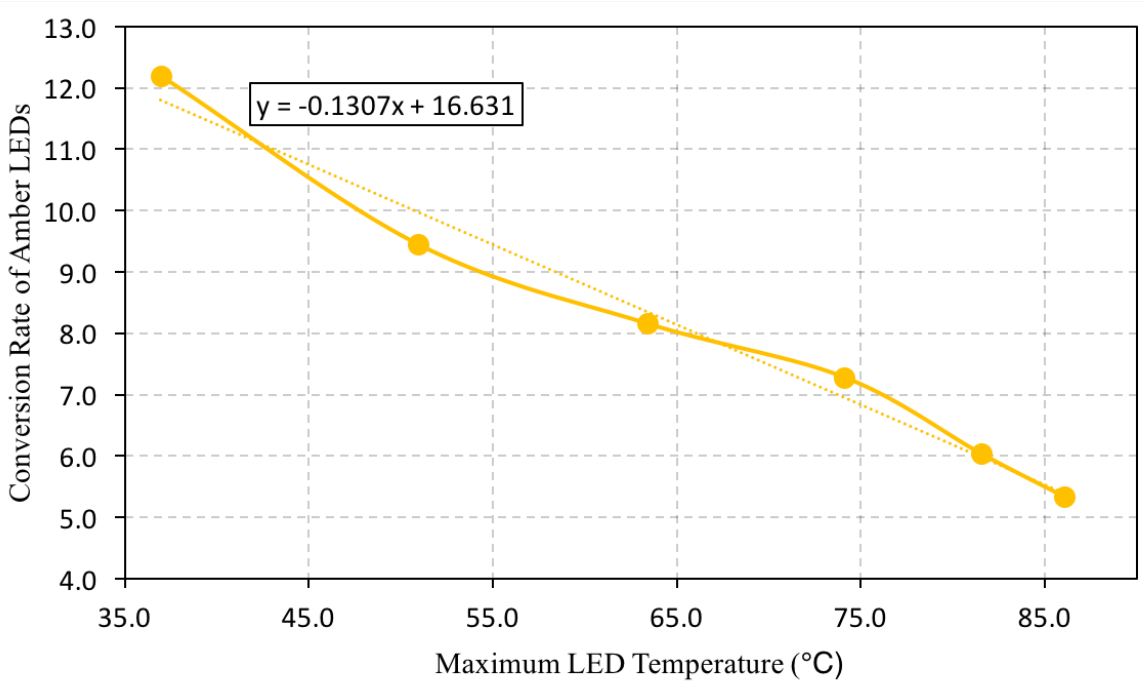

Figure 85: Relation between maximum LED temperature and conversion rate of amber LEDs

CHAPTER VI

COMPUTATIONAL THERMAL MODELS

A computational study has been performed to understand the impact over electronics components and LEDs providing the local temperature distribution. LED light engines populated with LEDs and electronics components are modeled by utilizing a commercial computational fluid dynamics (CFD) software (ANSYS Icepak 14.5) [49].

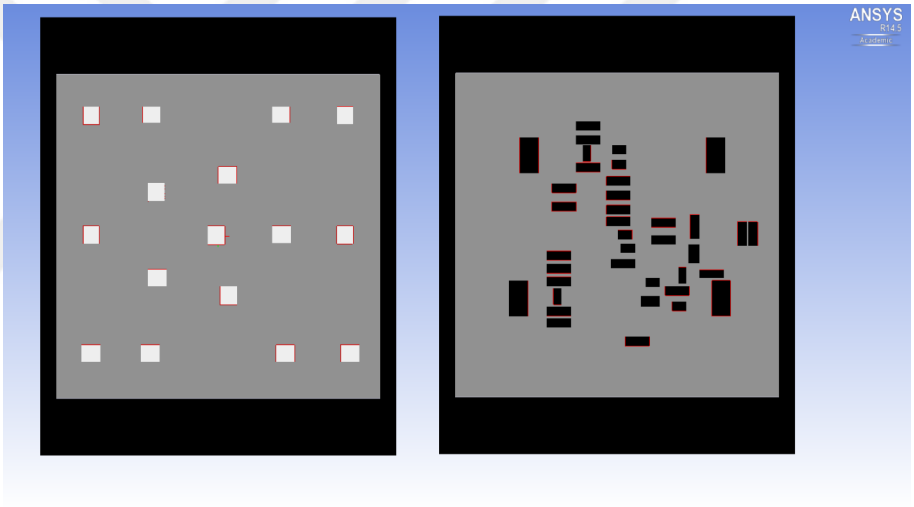

Figure 86: CFD model of the FR4 based board with LEDs and electronics

To achieve reliable solution in short computational time, computational models of the light engines are simplified in the computational model. Two different computational models are created for LED light engine with FR4 flex PCB and LED light engine with multilayer ceramic flex PCB. First of all, FR4 based LED light engine with FR4 flex PCB is modeled in the computational environment. In the computational model, substrate material is chosen as copper clad FR4 with thermal conductivity of 1 W/m-K. FR4 flex PCB is modeled as two layers which are 160 μm

FR4 and 40 μ m copper trace layers. While thermal conductivity of FR4 layer is 0.35 W/mK, thermal conductivity of copper trace layer is 50 W/mK. Copper layer in the flex PCB is not a monolith layer. There is only copper part under the electronic components and LEDs to provide electrical connection and the other parts of the layer is made of FR4. Therefore, effective thermal conductivity of the layer is calculated with respect to ratio of footprint areas of copper and FR4 material. LEDs and electronic components are modeled as rectangular blocks with identical dimensions of original components. To ensure heat generation of LEDs and electronic components, two-dimensional (2-D) heat sources are placed inside the LEDs and electronic components. Also, aluminum based LED light engine is modeled via only changing substrate material of the FR4 based LED light engine with FR4 flex PCB. Instead of copper clad FR4 substrate with 1 W/mK, Aluminum 6061-T6 is used as substrate material. Then, advanced heat spreader based LED light engine with FR4 flex PCB is modeled. Its substrate has orthotropic thermal conductivity due to thermal characteristics of the vapor chamber. Therefore, on x-plane and y-plane of the substrate, thermal conductivity is assigned as 4000 W/mK and on z-plane, thermal conductivity is assigned as 250 W/mK in computational model.

Secondly, FR4 based LED light engine with multilayer ceramic flex PCB is modeled with the same approach. Modeled multilayer ceramic flex PCB has identical physical and thermal properties with the original LED light engine. Details of the computational models can be seen from Table 13.

Table 12: Properties of the computational model of the LED light engines

Description of the LED light engine	*Thermal Conductivity of Substrate (W/mK)*	*Type of Flex PCB*	*Thermal Conductivity of Flex PCB(W/mK)*	*Thickness of the PCB Layer(μm)*
FR4 based LED light engine	1	FR4	50 (Cu trace) + 0.35 (FR4)	40 160
Al based LED light engine	167	FR4	50 (Cu trace) + 0.35 (FR4)	40 160
Adv. Heat Sp. based LED light engine	4000(k_x) 4000(k_y) 250(k_z)	FR4	50 (Cu trace) + 0.35 (FR4)	40 160
FR4 based LED light engine	1	Ceramic	0.8 (Adhesive) 400 (Copper x2) 4.1 (Ceramic)	127 70 x 2 152

In order to increase the mesh accuracy and decrease the computational time, separate assemblies are created for all LEDs and electronic components. In addition, an inclusive assembly which comprises of the components assemblies, flex PCBs and substrate is created. Non-conforming cell structure with unstructured mesh type is generated (see Figure 87).

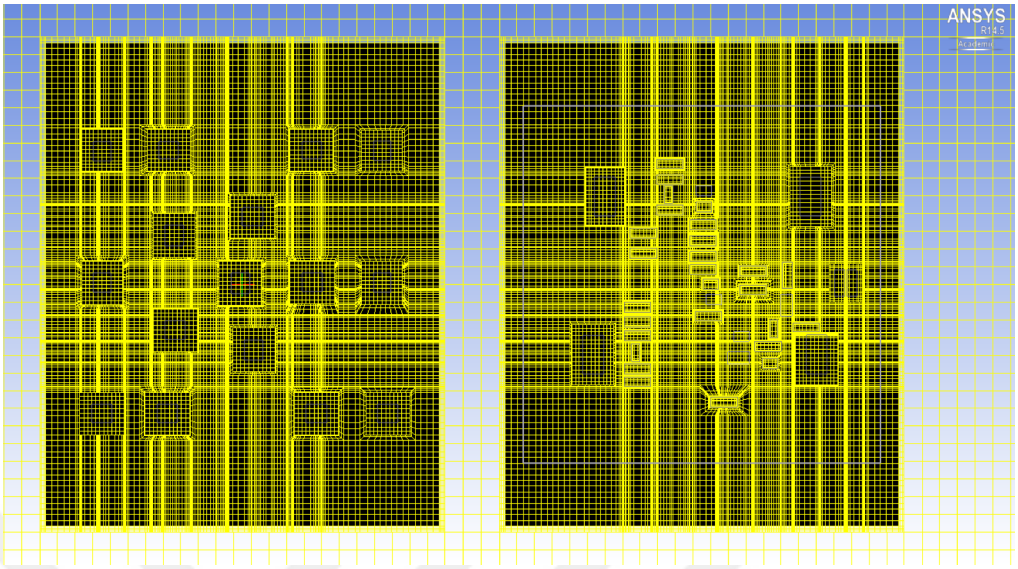

Figure 87: CFD model of the board with mesh structure

As it is presented in Table 13, mesh sensitivity analysis is conducted to computational model of the FR4 based LED light engine with the multilayer ceramic flex PCB. As a result of the sensitivity test, only 0.02% difference is obtained after grid size of 1.8E+06. Therefore, mesh independency of the model is proven with mesh sensitivity analysis.

Table 13: Mesh sensitivity analysis

Grid Size	*Maximum Temperature on LED6 (C)*
1.8E+06	62.0
2.2E+06	62.0
3.0E+06	62.0
4.2E+06	62.0

In order to validate the experimental results, computational study is also conducted and results are compared with the experimental data. As it is presented in

Figure 88 and Figure 89, similar temperature distribution is observed in experimental and computational results. While maximum temperature observed on LEDs' side is obtained 105.0°C as a result of experimental study, it is obtained as 103.3°C in computational study. On the other side of the light engine, maximum component temperature is experienced as 95.9°C in experimental study while it is obtained as 105.5°C in the computational study.

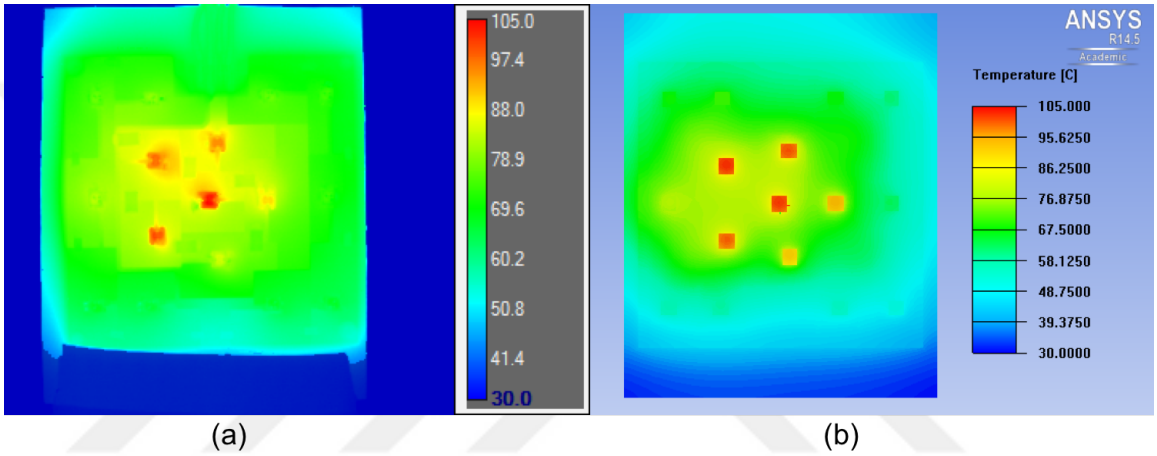

Figure 88: Contour plot for temperature distribution of (a) LEDs from experimental findings and (b) LEDs from computational model for FR4 based LED light engine with FR4 flex PCB at Case-4

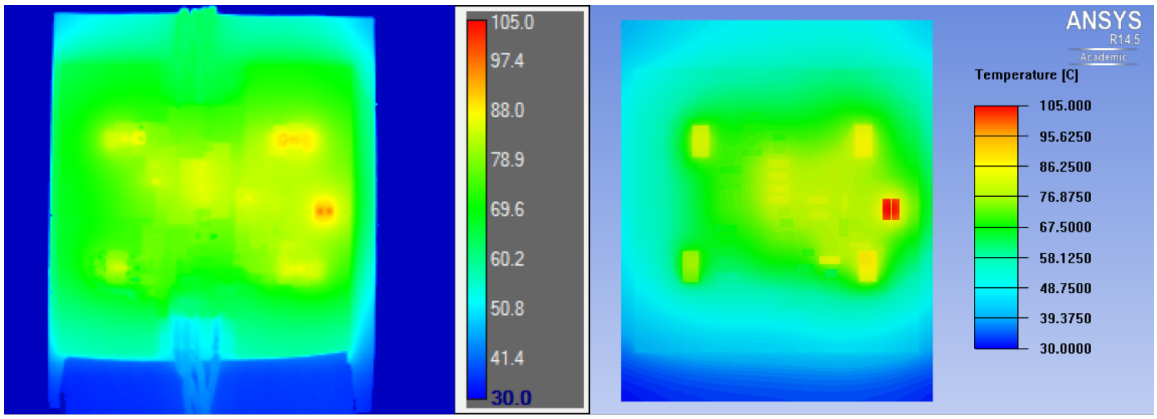

Figure 89: Contour plot for temperature distribution of (a) electronics from experimental findings and (b) electronics from computational model for FR4 based LED light engine with FR4 flex PCB at Case-4

In order to check accuracy of the computational study, experimental and computational findings are compared with each other. Maximum surface temperatures of all LEDs and several critical electronic components are obtained. Computational and experimental temperature results of these components are compared in Figure 90 for the FR4 based LED light engine with the FR4 flex PCB. Maximum difference between experimental and computational results at the light engine with the FR4 flex PCB is 18.2% while minimum difference is 0% on the LEDs' side of the light engine. On the other side of the light engine, maximum discrepancy between experimental and computational results of electronic components' temperatures is 10.0% while minimum difference is 2.9%.

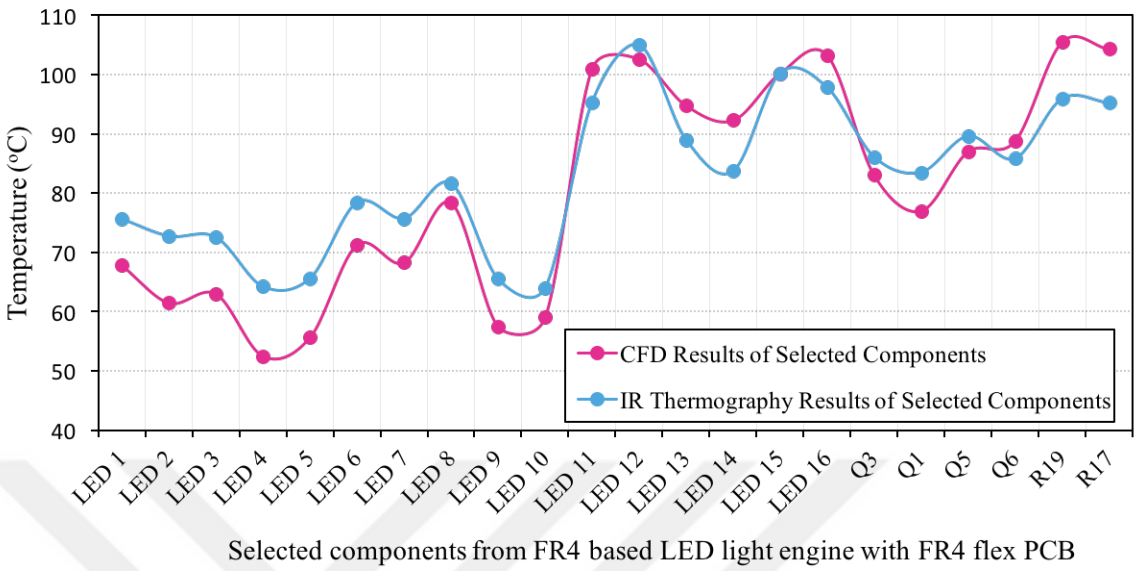

Figure 90: Comparison between experimental and computational findings of the FR4 based LED light engine with the FR4 flex PCB

As it is demonstrated in Figure 91 and Figure 92, similar temperature distribution is observed in experimental and computational results. However, board temperatures are seems quite different about 10%. While maximum temperature observed on LEDs' side is obtained 84.1°C as a result of experimental study, it is obtained as 79.8°C in computational study. On the other side of the light engine, maximum component temperature is experienced as 78.6°C in experimental study while it is obtained as 81.0°C in the computational study.

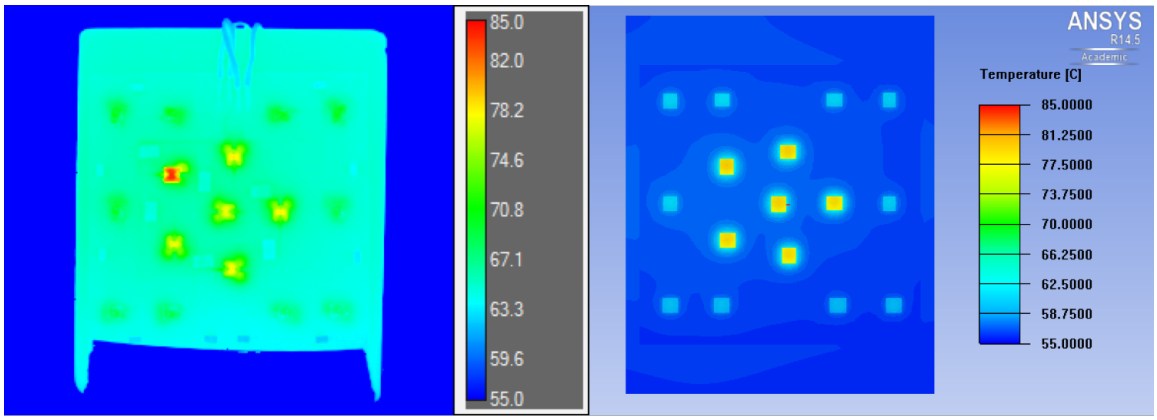

Figure 91: Contour plot for temperature distribution of (a) LEDs from experimental findings and (b) LEDs from computational model for aluminum based LED light engine with FR4 flex PCB at Case-4

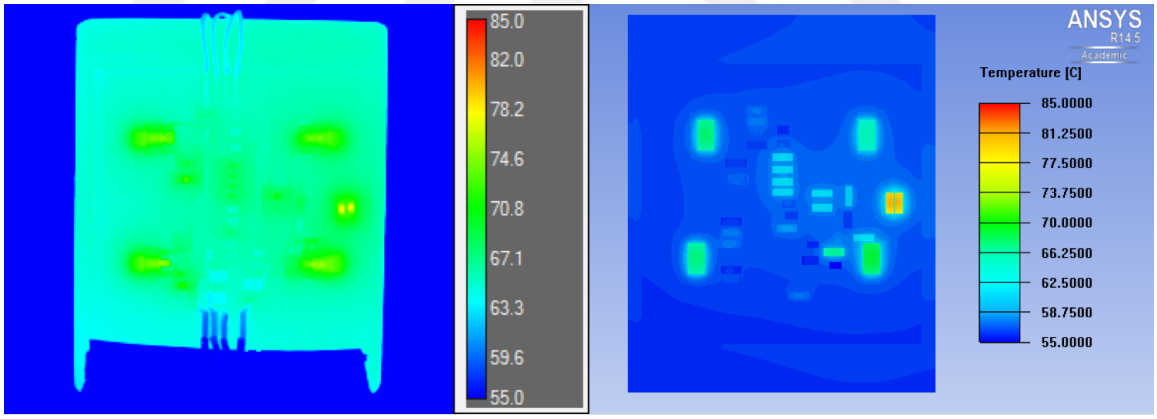

Figure 92: Contour plot for temperature distribution of (a) electronics from experimental findings and (b) electronics from computational model for aluminum based LED light engine with FR4 flex PCB at Case-4

Discrepancy between computational and experimental results are indicated in Figure 93 for the aluminum based light engine with the FR4 flex PCB. Maximum difference between experimental and computational results at the light engine with the

FR4 flex PCB is 12.9% while minimum difference is 1.4%. On the other side of the light engine, maximum discrepancy between experimental and computational results of electronic components' temperatures is 10.6% while minimum difference is 3.1%. When the light engine was modeled in a commercial software, geometry of elements was idealized. As expected, a difference between the experiment and the simulations were observed, but in reasonably low percentages. Thus, the comparison between the results shows good agreement with the experimental results.

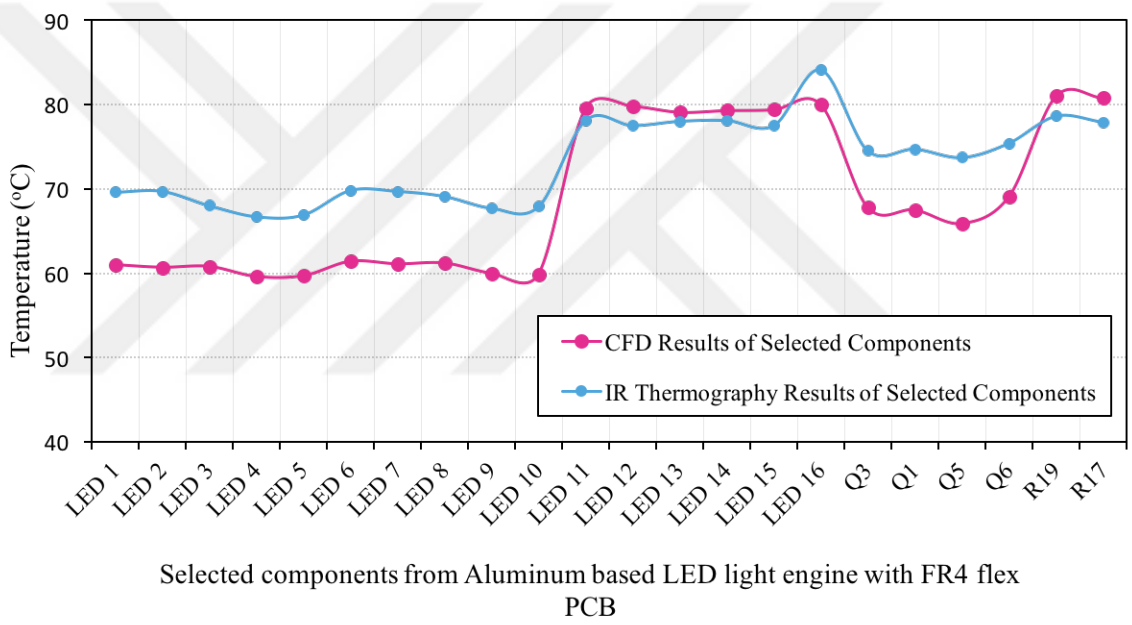

Selected components from Aluminum based LED light engine with FR4 flex PCB

Figure 93: Comparison between experimental and computational findings of the aluminum based LED light engine with the FR4 flex PCB

As it is indicated in Figure **??** and Figure **??**, similar temperature distribution is observed in experimental and computational results. However, there is also difference in board temperatures about 10%. While maximum temperature observed on LEDs' side is obtained 77.9°C as a result of experimental study, it is obtained as 79.2°C in computational study. On the other side of the light engine, maximum component temperature is experienced as 79.4°C in experimental study while it is obtained as

80.3°C in the computational study.

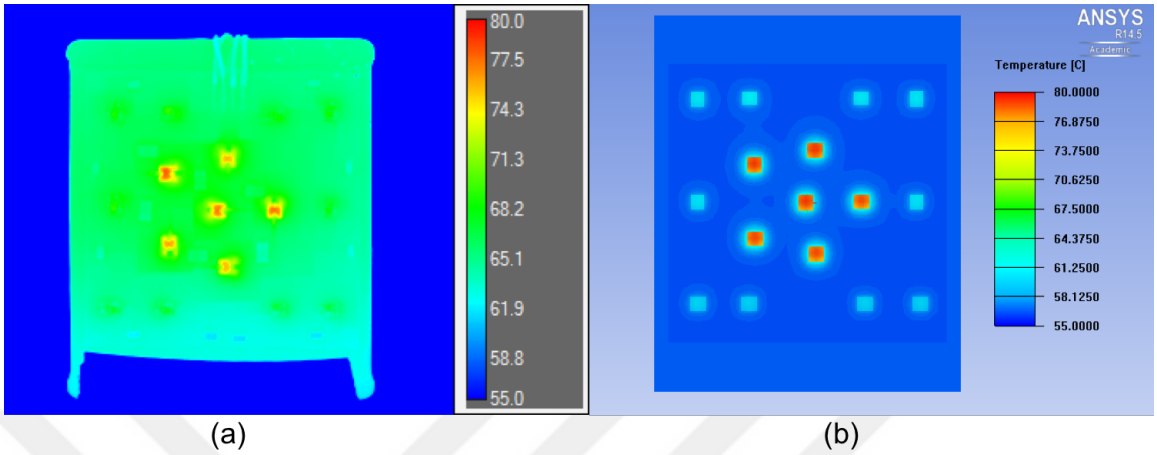

Figure 94: Contour plot for temperature distribution of (a) LEDs from experimental findings and (b) LEDs from computational model for advanced heat spreader based LED light engine with FR4 flex PCB at Case-4

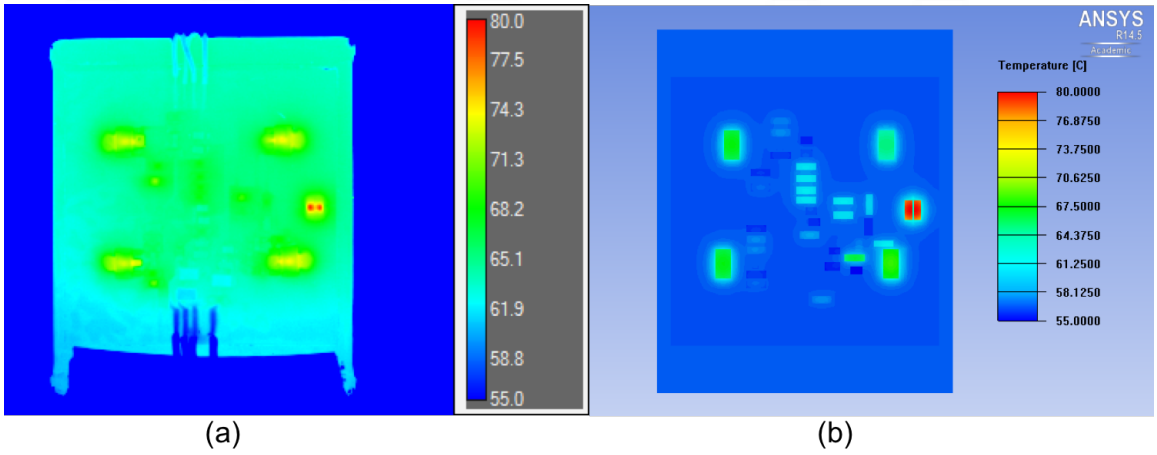

Figure 95: Contour plot for temperature distribution of (a) electronics from experimental findings and (b) electronics from computational model for advanced heat spreader based LED light engine with FR4 flex PCB at Case-4

Computational and experimental temperature results of these components are compared in Figure 93 for the advanced heat spreader based light engine with the

FR4 flex PCB. Maximum difference between experimental and computational results at the light engine with the FR4 flex PCB is 11.9% while minimum difference is 1.7%. On the other side of the light engine, maximum discrepancy between experimental and computational results of electronic components' temperatures is 11.6% while minimum difference is 1.1%. As it can be seen from the Figure 96, for most of the components and LEDs, computational results are lower than experimental results. It is expected results because in computational study, model and components have attached perfectly. However, in real LED light engines, there should be possible air gaps between boards and components which can increase thermal resistance of the system.

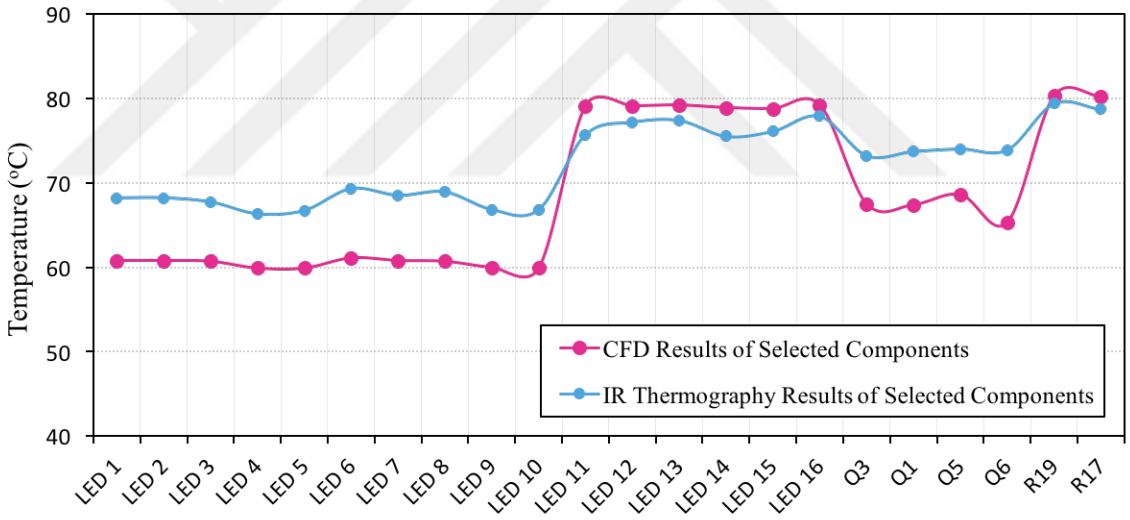

Selected components from advanced heat spreader based LED light engine with FR4 flex PCB

Figure 96: Comparison between experimental and computational findings of the advanced heat spreader based LED light engine with the FR4 flex PCB

As it is presented in Figure 97 and Figure 98, similar temperature distribution is observed in experimental and computational results. While maximum temperature observed on LEDs' side is obtained 76.9°C as a result of experimental study, it is

obtained as 75.3°C in computational study. On the other side of the light engine, maximum component temperature is experienced as 74.8°C in experimental study while it is obtained as 76.5°C in the computational study.

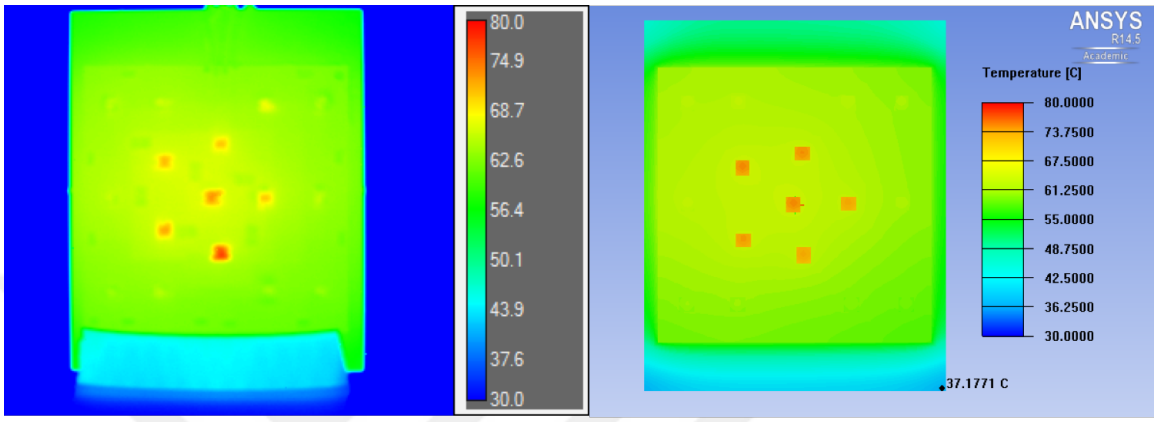

Figure 97: Temperature distribution of (a) LEDs from experimental findings and (b) LEDs from computational model for FR4 based LED light engine with ceramic flex PCB at Case-4

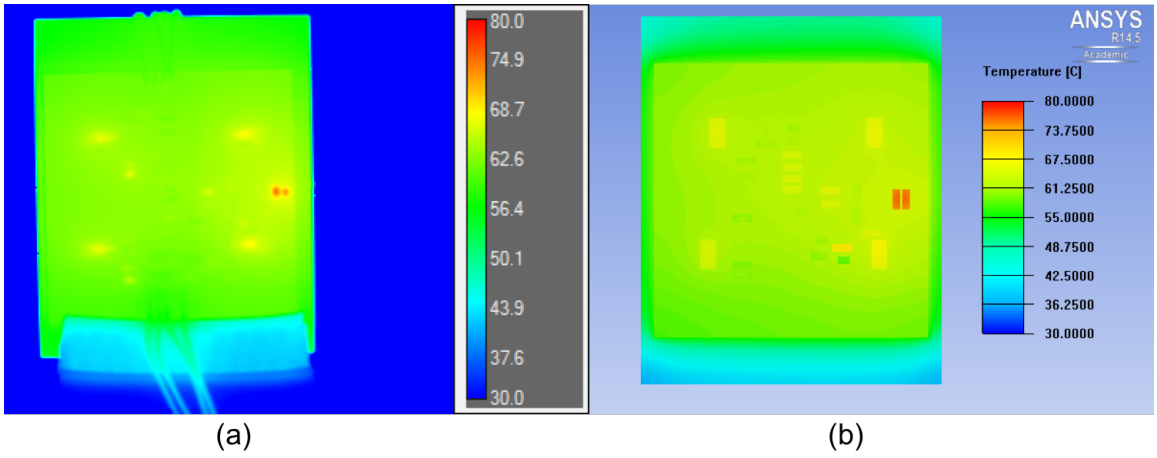

Figure 98: Temperature distribution of (a) electronics from experimental findings and (b) electronics from computational model for FR4 based LED light engine with ceramic flex PCB at Case-4

Computational and experimental temperature results of these components are compared in Figure 93 for the FR4 based light engine with the ceramic flex PCB. Maximum difference between experimental and computational results at the light engine with the FR4 flex PCB is 6.5% while minimum difference is 2.3%. On the other side of the light engine, maximum discrepancy between experimental and computational results of electronic components' temperatures is 5.5% while minimum difference is 0.6%. Good agreement between computational study and experimental study is achieved for FR4 based light engine with the ceramic flex PCB.

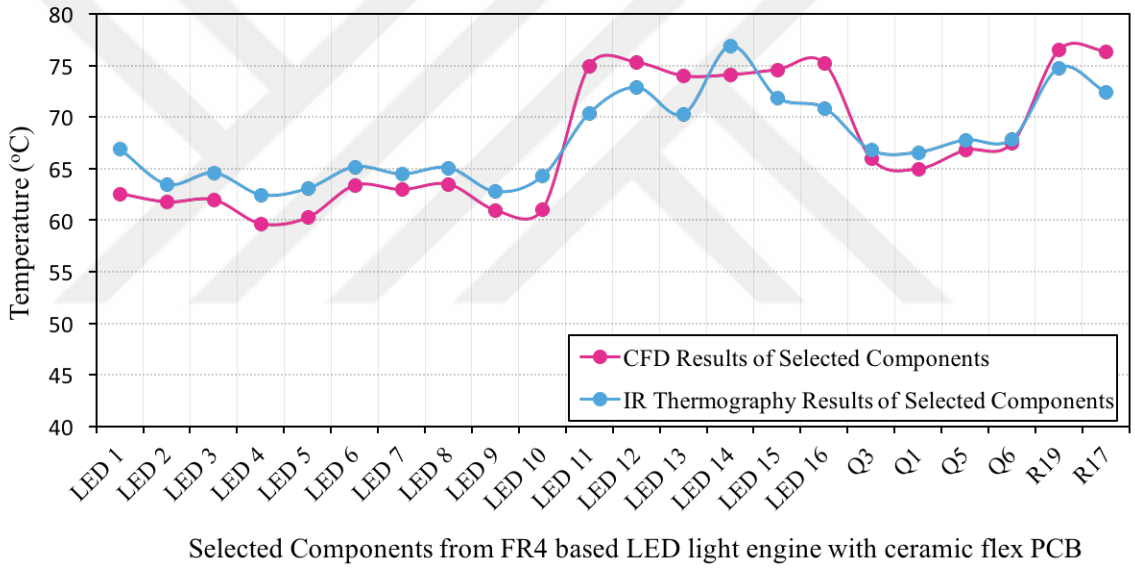

Figure 99: Comparison between experimental and computational findings of the FR4 based LED light engine with the multilayer ceramic flex PCB

LED light engines with FR4 flex PCB are compared computationally during Case-4. As it is represented in Figure 100 and Figure 101, while over the FR4 based LED light engine, local hotpots are experienced around the signal LEDs, high-power transistors and some resistors, over the aluminum and advanced heat spreader based LED light engines uniform temperature distribution is observed.

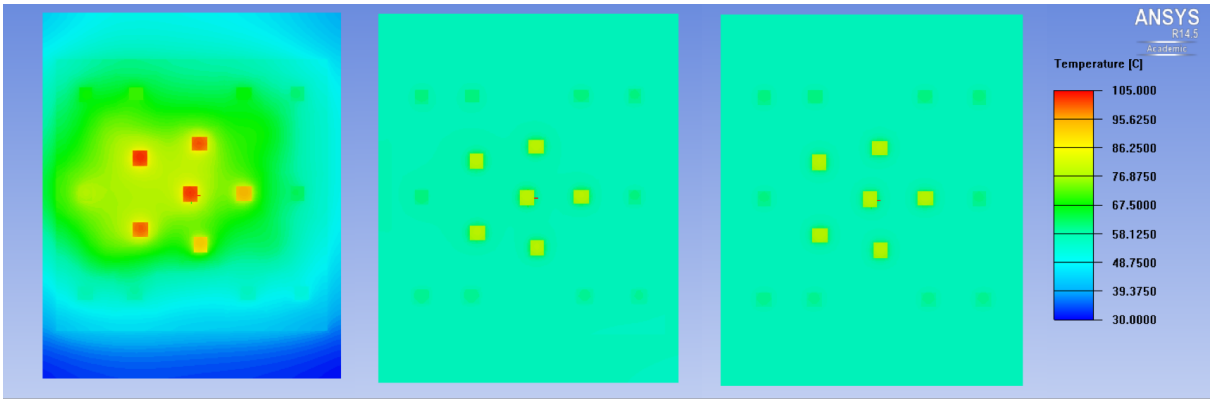

(a) (b) (c)

Figure 100: Comparison of computational results of FR4, aluminum and advanced heat spreader based LED light engines at Case-4 (from LEDs' side)

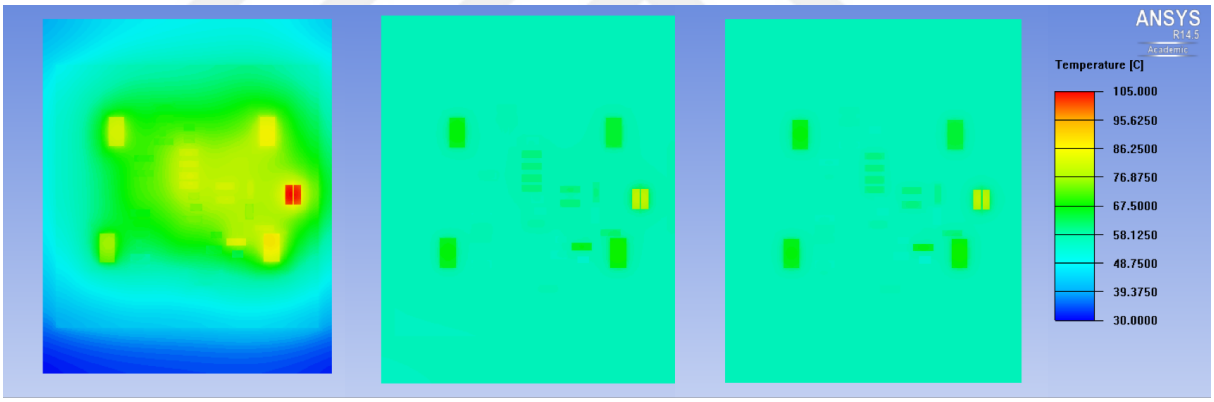

(a) (b) (c)

Figure 101: Comparison of computational results of FR4, aluminum and advanced heat spreader based LED light engines at Case-4 (from electronics' side)

Computational results of these two LED light engines are represented in Figure 102 and Figure 103. While maximum LED temperature is experienced as 103.3°C at the LEDs side of the light engine with the FR4 flex PCB, maximum temperature observed at the electronics side of the light engine with the FR4 flex PCB is 105.5°C. As maximum LED temperature is experienced as 75.3°C at the LEDs side of the

light engine with the multilayer ceramic flex PCB, maximum temperature observed at the electronics side of the light engine with the multilayer ceramic flex PCB is 76.5°C. According to computational findings, temperature distributes uniformly over the LED light engine with the multilayer ceramic flex PCB due to its higher thermal conductivity. Furthermore, more critical local hot spots over LEDs and electronics were observed over the light engine with the FR4 flex PCB.

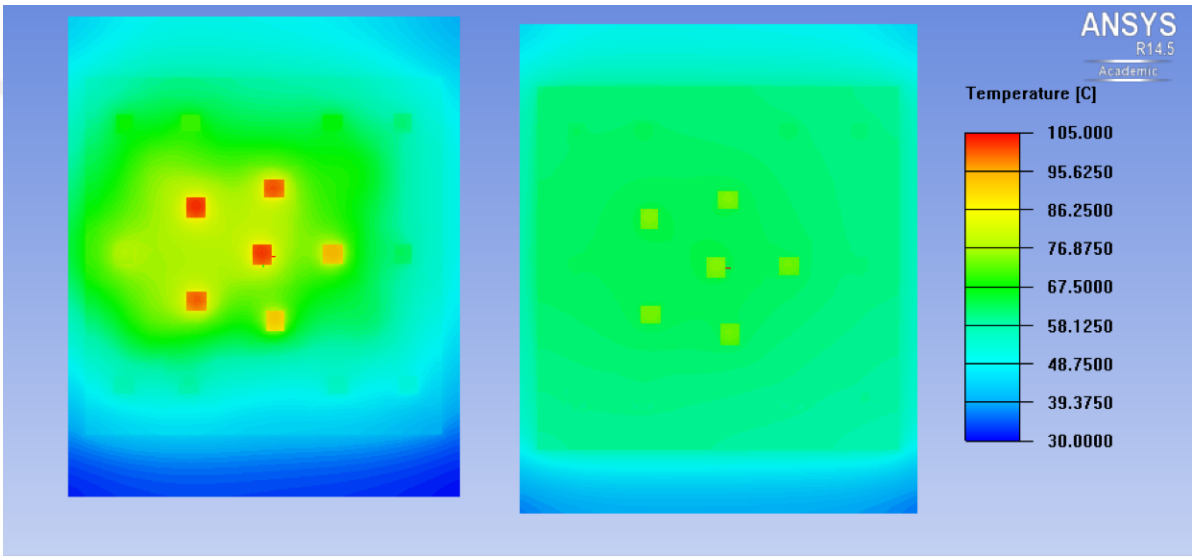

Figure 102: Contour plot for temperature distribution of LEDs from computational study of the LED light engine (a) with FR4 flex PCB and (b) with multilayer ceramic flex PCB

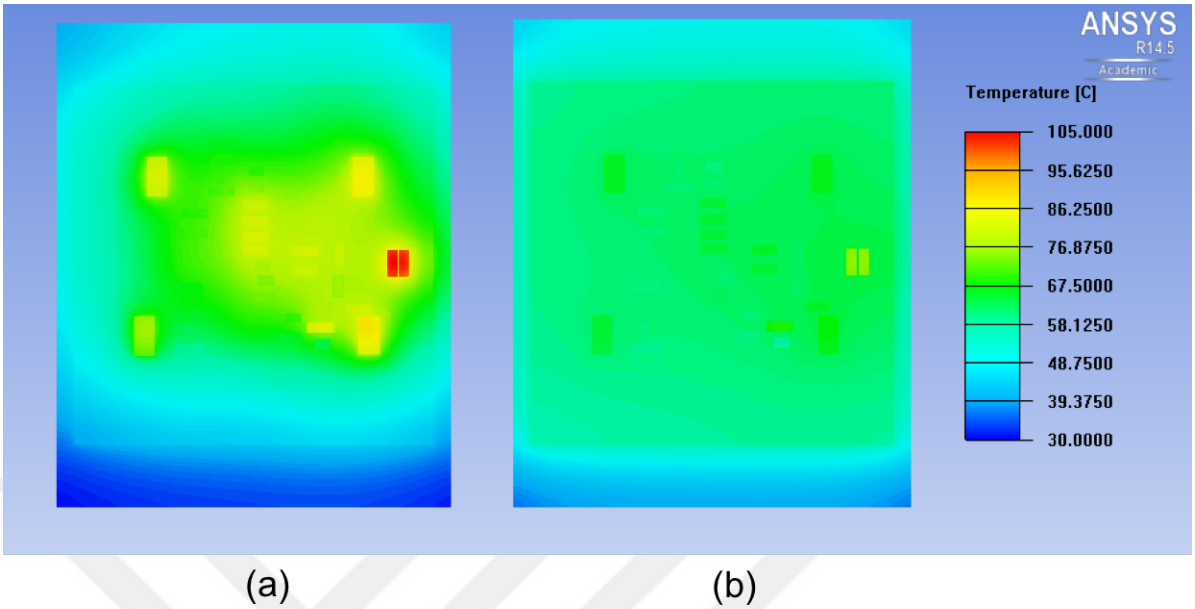

Figure 103: Contour plot for temperature distribution of electronics from computational study of the LED light engine (a) with FR4 flex PCB and (b) with multilayer ceramic flex PCB

Table 14: Comparison table of computational and experimental results of Properties of the FR4 based LED light engines with FR4 flex PCB

$Component$	$CFDResults$	$ExperimentalResults$	$Difference(\%)$
LED 1	67.8	75.6	10.3
LED 3	63	72.5	13.1
LED 5	55.7	65.6	15.1
LED 7	68.3	75.7	9.8
LED 9	57.5	65.5	12.2
LED 11	101	95.3	6.0
LED 13	94.8	89	6.5
LED 15	100.2	100.2	0.0
Q3	83.1	86.1	3.5
Q1	77	83.5	7.8
Q5	87	89.6	2.9
Q6	88.8	85.8	3.5
R19	105.5	95.9	10.0
R17	104.3	95.2	9.6

Table 15: Comparison table of computational and experimental results of Properties of the FR4 based LED light engines with ceramic flex PCB

$Component$	$CFDResults$	$ExperimentalResults$	$Difference(\%)$
LED 1	62.6	66.9	6.4
LED 3	62	64.6	4.0
LED 5	60.3	63.1	4.4
LED 7	63	64.5	2.3
LED 9	61	62.8	2.9
LED 11	75	70.4	6.5
LED 13	74	70.3	5.3
LED 15	74.6	71.9	3.8
Q3	83.1	86.1	3.5
Q1	66	66.8	1.2
Q5	66.8	67.8	1.5
Q6	67.5	67.9	0.6
R19	76.5	74.8	2.3
R17	76.4	72.4	5.5

CHAPTER VII

THERMAL PROBLEMS POSED BY COMPACT PACKAGING AND INTERNET OF THINGS (IOT) FOR SOLID STATE LIGHTING SYSTEMS

Vehicles are expected be one of the major part of the IoT due to their current electronics infrastructure [34]. Electronics have already been used in several purposes in a number of areas in vehicles. For instance, power electronics are used in lighting systems of automobiles in order to drive LEDs. These electronic systems can establish a substructure for IoT applications. Therefore, in this study, an LED light engine which is used in automotive rear lighting system will be analyzed. Rear lighting systems consists of three different functions which are signal, stop and position. Conventionally, for these three functions, three separate light engines are typically used. Due to unique advantages of LEDs, to integrate all these functions on a single light engine is possible. Although LEDs are energy efficient sources, if all three functions operate simultaneously, heat generation of combined LEDs and driver electronics increase. Industry preferred PCB material for light engines is FR4 due to availability, ease of processing and cost. However, due to poor thermal conductivity of FR4; heat generated from components over PCB cannot diffuse uniformly so local hot spots occur over components and PCB. Thus, junction temperature of LEDs can surpass 100°C which is the critical temperature for most LEDs [2]. Therefore, LEDs and driver electronics placed over separate PCBs due to thermal limitations of conventional boards. However, this study aims to combine electronic components and LEDs on a single compact PCB. When IoT features are added into current system, number of electronics and their power consumptions will increase so thermal problems will to

the continually increase. Therefore, proposed novel heat spreader board technology should be developed to overcome these thermal issues.

In order to observe thermal effect of possible power increase on driver electronics of LED light engine when IoT applications are adapted to current system, a computational study has been conducted in a commercial computational fluid dynamics software Icepak 14.5 [49]. CFD simulations allow users to change model parameters and experimental conditions easily. Therefore, the computational study consists of four cases which represent expected scenarios when IoT applications integrated to LED light engines. First case stands for current performance of LED light engine without any smart features addition. In second, third and fourth cases, only power levels of driver electronics are increased by 25%, 50% and 70%, respectively. Geometrical models of the LED light engines are identical for all cases. Computational models of FR4 based LED light engine and advanced heat spreader LED light engine which are explained in previous chapter is used.

IoT features integration to current technologies will soon be essential. These new features will cause an increase in the number of electronics and their power consumptions in same or smaller footprint areas. It is expected that overall heat generation of electronics may increase as much as 70%. Therefore, this study aims to investigate advanced heat spreader substrate technology to solve possible thermal problems of new generation electronic systems.

Since a very good agreement between computational and experimental results is observed as mentioned in previous chapters, model is solved for other CFD cases to analyze thermal performance of current LED engine with smart applications. It is expected that IoT features leads to a 70% increase in power consumption of electronics. Thus, the model is modified via increasing power consumptions of electronics by 25%, 50% and 70% which represents future smart LED engines. Firstly, computational model of the FR4 based LED light engine is solved for these four cases. Then,

to analyze thermal performance of the advanced heat spreader LED light engine, its computational model is solved for same cases.

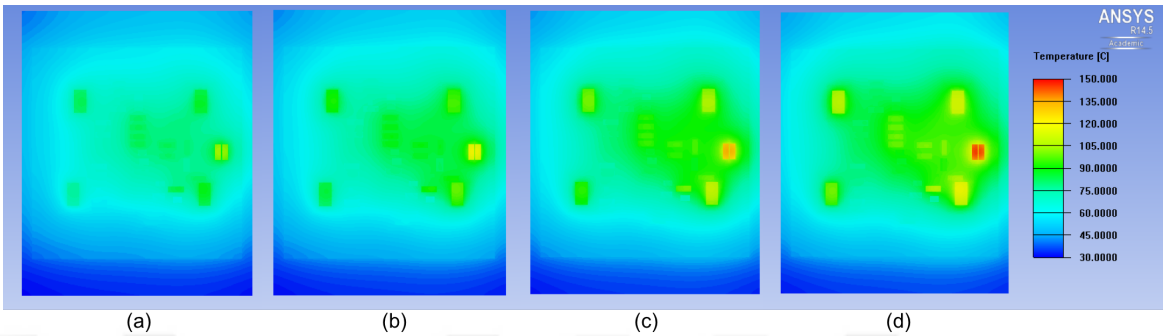

Figure 104: Temperature distribution of electronics components placed over light engine (a) Baseline without IOT added heat generation (b) 25% (c) 50% and (d) 70% added heat generation rates over electronics

Significance of the thermal problem can be seen from Figure 104. While power consumption of electronics increases by 70%, maximum temperatures that is experienced on electronics increase by +38.4%. Temperature rise on electronics is indicated in Figure 105. The maximum temperature on the light engine goes up to 145.6°C which can lead to catastrophic failures.

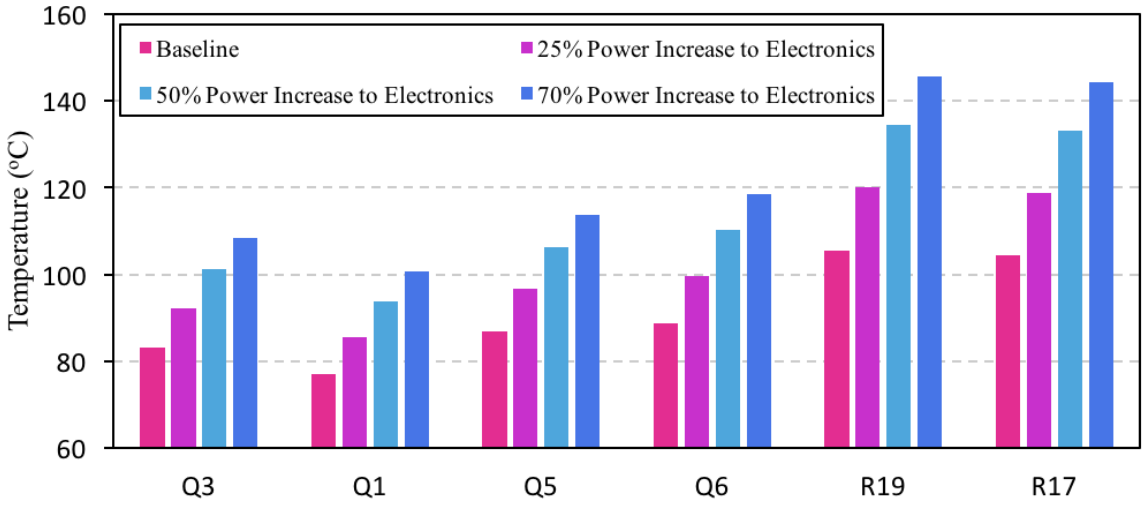

Figure 105: Temperature increase of electronic components as a result of power increase

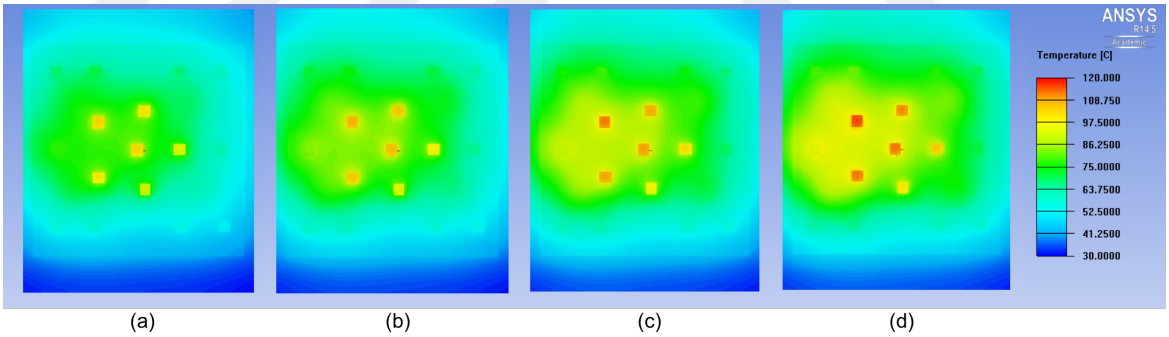

Figure 106: Temperature distribution of some LEDs placed over light engine (a) Baseline without IOT added heat generation (b) 25% (c) 50% and (d) 70% added heat generation rates over electronics

Although power consumptions of LEDs are not changed in different cases, as it is shown in Figure 106, temperatures of LEDs and thermal distribution over the board is changed due to power addition to electronics. As it is indicated in Figure 106 and 107, while maximum temperatures of red LEDs increased by +15.4%, a

+12.5% temperature rise is experienced on amber LEDs. While with 25%, 50% and 70% power addition to electronics, maximum temperature experienced on LED-16 reached to 103.3°C, 107.9°C and 112.7°C from 116.2°C, respectively. Because of the fact that when FR4 material used as substrate, junction temperature of LEDs exceeds critical temperature even in the current situation when there is no IOT added power, an additional heat generation in electronics gets this situation more critical.

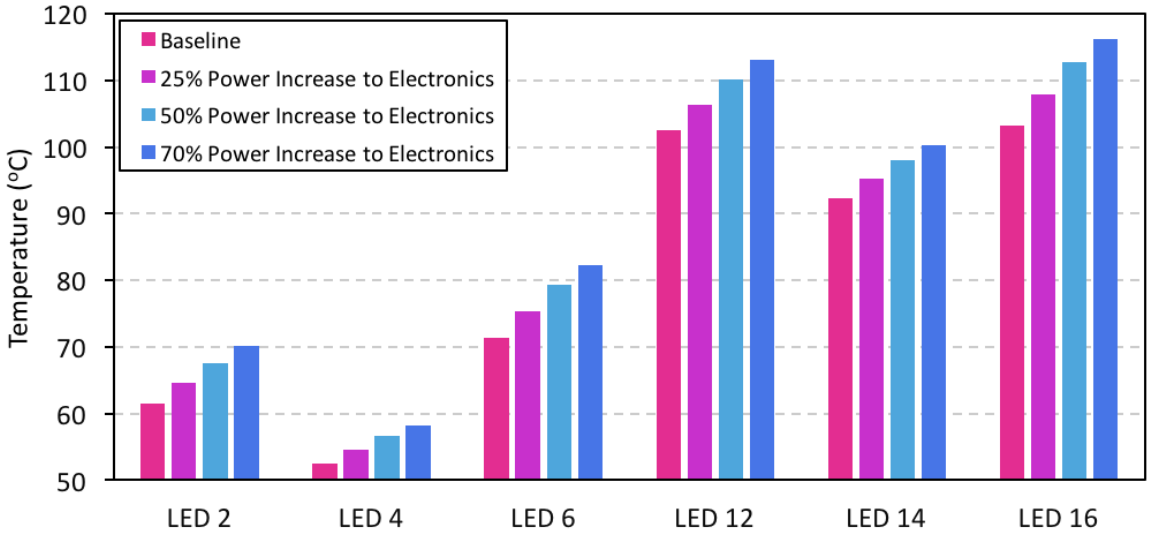

Figure 107: Temperature increase of amber LEDs as a result of power increase to electronic components

It is found that the highest temperature is observed on the amber LEDs especially LED 12 and LED 16 due to the fact that local heat generation is highest and the heat transfer path is rather limited compared to other LEDs on the light engine. Although there is approximately 15.4% elevation in temperature, this can be perhaps eliminated by improving the conduction performance of the board by having either highly conductive boards. When real automotive environment is evaluated, ambient temperature will be considerably higher than room temperature. It can be inferred that if IoT features added to current system, system will be more compact than

today so current thermal problems will be harder. Therefore, while FR4 substrate is not adequate for even current application, for future more complex technologies, a novel heat spreader PCB substrates should be developed. Therefore, computational study for an advanced heat spreader LED light engine is conducted for higher power applications.

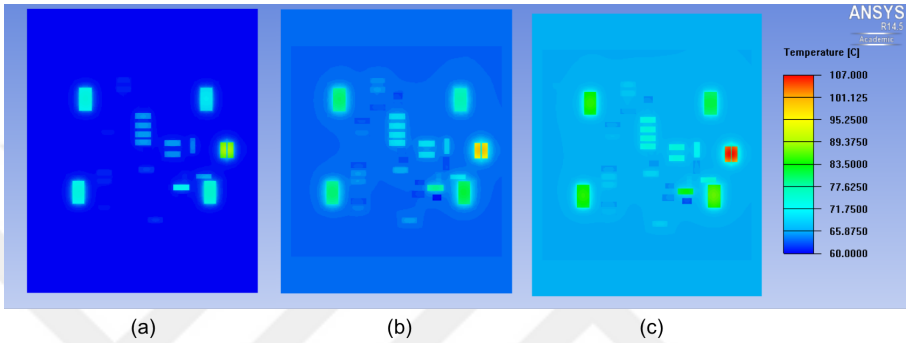

Figure 108: Temperature distribution of electronics components placed over the advanced heat spreader LED light engine (a) Baseline without IOT added heat generation (b) 25% (c) 50% and (d) 70% added heat generation rates over electronics

At the advanced heat spreader LED light engine, while power consumption of electronics increases by 70%, maximum temperatures that is experienced on electronics increase by +33.1%. Temperature rise on electronics is showed in Figure 109. The maximum temperature on the light engine goes up to 106.7°C which is tolerable temperature for electronic components.

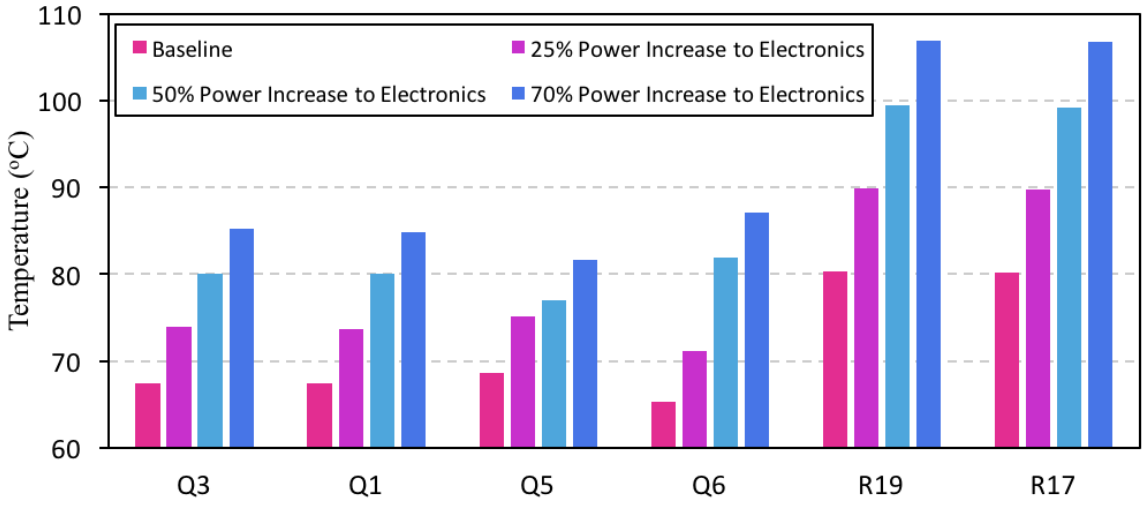

Figure 109: Temperature increase of electronic components as a result of power increase at the advanced heat spreader based LED light engine

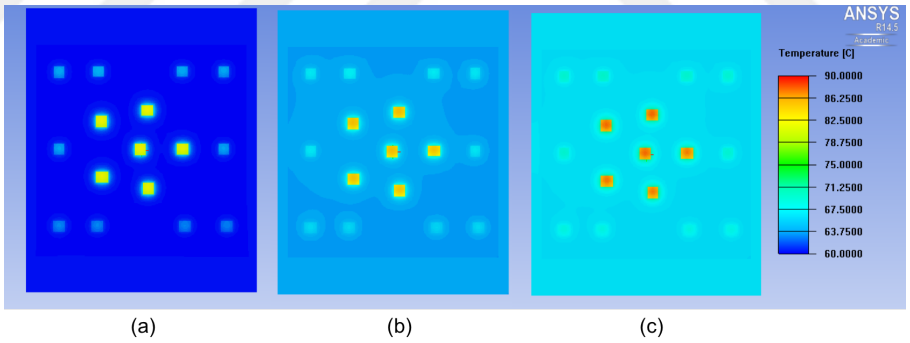

Figure 110: Temperature distribution of some LEDs placed over the advanced heat spreader LED light engine (a) Baseline without IOT added heat generation (b) 25% (c) 50% and (d) 70% added heat generation rates over electronics

Although power consumptions of LEDs are not changed in different cases, as it is shown in Figure 110, temperatures of LEDs and thermal distribution over the board is changed due to power addition to electronics. As it is indicated in Figure 110 and 111, while maximum temperatures of red LEDs increased by +14.2%, a +11.1%

temperature rise is experienced on amber LEDs, respectively. While with 25%, 50% and 70% power addition to electronics, maximum temperature experienced on LED-16 reached to 79.2°C, 82.4°C and 85.5°C from 87.9°C, respectively. According to results, although 70% power addition is applied to electronics, temperatures of red and amber LEDs stay under the critical LED temperature. In addition, while there is temperature difference between same type of LEDs which are mounted to FR4 LED light engine, uniform temperature distribution is obtained across the advanced heat spreader LED light engine. Therefore, advanced heat spreader technology constitutes a potential as electronic board substrate for smart IoT applications.

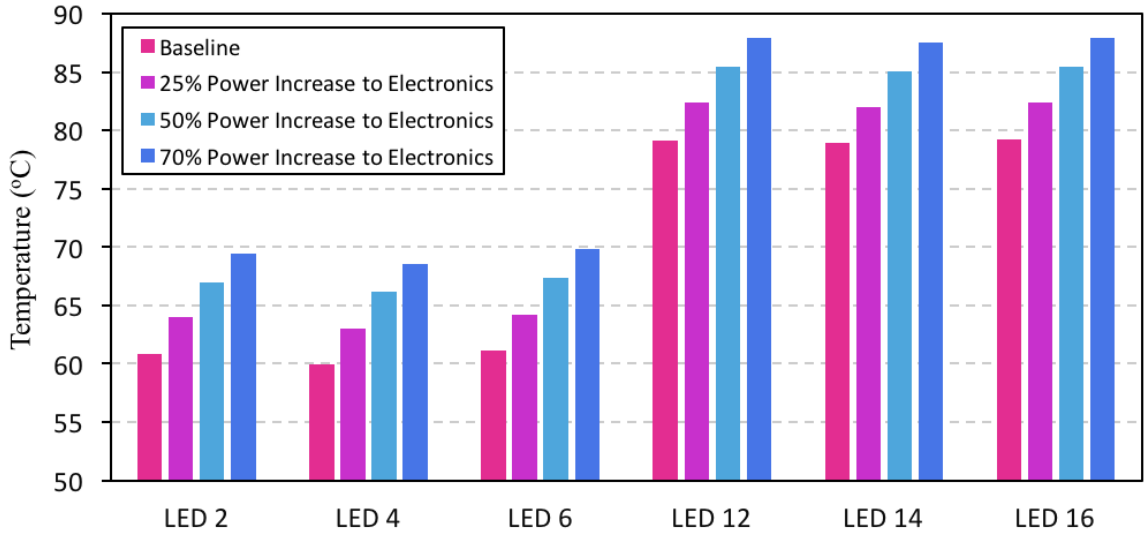

Figure 111: Temperature increase of amber LEDs as a result of power increase to electronic components at the advanced heat spreader based LED light engine

CHAPTER VIII

SUMMARY AND CONCLUSIONS

This study aims to enhance the thermal management of an LED light engine for automotive exterior lighting with an advanced heat spreader. Although LEDs have many advantages, their applications require an accurate thermal management. To house driver electronics and LEDs in a typical automotive exterior lighting, conventionally FR4 based printed circuit board is usually used. Over the board, local hotspots are observed due to low thermal conductivity of FR4 based PCB and high heat flux caused by LEDs and electronics. LEDs in automotive back lighting units operated with different input power for position, stop and signal lights. Moreover, in some instances, these three lights perform simultaneously in the automobiles. Therefore, heat flux dissipation over LEDs and electronics become abundant making thermal performance of the FR4 board inadequate to diffuse this flux. Thus, metal core printed circuit boards are investigated to enhance the thermal performance. Although a high conductivity of metal core printed circuit board improves thermal performance significantly, still a novel technology is needed in order to dissipate heat efficiently over PCB. Thus, in this study, an advanced heat spreader board technology was investigated and compared with the conventional FR4 based and Al metal core printed circuit boards. An experimental study was conducted via thermal imaging technique in order to inspect local hot spots in Chapter III. Also, in Chapter IV, an optical performance investigation for advanced heat spreader based LED light engine was conducted. Then, in Chapter VI, a numerical analysis was also performed in order to validate experimental results. A number of findings can be given as;

- Maximum temperatures of FR4, Al and advanced heat spreader board were

observed as 105.0°C., 84.1°C and 77.9°C, respectively in Case 4.

- More uniform thermal pattern was observed on Al and advanced heat spreader boards than FR4 based board due to low thermal conductivity of FR4 substrate.
- According to experimental data, advanced heat spreader has performed 7.4% better thermal performance than Al metal core board and %25.8 FR4 based board.
- At the Case-4, aluminum and advanced heat spreader based LED light engines showed 7.1% and 16.3% better performance in terms of radiant flux, respectively.
- When advanced heat spreader board base used instead of FR4 board base, luminous efficacy can be improved by 25.9%.
- FR4 substrate is not sufficient for this 3- purpose lamp due to its thermal performance.
- Maximum difference between experimental and computational results was 18.2%.

In addition, improving thermal spreading capability of PCBs is one of the alternative solution in order to distribute heat from source, efficiently. Various type of materials is investigated to improve thermal characteristics of PCBs. In this study, multilayer ceramic flex PCB was analyzed as alternative PCB solution to overcome thermal problems. To analyze thermal performance of the PCB, it was compared with that of FR4 flex PCB experimentally and computationally. Experimental and computational findings of the study can be summarize as following:

- More uniform temperature distribution was observed at the LED light engine with multilayer ceramic flex PCB due to its higher thermal conductivity.

- While thermal performance degraded by 36.5% when FR4 flex PCB was used, radiant flux and luminous flux of the LED light engine decreased by 13.3% and 14.6%, respectively.

- Peak wavelength shift by 3nm in the amber region of the spectrum was experienced due to rise of the junction temperature when FR4 flex PCB was utilized instead of multilayer ceramic flex PCB.

Besides, there is strong dependency between photometric, electrical and thermal properties of LEDs. Hence, designers should be consider this dependency between optical, thermal and electrical parameters of the lighting system to obtain desired performance. Success of thermal management of the lighting systems is critical for optical output of the system so that luminous efficacy of the LED systems is highly sensitive to junction temperature of the LEDs. In Chapter V, the relationship between photometric, electrical and thermal parameters of the FR4 LED light engine with FR4 flex PCB was analyzed. Findings of the study can be summarized as following:

- The results of this investigation showed that when input power of the red LEDs exceeded the 930 mW, luminous efficacy started to decrease sharply due to elevation of the junction temperature.

- The second major finding of this chapter was that as input power increased from 432.8 mW to 1928.5 mW, luminous efficacy of amber LEDs decreased by 24.6 lm/W. Until forth experimental case, luminous efficacy increased slowly, after that it started to decrease with positive acceleration. Decreasing in luminous flux causes the luminous efficacy degradation. Therefore, power level of 1600 mW was critical for amber LEDs in this study.

On the other hand, in recent years, paradigm of Internet of Things which will be effective in all areas of our lives is in the foreground and lighting systems with over

500 billion fixtures globally are seen as a great opportunity for a widespread application. In addition, automobiles may constitute a platform for IoT applications due to their current electronics system and mobility feature. Thus, in this study, a possible candidate automotive rear LED lighting system is evaluated in terms of thermal performance for new generation IoT added applications. Firstly, thermal performance of FR4 based LED engine is evaluated and it is modeled in a CFD program. Then, in Chapter VII, computational model is solved for different cases such as; 25%, 50% and 70% power addition to electronics to determine the adverse effects due to IOT power needs. Metal and advanced heat spreader substrate technologies are presented as solution to overcome thermal problems. Consequences of the Chapter VII can be listed as follows:

- While power consumption of electronics increases by 70%, maximum temperatures that was experienced on electronics increase by +38.4%. Maximum temperatures of amber LEDs increased by +15.4%, when temperature rise of +11.2% was experienced on red LEDs.

- At the advanced heat spreader LED light engine, while power consumption of electronics increases by 70%, maximum temperatures that was experienced on electronics increase by +33.1%. Maximum temperatures of amber LEDs increased by +14.2%, when temperature rise of +11.1% was experienced on red LEDs.

- In case of 25%, 50% and 70% power addition to electronics, maximum temperature experienced on the amber LED which had the highest temperature reached to 103.3°C, 107.9°C, 112.7°C and from 116.2°C, respectively.

- As conventional FR4 substrate is not adequate for future electronic systems, advanced heat spreader board technology which consists of vapor chamber structure can be a possible substrate technology for new generation smart applications.

CHAPTER IX

FUTURE WORK

Advanced heat spreader technology that offered in this study presents high potential for applications which requires highly dense electronic packages. Therefore, this technology can be improved to integrating with IoT applications in future years.

On the other hand, compactness is an important issue for electronic packages especially for automotive lighting system. Thus, novel advanced heat spreader substrates with low volume provides a better solution to enhance thermal performance of this kind of systems. Besides, novel advanced heat spreader substrates with thinner structure can increase thermal performance of the electronic boards via decreasing thermal resistance of the substrate. Therefore, EVATEG Center offers a novel compact heat spreader substrate with dimensions of 55mm X 55mm X 1mm.

Bibliography

[1] X. Luo, R. Hu, T. Guo, X. Zhu, Z. Mao, and S. Liu, "Low thermal resistance led light source with vapor chamber coupled fin heat sink," *IEEE Electronic Components and Technology Conference (ECTC)*, vol. Proceedings 60th, pp. 1347–1352, 2010.

[2] M. Arik, C. Beckerb, S. Weaverb, and J. Petroski, "Thermal Management of LEDs: Package to System," *Third International Conference on Solid State Lighting*, vol. Proc. SPIE, no. 5187, 2004.

[3] J. Yoo, J. Jang, J. Kwon, H.C.Kim, D.W.Song, and S.Y.Jung, "Demonstration of vehicular visible light communication based on led headlamp," *International Journal of Automotive Technology*, vol. 17, no. 2, pp. 347–352, 2016.

[4] D. Pounds, B. III, and R. W., "High heat flux heat pipes embedded in metal core printed circuit boards for led thermal management," *14th IEEE ITHERM Conference*, vol. IEEE, 2014.

[5] N. Kafadarova and A. Andonova, "Pcb thermal design improvement through thermal vias," *Recent Advances in Circuits, Systems, Electronics, Control and Signal Processing*, 2009.

[6] K. Yung, H. Liem, H. Choy, and Z. Cai, "Thermal investigation of a high brightness LED array package assembly for various placement algorithms," *Elsevier Applied Thermal Engineering*, vol. 63, pp. 105–118, Nov. 2013.

[7] K. M. Kota, "Design and experimental study of an integrated vapor chamber thermal energy storage system," *University of Central Florida Orlando*, 2008.

[8] S. Hsieh, R. Lee, J. Shyu, and S. Chen, "Thermal performance of flat vapor chamber heat spreader," *Energy Conversion and Management 49 (2008)*, vol. Elsevier, pp. 1774–1784, 2008.

[9] J. Wang and C. L. Huang, "Vapor chamber in high power leds," *Microsystems Packaging Assembly and Circuits Technology Conference (IMPACT)*, vol. 2010 5th International, no. 4, pp. 1–4, 2010.

[10] R. Lenk and C. Lenk, *Practical Lighting Design With LEDs*, vol. ISBN 978-0-470-61279-8. John Wiley & Sons, Ltd, 2011.

[11] C. J. M. Lasance and A. Poppe, *Thermal Management for LED Applications*. Solid State Lighting Technology and Application Series, New York, US: Springer, 2014.

[12] Commercial Buildings Energy Consumption Survey (CBECS), *Trends in Lighting in Commercial Buildings*. www.eia.gov, US, 2017.

[13] S. Shanmugan, D. Mutharasu, and I. Kamarulazizi, "Bn thin film as thermal interface material for high power led: Thermal resistance and optical analysis," *Optical & Quantum Electronics*, vol. Springer Science & Business Media B.V, 2013.

[14] E. F. Schubert, *Light-Emitting Diodes*. Second Edition, Cambridge, UK: Cambridge University Press, 2006.

[15] W. Jing, L. P. W. Yumei, and, and W. Sanshan, "Junction-temperature estimation in algainp light-emitting diodes using the luminescence spectra method," *Journal of Semiconductor*, vol. 37, no. 6, p. 064010, 2016.

[16] E. Tamdogan, G. Pavlidis, S. Graham, and M. Arik, "A comparative study on the junction temperature measurements of leds with raman spectroscopy, microinfrared (ir) imaging, and forward voltage methods," *IEEE Transactions on Components, Packaging and Manufacturing Technology*, vol. doi: 10.1109/TCPMT.2018.2799488, 2018.

[17] S. Jang and M. W. Shin, "Thermal analysis of led arrays for automotive headlamp with a novel cooling system," *IEEE Transactions on Device and Materials Reliability*, vol. 8, no. 3, pp. 561–564, 2008.

[18] F. S. Khosroshahi, M. Arik, and C. Tfekci, "Conduction driven cooling of led based automotive led lighting systems for abating local hot spots," *11th International Conference on Heat Transfer, Fluid Mechanics and Thermodynamics*, 2015.

[19] H. Dieker, C. Miesner, D. Pttjer, and B. Bachl, "Comparison of different LED packages," *Manufacturing LEDs for Lighting and Display*, vol. Proc. SPIE 6797, no. 67970I, 2007.

[20] O. Kckmann, "High-power led arrays: special requirements on packaging technology," *Light-Emitting Diodes: Research, Manufacturing, and Applications X*, vol. Proc. SPIE, no. 6134, 2006.

[21] E. C. W. de Jong, B. J. A. Ferreira, and P. Bauer, "Toward the next level of pcb usage in power electronic converters," *IEEE Transactions on Power Electronics*, vol. 23, no. 6, pp. 3151–3163, 2008.

[22] D. L. Saums, R. A. Hay, M. Ryals, B. Edward, and P. Ruzicka, "Application of conduction-cooled pcbs and composite materials in an aerospace system," *2016 IEEE International Symposium on Phased Array Systems and Technology*, pp. 1–9, 2016.

[23] E. Juntunen, A. Sitomaniemi, O. Tapaninen, R. Persons, M. Challingsworth, and V. Heikkinen, "Thermal performance comparison of thick-film insulated aluminum substrates with metal core pcbs for high-power led modules," *IEEE Transactions on Components, Packaging and Manufacturing Technology*, vol. 2, no. 12, pp. 1957–1964, 2012.

[24] M. Weilguni, J. Nicolics, R. Medek, M. Franz, G. Langer, and F. Lutschounig, "Characterization of the thermal impedance of highpower led assembly based on innovative printed circuit board technology," *33rd International Spring Seminar on Electronics Technology*, vol. ISSE 2010, Warsaw, pp. 238–244, 2010.

[25] U. Z. Uras, M. Ark, and E. Tamdoan, "Thermal performance of a light emitting diode light engine for a multipurpose automotive exterior lighting system with competing board technologies," *ASME.J. Electron. Packag.*, vol. 139, no. 2, pp. 020907–020907–8, 2017.

[26] E. Tamdogan and M. Arik, "Natural convection immersion cooling with enhanced optical performance of light-emitting diode systems," *ASME.J. Electron. Packag.*, vol. 137, no. 4, pp. 041006–041006–8, 2015.

[27] M. Arik and Y. Utturkar, "A computational and experimental investigation of synthetic jets for cooling of electronics," *ASME.J. Electron. Packag.*, vol. 137, no. 2, pp. 021005–021005–10, 2015.

[28] D. Thomas, R. McPherson, G. Paul, and J. Irvine, "Optimizing power consumption of wi-fi for iot devices: An msp430 processor and an esp-03 chip provide a power-efficient solution," *IEEE Consumer Electronics Magazine*, vol. 5, no. 4, pp. 92–100, 2016.

[29] H. Jayakumar, K. Lee, W. S. Lee, A. Raha, Y. Kim, and V. Raghunathan, "Powering the internet of things," *2014 IEEE/ACM International Symposium on Low Power Electronics and Design (ISLPED)*, pp. 375–380, 2014.

[30] T. Islam, S. C. Mukhopadhyay, and N. K. Suryadevara, "Smart sensors and internet of things: A postgraduate paper," *IEEE Sensors Journal*, vol. 17, no. 3, pp. 577–584, 2017.

[31] J. A. Stankovic, "Research directions for the internet of things," *IEEE Internet of Things Journal*, vol. 1, no. 1, pp. 3–9, 2014.

[32] D. Bandyopadhyay and J. Sen, "Internet of things: Applications and challenges in technology and standardization," *Wireless Personal Communications*, vol. 58, no. 1, pp. 49–69, 2011.

[33] Q. Ju and Y. Zhang, "Predictive power management for internet of battery-less things," *IEEE Transactions on Power Electronics*, vol. 33, no. 1, pp. 299–312, 2018.

[34] G. Lowe, "Driving the internet of things," *IEEE Design & Test*, vol. 31, no. 2, pp. 22–27, 2014.

[35] The Bergquist Company, *Thermal Clad HT-07006 (High Temperature)*. www.bergquistcompany.com, Minnesota, US. PDS_HT_6mil_1113.

[36] Henkel Corporation, *Selection Guide: Thermal Interface Materials*. www.henkel-adhesives.com/thermal, California, US, 2016. 4282_US/LT8116 (2/16).

[37] OSRAM Opto Semiconductors GmbH, *Datasheet: Power TOPLED LR E6SF*. www.osram.com, Regensburg, DE, Nov. 2013. Version 1.2.

[38] OSRAM Opto Semiconductors GmbH, *Datasheet: Advanced Power TOPLED LA G6SP*. www.osram.com, Regensburg, DE, 2013. Version 1.0.

[39] J. Garg, M. Arik, S. Weaver, and S. Saddoughi, "Microfluidic jets for thermal management of electronics," *2004 ASME Heat Transfer/Fluids Engineering Summer Conference*, vol. Proceedings of HT-FED04, 2004.

[40] A. Corfa, A. Gasse, and S. Bernabe, "Analytical and FEM Simulations of the Thermal Spreading Effect in LED Modules and IR Thermography Validation," *2010 11th International Thermal, Mechanical and Multi-Physics Simulation, and Experiments in Microelectronics and Microsystems*, vol. IEEE, no. 11306235, 2010.

[41] C. Meola, *Infrared Thermography Recent Advances and Future Trends*, vol. ISBN: 978-1-60805-521-0. Bentham Science Publishers, 2012.

[42] W. Minkina and S. Dudzik, *Infrared Thermography Errors and Uncertainties*, vol. ISBN 978-0-470-74718-6. John Wiley & Sons, Ltd, 2009.

[43] Flir Systems, AB, *The Ultimate Infrared Handbook for R&D Professionals*. www.flir.com/thg.

[44] Keithly, *S2220, 2220G ,2230, 2230G Multi Channel USB and USB/GPIB Programmable DC Power Supplies Data Sheet*. Keithly Inc., US, 2013.

[45] FLIR SYSTEMS, *ThermaCAM SC5000 Technical Specifications*. FLIR Systems, Inc., 2005.

[46] Keysight Technologies, *Technical Overview*. USA, 2012-2014.

[47] E. Hong and N. Narendran, "A method for projecting useful life of LED lighting systems," *Third International Conference on Solid State Lighting*, vol. Proc. SPIE, no. 5187, 2004.

[48] Keysight Technologies, *Evaluating Current Probe Technologies for Low-Power Measurements*. www.keysight.com, USA, Dec. 2017.

[49] ANSYS Icepak, *ANSYS Icepak Tutorials*. ANSYS, Inc., US, 2013.

[50] MM.

[51] D. E. Knuth, *TEX: The Program*, vol. B of *Computers & Typesetting*. Reading, Massachusetts: Addison-Wesley, 1986.

[52] D. E. Knuth, "A torture test for TEX, version 1.3," Tech. Rep. STAN-CS-84-1027, Computer Science Department, Stanford University, Stanford, California, Nov. 1984.

[53] R. K. Furuta and P. A. MacKay, "Two TEX implementations for the IBM PC," *Dr. Dobb's Journal*, vol. 10, pp. 80–91, Sept. 1985.

[54] J. Désarménien, "How to run TEX in french," Tech. Rep. SATN-CS-1013, Computer Science Department, Stanford University, Stanford, California, Aug. 1984.

[55] A. L. Samuel, "First grade TEX: A beginner's TEX manual," Tech. Rep. SATN-CS-83-985, Computer Science Department, Stanford University, Stanford, California, Nov. 1983.

[56] L. Lamport, *LATEX: A Document Preparation System. User's Guide and Reference Manual*. Reading, Massachusetts: Addison-Wesley, 1986.

[57] M. D. Spivak, *The Joy of TEX*. American Mathematical Society, 1985.

[58] O. Patashnik, *BibTEXing*. Computer Science Department, Stanford University, Stanford, California, Jan. 1988. Available in the BibTEX release.

[59] O. Patashnik, *Designing BibTEX Styles*. Computer Science Department, Stanford University, Jan. 1988.

[60] D. Fuchs, "The format of TEX's DVI files version 1," *TUGboat*, vol. 2, pp. 12–16, July 1981.

[61] D. Fuchs, "Device independent file format," *TUGboat*, vol. 3, pp. 14–19, Oct. 1982.

[62] J. You, Y. He, and F. Shi, "Thermal management of high power leds: Impact of die attach materials," *Microsystems, Packaging, Assembly and Circuits Technology*, vol. IMPACT 2007. International, pp. 239–242, 2007.

[63] K. Yung, H. Liem, and H. Choy, "Heat transfer analysis of a high- brightness led array on pcb under different placement configurations," *International Communications in Heat and Mass Transfer 53 (2014)*, vol. Elsevier, pp. 79– 86, 2014.

[64] U. Uras and M. Arik, "Thermal and optical challenges in multi-purpose automotive exterior lighting systems," *Lighting Professional Symposium- LPS 2016*, 2016.

VITA

Umut Zeynep Uras received her bachelor degree in Mechanical Engineering from Ozyegin University in 2015. She is continuing her master education in Mechanical Engineering department of Ozyegin University under advisory of Professor Mehmet Arik. She worked as a teaching and a research assistant at Ozyegin University. Also, she worked as management representative at EVATEG Center (Energy Efficient Electronics and Lighting Technologies Research, Development, and Demonstration Center) between September 2016- May 2018. Now, she is working in TUSAS Engine Industries as thermal system design engineer. Her research areas consist of electronics cooling, thermal management of LEDs, effect of thermal issues on optical performance of LEDs and LED automotive exterior lighting.